



## City Research Online

### City, University of London Institutional Repository

---

**Citation:** Chan, W-L (1999). Integrated monitoring and control for intelligent power substations. (Unpublished Doctoral thesis, City, University of London)

This is the accepted version of the paper.

This version of the publication may differ from the final published version.

---

**Permanent repository link:** <https://openaccess.city.ac.uk/id/eprint/30673/>

**Link to published version:**

**Copyright:** City Research Online aims to make research outputs of City, University of London available to a wider audience. Copyright and Moral Rights remain with the author(s) and/or copyright holders. URLs from City Research Online may be freely distributed and linked to.

**Reuse:** Copies of full items can be used for personal research or study, educational, or not-for-profit purposes without prior permission or charge. Provided that the authors, title and full bibliographic details are credited, a hyperlink and/or URL is given for the original metadata page and the content is not changed in any way.

**INTEGRATED MONITORING AND CONTROL  
FOR  
INTELLIGENT POWER SUBSTATIONS**

by

**Wai-Lok Chan**

This thesis is submitted for the degree of

**Doctor of Philosophy**

at

Department of Electrical, Electronics and Information Engineering

**City University**

July, 1999.

## TABLE OF CONTENTS

TABLE OF CONTENTS .....	ii
LIST OF FIGURES .....	v
LIST OF TABLES .....	ix
ACKNOWLEDGMENTS .....	x
DECLARATION .....	xi
ABSTRACT .....	xii
Chapter I: INTRODUCTION .....	1
1.1 Advantages of artificial intelligence .....	2
1.2 Problems of conventional power substations .....	2
1.3 Features of an intelligent substation .....	5
1.4 Scope of the thesis .....	6
1.5 Organisation of the thesis .....	7
1.6 Statement of originality .....	8
1.7 List of publications .....	8
Chapter II: DISTRIBUTED SUBSTATION MONITORING SYSTEM .....	11
2.1 CLP power transmission system .....	12
2.2 Maintenance philosophy .....	13
2.3 Monitoring 400 kV substations .....	15
2.4 Concept of distributed monitoring .....	18
2.5 Details of the monitoring system .....	19
2.5.1 System hardware .....	19
2.5.2 Software .....	21
2.6 System performance .....	22
2.7 Advantages of the system .....	30
Chapter III: INTERNET BASED SUBSTATION MONITORING SYSTEM .....	32
3.1 System implementation .....	32
3.2 The remote vision system .....	34
3.2.1 Illumination level detection .....	36
3.2.2 Intruder detection .....	38
3.2.3 Fire alarm zone detection .....	39

	3.2.4	Substation meter reading .....	40
	3.2.5	Other useful features .....	44
Chapter IV:		FUZZY LOGIC APPLICATIONS IN SUBSTATIONS .....	50
4.1		Fuzzy sets and properties .....	50
4.2		Fuzzy expert systems .....	53
4.3		Application in capacitor switching .....	55
	4.3.1	Choice of control variable .....	55
	4.3.2	Discrete and continuous actuation .....	59
	4.3.3	Fuzzy control .....	60
	4.3.4	Fuzzification .....	60
	4.3.5	The rule base .....	62
	4.3.6	The inference engine and defuzzification .....	63
	4.3.7	Hardware design .....	64
	4.3.8	Performance of controller .....	65
4.4		Application in harmonic load recognition .....	66
	4.4.1	Harmonics patterns of system loads .....	67
	4.4.2	Concept of fuzzy numbers .....	69
	4.4.3	The harmonics templates .....	70
	4.4.4	Fuzzy number representation of harmonics spectrum .....	73
	4.4.5	Setting up the fuzzy linear equations .....	74
	4.4.6	Solving the fuzzy equations by optimisation .....	75
	4.4.7	Measurements on site and recognition .....	76
	4.4.8	Harmonics pollution indicator .....	77
4.5		Relationship with intelligent sub-stations .....	78
Chapter V:		NEURAL NETWORK APPLICATIONS IN SUBSTATIONS .....	79
5.1		Real-time frequency and harmonic evaluation .....	80
	5.1.1	Non-linear least-squares .....	82
	5.1.2	Neural network formulation .....	83
	5.1.3	Model validation by simulation .....	85
	5.1.4	Real application of the system .....	86
5.2		Complex artificial neural networks .....	89
	5.2.1	Conventional ANN for real numbers .....	90

5.2.2	New ANN for complex numbers .....	92
5.2.3	Comparison of the two ANNs by computer simulation .....	93
5.2.4	Application of "complex" ANN to load flow analysis .....	95
Chapter VI:	<b>EVOLUTIONARY PROGRAMMING APPLICATION</b>	
	<b>IN SUBSTATIONS .....</b>	<b>102</b>
6.1	Evolutionary computation .....	102
6.2	Motor incipient fault detection .....	103
6.3	The machine model .....	106
6.4	The parameter estimation .....	107
6.5	Evolutionary programming .....	108
6.6	The experimental setup .....	110
6.7	Experimental results .....	112
6.8	Applications in intelligent sub-stations .....	118
Chapter VII:	<b>CONCLUSION AND FURTHER WORKS .....</b>	<b>121</b>
7.1	Major achievements .....	121
7.2	Future works .....	123
7.3	A final remark .....	126
References	.....	127

## LIST OF FIGURES

<i>Number</i>		<i>Page</i>
Figure 2.1	The CLP 400 kV Transmission Network	13
Figure 2.2	The Castle Peak 400 kV Substations	15
Figure 2.3	Floor Plan of Castle Peak 400 kV Substation	16
Figure 2.4	Schematic diagram of single microcontroller	19
Figure 2.5	Schematic diagram of the CB timing circuit	20
Figure 2.6	Wiring diagram of one monitoring unit	21
Figure 2.5	SF <sub>6</sub> gas pressure variation of CB X830	23
Figure 2.8	The Tsz Wan Shan 400 kV Substation	24
Figure 2.9	132 kV Circle Breaker	25
Figure 2.10	The 132 kV 80 MVA Reactor	25
Figure 2.11	Current waveform for closing of reactor CB	25
Figure 2.12	Current waveform for tripping of reactor CB	26
Figure 2.13	Temperature variation of a 132 kV reactor	27
Figure 2.14	Typical circuit breaker waveforms	27
Figure 2.15	CB closing time	28
Figure 2.16	CB tripping time	28
Figure 2.17	Typical temperature profiles of eight sensing points	28
Figure 2.18	SF <sub>6</sub> gas pressure variation for two weeks	29
Figure 2.19	Typical battery voltage variation for two weeks	29
Figure 2.20	Air compressor on/off timing	30
Figure 3.1	The Whole Internet Based Monitoring System	33
Figure 3.2	The Airport 'A' Substation	34
Figure 3.3	Another view of the Airport 'A' Substation	34
Figure 3.4	The Fire Alarm Panel monitored by Remote Vision System	34
Figure 3.5	An Image of the Fire Alarm Panel	34
Figure 3.6	The Remote Vision System	35
Figure 3.7	Installation of a Video Camera	36
Figure 3.8	Installation of a Lighting Contactor	36
Figure 3.9	A View of the 11 KV Switchgear Room at Night	37

Figure 3.10	The View of the 11 kV Switchgear Room when the Lighting Contactor is Switched on	38
Figure 3.11	The Image of the Fire Alarm Panel when Alarms are Occurred	40
Figure 3.12	The Threshold of the Subtracted Images	40
Figure 3.13	An illustration of the "maximum" operation	42
Figure 3.14	An illustration of the Subtraction Operator	42
Figure 3.15	The Extracted Meter Pointer	43
Figure 3.16	The Flowchart of the Method	43
Figure 3.17	Front Page of the Monitoring Homepage	46
Figure 3.18	Monitoring Homepage for Po Lam Transmission Sub-station	47
Figure 3.19	Layout of Authorised User's Page	47
Figure 3.20	Image of Fire Alarm Panel on Homepage	48
Figure 3.21	Homepage showing Current Waveforms of Latest 132 kV SF <sub>6</sub> GCB Operation	48
Figure 4.1	An Example of Defuzzification	54
Figure 4.2	A Simplified Single Line Diagram	57
Figure 4.3(a)	Industrial Loading	58
Figure 4.3(b)	Residential Loading	58
Figure 4.3(c)	Commercial Loading	58
Figure 4.4	Membership Function of the Input Variables	61
Figure 4.5	Block Diagram of the Controller	64
Figure 4.6	Variation of P and Q	65
Figure 4.7	Variation of Power Factor and Q	65
Figure 4.8	Variation of Power Factor and Q	66
Figure 4.9(a)	Magnitude Spectrum of PC1	68
Figure 4.9(b)	Phase Spectrum of PC1	68
Figure 4.10(a)	Magnitude Spectrum of PC2	68
Figure 4.10(b)	Phase Spectrum of PC2	68
Figure 4.11(a)	Harmonics Pattern of PC1	71
Figure 4.11(b)	Harmonics Pattern of PC2	71
Figure 4.12	Harmonics Pattern of 200W Dimmer	72
Figure 4.13	Harmonics Pattern of 200kVA Transformer	72

Figure 4.14	Harmonics Pattern of Fluorescent Tubes (120W)	72
Figure 4.15	Star Diagram of 3 Transformers Plus 1 Dimmer	72
Figure 4.16	Star Diagram of 1 Transformer Plus 2 PC's	72
Figure 4.17	Star Diagram of Mixture of Fluorescent Tubes, Personal Computers and Dimmer	72
Figure 4.18(a)	3rd Harmonics Measurement (Real Part)	74
Figure 4.18(b)	3rd Harmonics Measurement (Imaginary Part)	74
Figure 4.19(a)	Fuzzy Number Representing Real Part	74
Figure 4.19(b)	Fuzzy Number Representing Imaginary Part	74
Figure 5.1	The Neural Network System for Frequency and Harmonic Evaluation	84
Figure 5.2(a)	Instantaneous waveform by simulation	86
Figure 5.2(b)	Extracted fundamental amplitude	86
Figure 5.2(c)	Extracted 15 th harmonic amplitude	86
Figure 5.2(d)	Extracted frequency variation	86
Figure 5.2(e)	Extracted fundamental based on DFT	87
Figure 5.2(f)	Extracted 15 th harmonic amplitude based on DFT	87
Figure 5.3(a)	Instantaneous supply voltage waveform	87
Figure 5.3(b)	Extracted fundamental voltage by neural network	87
Figure 5.3(c)	Extracted 3 rd and 5 th harmonic by neural network	88
Figure 5.3(d)	Extracted main frequency by neural network	88
Figure 5.3(e)	Extracted voltage harmonics spectrum at $t = 0.5$ s	88
Figure 5.3(f)	Extracted phase spectrum at $t = 0.5$ s	88
Figure 5.4	A Typical ANN for Real Numbers	91
Figure 5.5	Basic Elements of Newly Designed "Complex" ANN	91
Figure 5.6	The New ANN for Complex Numbers	93
Figure 5.7	Error History of 2 ANNs under Training	94
Figure 5.8	The 6-Bus Network for Load Flow Computation	95
Figure 5.9	Training Errors of 2 ANNs for Power Load Flow	98
Figure 6.1(a)	Waveform of $i_{ac}$ and $i_{am}$ (dash)	108
Figure 6.1(b)	Waveform of $i_{bc}$ and $i_{bm}$ (dash)	108
Figure 6.2	The A.C. motor - D.C. generator test bed	111
Figure 6.3	The ABB Variable Speed Drive	111

Figure 6.4	Yokogawa High Speed Digital Recorder	112
Figure 6.5	Start-up Current of Red Phase by DOL	113
Figure 6.6	Torque Variation during Start-up by DOL	113
Figure 6.7	Start-up Voltage of Red Phase by DOL	114
Figure 6.8	Rotor Speed Variation during Start-up (DOL)	114
Figure 6.9	Current Waveform during Soft Start-up	116
Figure 6.10	Voltage Waveform during Soft Start-up	116
Figure 6.11	Torque Variation during Soft Start-up	117
Figure 6.12	Rotor Speed Variation during Soft Start-up	117

## LIST OF TABLES

<i>Number</i>		<i>Page</i>
Table 2.1	400 kV CB Operation at Castle Peak	22
Table 2.2	132 kV CB operation at Tsz Wan Shan	24
Table 5.1	A Data Set with Nine Training Examples	94
Table 5.2	Network Parameters of the 6-Bus Network	96
Table 5.3	Load information of the Load Flow Study	96
Table 5.4	Training Examples for the Load Flow Study	98
Table 5.5	Test Cases for the Load Flow Study	99
Table 5.6	Results of the Load Flow Study	100
Table 6.1	Evaluated Parameters for Different Initial Guesses	115

## ACKNOWLEDGEMENTS

The author would like to thank Dr. L.L. Lai for his continuous guidance and supervision on the project since its commencement in 1995. Particular thanks are given to Dr. Albert So for his continuous support and creative idea over the research period. Special thanks are also given to Mr. T.M. Chan and Mr. S.L. Pang of CLP Power for their technical support in the installation of the systems on trial. The author is also indebted to Prof. A.K. David, Prof. S.L. Ho and Dr. C.T. Tse for their invaluable advice during the preparation of the thesis.

## DECLARATION

The author hereby grant powers of discretion to the City University Librarian to allow this thesis to be copied in whole or in part without further reference to the author. This permission covers only single copies made for study purposes, subject to normal conditions of acknowledgment.

City University, London.

## ABSTRACT

Power substations can be considered the major component of an electric power transmission system, influencing the reliability, security and efficiency of all functions of the system. The idea of "intelligent sub-stations" is the main theme of this thesis.

First of all, a distributed monitoring system was developed so that the concept of sub-station automation could be realised. The monitoring system was successful in interfacing all major components inside a sub-station using simple hardware and off-the-shelf personal computers. This system formed the foundation of all subsequent research work described in this thesis. It was further developed to possess two outstanding functions, namely computer vision and Internet access. Using computer vision, the human operators in the central control centre were able to get the full picture of what happened in the sub-station with full confidence under a real-time mode. With Internet access, relevant information could be made available to all personnel concerned with the normal operation and maintenance and ad hoc emergency fault attendance as well.

With this basic hardware and software being successfully implemented in three sub-stations in Hong Kong, advanced features involving techniques in artificial intelligence were employed for enhancing the existing functions of the distributed monitoring system. Fuzzy logic was extensively applied for reactive power control and power harmonics signature recognition. The response and accuracy of reactive power control which was so important in maintaining a constant voltage level of the power system could be improved. With power harmonics signature recognition, the concept of power quality control could be realised as this problem was getting more and more serious as power electronics equipment was extensively utilised. Artificial neural networks were employed to evaluate the harmonics spectra of the power line, which could be a useful partner to the fuzzy system. The fundamental frequency could be evaluated on a real-time basis. The artificial neural networks were extended from the conventional real space into the complex space which saw great application in power system analysis. Finally, evolutionary programming was used to

estimate the parameters of rotating machines during the state of transient operation. With the modern field oriented control strategy, accurate parameter estimation was more and more demanding. Further to that, parameter estimation could be a useful aid to the policy of condition based maintenance which was widely used in the power industry.

As future research work, preliminary studies on the application of thermography in power sub-stations and virtual reality were carried out. A brief report on these studies is included in the concluding chapter. As a final remark, the systems described in this thesis may also be useful to aid the successful implementation of the policy of deregulation of power systems in the future.

*Chapter I*

**INTRODUCTION**

This thesis reports research works carried out on new monitoring and control systems for intelligent power substations. This chapter highlights existing problems of conventional power sub-stations and then describes the evolution of conventional control and monitoring features of power substations with the introduction of technologies in artificial intelligence. In modern power systems, the main function of the transmission and distribution system is to deliver bulk power from generation sources to users at different load centres. Transmission facilities generally include step-up transformers, interconnecting transmission lines, switching stations and step-down transformers. The distribution system comprises primary distribution lines, service transformer banks and secondary networks. As an integral part of the transmission system, the power substation or switching station functions as the connection and switching point for transmission lines, sub-transmission feeders, generating circuits, and step-up/step-down transformers [1]. Primarily, the substation design objective is to provide maximum reliability, flexibility and continuity of service. Moreover, there are a lot of electrical equipment in a typical substation, including protection relays, circuit breakers, isolators and ground switches, current and voltage transformers, power transformers, shunt reactors and capacitors, buses and cables, and other building services equipment. All of them are closely related to the reliability of a substation [1,2]. Since power substations have an important role in the security and quality of supplies in a distribution system, it is necessary to pay particular attention to maintain a good system performance and to prevent damage in the equipment. Many technological advances have indeed been made in the area of substation automation [3,4], including the introduction of fuzzy expert systems, artificial neural networks and evolutionary computation. Thus, there is an excellent potential for electrical engineers to consider the application of intelligent system and information technology in the realisation of intelligent substations [5,6]. In essence, an intelligent system can be defined as a system which exhibits intelligence, where intelligence in this context is artificial intelligence (AI) [7].

## 1.1 ADVANTAGES OF ARTIFICIAL INTELLIGENCE

An intelligent system is one which employs AI techniques to fulfil some of its computational requirements. Moreover, intelligent systems also aim to blend the speed and reliability of computers with the adaptability and abstract thinking abilities of humans. Hence, the building of intelligent systems that can model human behaviour has captured the attention of the world for years. So far, the application of intelligent soft-computing methods has the greatest impact on the discipline of power engineering [8-11]. Many practical power system problems often require logical reasoning, heuristic search, perception, and the ability to handle uncertainties. Some of the main advantages offered by the application of AI based systems are:

- i) accurate mathematical model of the target system is not required;
- ii) system performance is enhanced substantially;
- iii) design is exclusively based on the linguistic information available from experts;
- iv) less tuning effort is required;
- v) design can be based on the response data in the absence of the necessary expert knowledge;
- vi) generalisation is extremely good and thus the performance is independent of the particular characteristics of the system;
- vii) adaptive to new data or information;
- viii) solutions to problems which are intractable by conventional methods;
- ix) inexpensive to implement;
- x) easy to extend and modify.

## 1.2 PROBLEMS OF CONVENTIONAL POWER SUBSTATIONS

It seems that electric power substations operate well because thousands of them have been operating everywhere in the world for decades. However, when one takes a closer look at the current operation of most power substations, it can be noticed that the existing design of substations together with the current features have, in fact, many shortcomings.

## Chapter I

The first major problem with conventional power substations is their high reliance on human intervention. The current practice of power utilities in Hong Kong is to send teams of duty staff to visit substations on a regular and ad hoc basis. This kind of surveillance, very often, is not systematic enough to discover abnormal situations that are not obviously visible. However, such surveillance is still essential from the power company's point of view to ensure the complete integrity of the system. In addition, there is always the possibility of an incident occurring in between the two visits of the duty staff. Due to the large number of sub-stations in the city, the frequency of visits by the duty staff cannot be too high. In this way, it is common for the power companies to use the policy of breakdown maintenance for all the non-critical systems such as ventilation fans, lightings and elevators etc. within the substations. For critical systems such as protective relays, switchgear and compressors, a planned preventive maintenance policy is carried out. With the growing sophistication and advance in technology, condition based maintenance should be the main trend although it cannot be adopted in conventional substations. Conventionally, trend loggers have been installed in certain critical systems where the status of each device is recorded continuously using, say, a chart recorder. Nevertheless, this important information cannot be assessed by professionals from the control centres. Duty staff need to physically visit a particular substation and bring the information back for further analysis. Furthermore, when an abnormal situation occurs in a remote substation, an alarm might be fed back to the control centre and only then a duty staff is summoned to attend the fault. This might however take a long time from minutes to hours if a traffic occurs.

Secondly, the importance of remote control and monitoring is getting more and more important in ensuring fast response to load changing and ad hoc occurrences. In China Light and Power (now renamed as CLP Power) systems, all the 400 kV and 132 kV switchgear can be controlled remotely. Most 11 kV switchgear has no remote control functions. Local and manual operation of 11 kV switchgear is necessary in conventional substations. Essential signals such as that of the fire and intruder alarms are generally wired back to the control centre. Nevertheless, the duty staff in the control centre cannot discriminate a genuine alarm from a false alarm that occurs very frequently in practice. Human resources are therefore wasted in attending the site and carrying out the alarm attendance. Furthermore, flooding of

## Chapter I

a substation is unknown to the control centre. Only when certain electrical equipment are short-circuited that the control centre is aware of such faults due to the occurrence of a fire or the tripping of protective devices. Real time image retrieval and analysis for intelligent decision making may thus be a solution to these problems.

Voltage and reactive power control are just two of the major responsibilities of a power substation. At present, voltage control is done by automatic tap changers in each substation. Reactive power control is troublesome in that it needs remote manual control by the system control engineer in the control centre through the Supervisory Control and Data Acquisition System (SCADA) on a daily basis. Technical staff are required to switch off the local reactors and switch in the local capacitor banks during peak hours and vice versa during off-peak hours. Improvement in this aspect is highly desirable.

At present, all relevant information related to the status and parameters of a power substation are fed back to the central control centre that is responsible for transmitting the selected data to concerned personnel, thus rendering the communication process highly inefficient. Thanks to the advancement of information technology nowadays, such mechanism can be modernised using an information superhighway, including both the Internet and the Intranet. With the aid of these modern systems, information can be made available to all authorised personnel within the power company, thereby speeding up enormously the response rate of control, fault finding and fault rectification.

Finally, the idea of optimal switching based on real-time load flow calculation is becoming more and more popular. Another issue is the growing concern of power quality of the substations outgoing feeders. The problem may come from the consumers or some intrinsic defects of the power system. Remedial preparation works could be done swiftly by the control centre if data regarding the power quality can be made available to the duty staff of the control centre. However, such concepts involving intelligent decision making can never be implemented in conventional substations.

### 1.3 FEATURES OF AN INTELLIGENT SUBSTATION

To improve the numerous short-comings of conventional substations, this thesis reports the development of a series of new systems using artificial intelligent techniques to enhance the features of these substations both reliably and economically. A modern intelligent power substation should at least possess the following functions [12]:

- i) power system protection
- ii) supervisory control and data acquisition
- iii) statistical revenue metering
- iv) local control
- v) voltage regulation
- vi) station battery monitoring
- vii) digital fault recording
- viii) sequence of events recording
- ix) power quality analysis

Some of the research work related to intelligent power substations has been done by others. A hybrid intelligent tool for distribution system fault diagnosis was implemented [13]. Neural networks were used for fault location in substations [14]. These neural networks as reported were also used to detect and classify faults in power systems [15]. A fuzzy rule based expert system for power system fault diagnosis was also developed [16]. Intelligent digital relays were constructed to improve the protection ability of large transformers [17]. Intelligent control of the cooling pumps of large transformers was also developed [18]. A neural network based partial discharge monitoring system was established to study the performance of a gas insulated switchgear [19]. Techniques using fuzzy logic and neural networks in load modelling and forecasting has been reported as well [20].

In summary, successful applications of intelligent systems to power systems have helped to open the door to a new challenging field. This thesis will demonstrate how the application of artificial intelligence can be beneficial to the various systems within a standard substation.

### 1.4 SCOPE OF THE THESIS

First of all, a microcontroller based distributed substation monitoring system was proposed and successfully implemented as the first contribution of this thesis. The system had been tested in the Castle Peak 400 kV substation, Tze Wan Shan 400 kV substation and Po Lam 132 kV substation of the CLP power company for two years, and it has been well proven up to the present moment. The system was later upgraded to possess some superior features such as computer vision aided alarm analysis and Internet based data distribution facility as the enhanced version of the system. The application of computer vision and Internet technologies in substation monitoring is the second contribution of this thesis. The new system was also satisfactorily implemented in the new airport substation at Chek Lap Kok. This distributed monitoring system was considered as the operating platform of the whole concept of intelligent substation. Throughout the research process, CLP Power had kindly supported the project in terms of the provision of site, staff and equipment for the installation of the whole system and the reporting of performance of systems on trial.

AI based features were studied, designed and verified in the laboratory, and hopefully, will be implemented onto the platform in the near future. The first AI based feature was the development of an automatic reactive power controller employing a fuzzy expert system as the third contribution of this thesis. Fuzzy number techniques were used to determine the constitution of various harmonics loads connected to the substation based only on the load current measurement as the fourth contribution. Such information will be very useful for power quality control in the future. Secondly, artificial neural networks (ANNs) were used to construct a real-time power harmonics analyzer which could accurately determine the fundamental frequency of the system as well as the fifth contribution. The conventional ANNs on real-number domain was further extended to the complex-number domain to provide an effective means of estimating power load flow at the substation as the sixth contribution. Finally, techniques in evolutionary programming were employed for machine parameter estimation as the seventh contribution. The results will be very useful for the real-time control of machines and for the possible implementation of condition based maintenance policy of rotating machines inside a power substation. These additional features have all been

successfully tested in the laboratory and they will soon be integrated into the existing distributed monitoring systems inside the substations in Hong Kong.

### 1.5 ORGANISATION OF THE THESIS

Chapter I gives an overview of the intelligent substation development. The first contribution of the thesis is to provide the foundation work for the future implementation of intelligent power substations.

Chapter II will give the basic hardware and software details of the microprocessor based distributed monitoring system [21]. Relevant waveforms of real-time monitored parameters are included to demonstrate the usefulness of the system.

Chapter III provides details of the implementation of the upgraded features of the system described in Chapter II. The features are computer vision and Internet based information delivery [22]. The application of computer vision and Internet techniques are very useful in power substation monitoring.

Chapter IV discusses applications of fuzzy expert systems on reactive power control [23] and the solution of fuzzy equations for harmonic signature recognition [24].

Chapter V discusses the applications of artificial neural networks in the power substations. A Hopfield type ANN on real space is used to evaluate the harmonic spectra of the power line and the fundamental frequency [25]. A new development of designing the ANN on the complex space has also been successful in a more accurate power load flow estimation with a guaranteed high speed of convergence [26,27].

Chapter VI introduces the application of evolutionary programming. A real-time machine parameter estimator has been developed for field oriented control and condition based maintenance [28].

Chapter VII gives a conclusion of all the achievements mentioned in this thesis with some new ideas for future research works are given. Two topics treated as future work, are being looked into and they are automatic diagnosis of power equipment using thermography [29] and the development of a virtual reality based system to help the maintenance engineers to visualise the condition of any piece of power equipment with both a visible and an infrared spectra [30].

### 1.6 STATEMENT OF ORIGINALITY

There are altogether eight original contributions of this thesis to the field of electric power engineering and they are as follows. The hardware implementation of a distributed monitoring system was original when it was first designed in 1996. Then, the application of computer vision and Internet technologies in substations could be considered as two significant contributions to the area of power engineering. Fuzzy reactive power compensation and application of fuzzy numbers for harmonics signature recognition were another two original contributions of the thesis. Real time harmonics calculation using neural networks and the development of ANN in complex domain for load flow calculation were two more contributions to the area of power engineering. Finally, the use of evolutionary programming in machine parameter estimation was also a new contribution to the field.

### 1.7 LIST OF PUBLICATIONS

Four papers have been published during this period in leading international journals, three in IEEE Transactions and one in Fuzzy Sets and Systems. Two more papers are now under review by IEEE Transactions on Power Systems. Four papers have been presented in international conferences and published in the proceedings.

#### Refereed Journal Papers

- 1 W.L. Chan, T.M. Chan, S.L. Pang and A.T.P. So, "A distributed on-line hv transmission condition monitoring information system", *IEEE Transactions on Power*

*Delivery*, Vol. 12, No. 2, 1997, pp. 707-713.

- 2 W.L. Chan, A.T.P. So and L.L. Lai, "Internet based transmission substation monitoring", *IEEE Transactions on Power Systems*, Vol. 14, No. 1, 1999, pp. 293-298.
- 3 W.L. Chan and A.T.P. So, "Power harmonics pattern recognition by solving fuzzy equations", *Fuzzy Sets and Systems*, Vol. 67, No. 3, 1994, pp 257-266
- 4 L.L. Lai, W.L. Chan, C.T. Tse and A.T.P. So, "Real-time frequency and harmonic evaluation using artificial neural networks", *IEEE Transactions on Power Delivery*, Vol. 14, No. 1, 1999, pp. 52-59.
- 5 W.L. Chan, A.T.P. So and L.L. Lai, "Complex artificial neural networks and its initial applications to load flow analysis", submitted to *IEEE Transactions on Power Systems* for consideration.
- 6 W.L. Chan, A.T.P. So and L.L. Lai, "Evolutionary programming based machine parameters estimation for field oriented control", submitted to *IEEE Transactions on Power Systems* for consideration.

Conference Papers

- 1 A.T.P. So, W.L. Chan and C.T. Tse, "Fuzzy logic based automatic capacitor switching controller for reactive power compensation", *Proceedings of Second International Forum on Applications of Neural Networks to Power Systems*, Yokohama, April 1993, pp. 41-46.
- 2 W.L. Chan and A.T.P. So, "Development of a new artificial neural network in complex space", *Proceedings of 2nd Biennial Australian Engineering Mathematics Conference*, Sydney, July 1996, pp. 225-230.

## Chapter I

- 3 Lai L.L., Chan W.L. and So A.T.P., "A two-ann approach to frequency and harmonic evaluation", *Proceedings of 5th Int. Conf. Artificial Neural Networks*, IEE, Cambridge, July, 1997, pp. 245-250.
- 4 W.L. Chan, A.T.P. So and L.L. Lai, "Evolutionary programming based machine parameters estimation for field oriented control", *Proceedings of IEEE International Electric Machines and Drives Conference*, Seattle, May 1999, pp. 534-536.

*Chapter II*

**DISTRIBUTED SUBSTATION MONITORING SYSTEM**

Having established the objectives of the thesis in Chapter I, the development of intelligent substations is described sequentially right from this chapter. The application of distributed microcontroller is discussed first. The most significant advantage offered by microprocessor technology is that it makes system integration of various automation and data-acquisition function possible. By efficiently combining functions in common hardware and software, one can achieve synergistic performance results and even perform functions which are previously not achievable. In particular, the concept of integrating several functions in one hardware solution provides a very cost-effective design which is one of the main advantages of using microprocessor-based technology. In general, the more functions that can be implemented in common hardware using the same or similar data base, the lower is the cost per function. Therefore, a significant advantage of integrated microprocessor systems for substations is the potential for cost effectiveness. The term "integrated" here describes the fact that all the functions are included in one computer system consisting of a network of several microcontrollers. The main design feature of the system is the distribution of the processing power to a number of microprocessors that are interconnected between one another. At least three different processing levels can be recognised [31]. One level is the data-acquisition level which comprises the data-acquisition units located in the switch-yard near the power apparatus, the other level being the processing level for certain time-critical functions, and the third level is the overall substation level. All adjacent levels are interconnected using various communication links. This communication facility is what makes the overall design to appear as one system for the entire substation. It can be observed that an obvious advantage is the possibility to monitor the entire substation automation system as well as all the power apparatus in a substation through a common database. This database is located at the third processing level in the integrated system hierarchy. An operator may access the database for the purpose of using such data for different control and analytical purposes. The details of a newly developed one-line distributed monitoring system is present in the following

sections.

### 2.1 CLP POWER TRANSMISSION SYSTEM

In the CLP Castle Peak power plant, 18 kV (A-station) and 23 kV (B-station) electric supplies are generated by 350 MW and 660 MW generators respectively. The voltage is then stepped up by generator transformers to 400 kV for transmission. A copy of the map of the 400 kV transmission system is shown in Figure 2.1. The intermediate control between those transformers and the major 400 kV overhead transmission system lies with a standard "One and a half Breaker Configuration" switch substation. The 400 kV substation consists of twenty four groups of 3 single phase encapsulated SF<sub>6</sub> CBs and each CB is remotely controlled by the main control centre at Tai Po. These CBs form a major channel of power flow between the generators and the transmission system and any breakdown during normal operation will significantly reduce the generation output or the system security. At the urban centres, the 400 kV is stepped down to 132 kV for further transmission or 11 kV for distribution. The Tsz Wan Shan 400 kV substation is one of the most important substations for the Kowloon Peninsula where standard "Double Busbar-Breaker Arrangement with Sectioner in 132 kV" is employed. Subject to the importance of all these CBs and the integrity of our modern electric power supply system, an appropriate predictive maintenance scheme by on-line computerised monitoring must be implemented onto these CBs.

The newly developed on-line distributed monitoring system which is going to be discussed will form part of the main features of the maintenance policy and it was specified in the 1995's target plan of the maintenance section. Castle Peak 400 kV substation has been in service for over ten years and there had been increasing defects being experienced during the past few years, particularly with respect to the closing time of CBs, the hydraulic system and the problems due to partial discharge etc. This substation is located in a remote area and thus the installation of an on-line monitoring system is considered necessary and efficient.

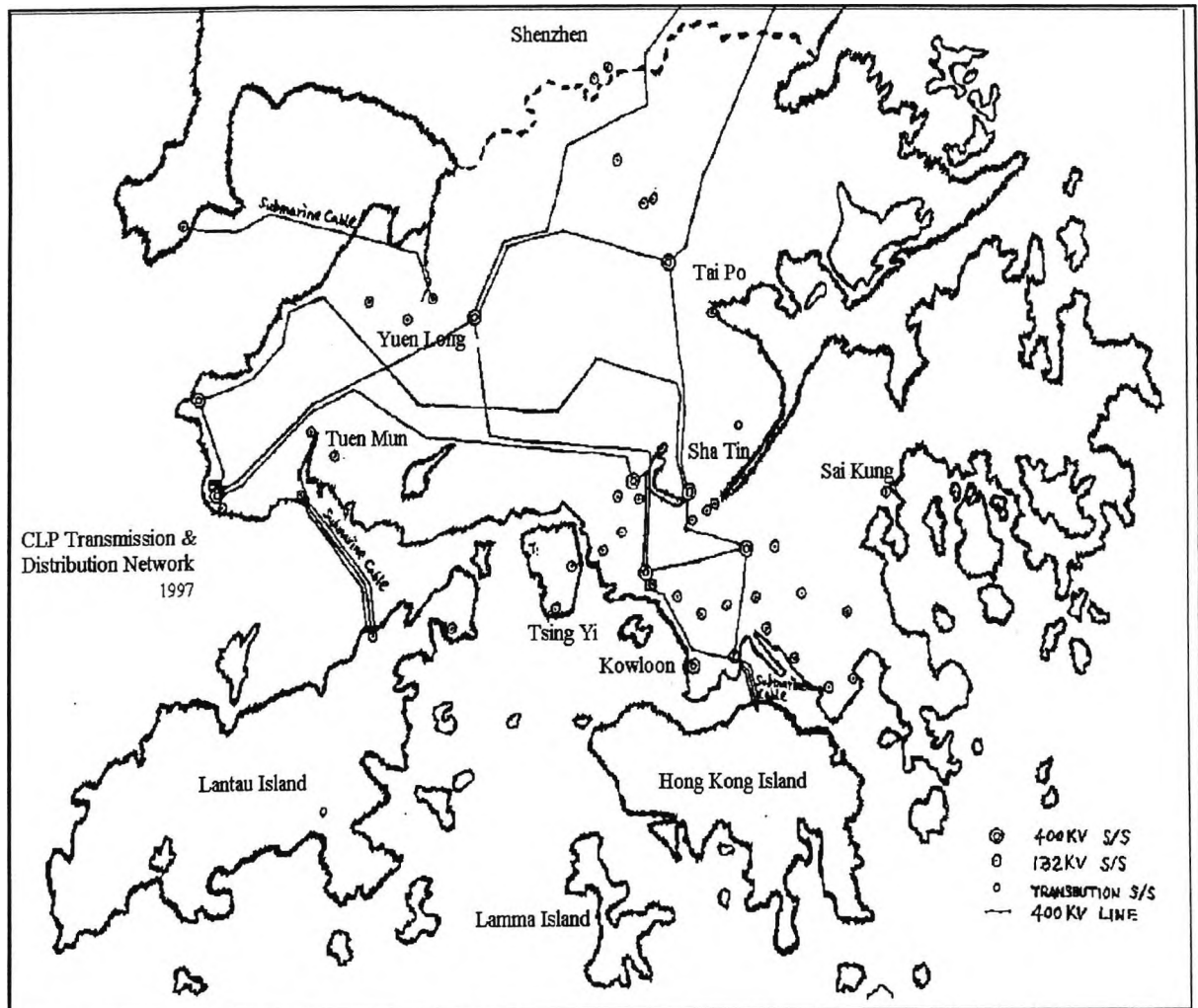


Figure 2.1 The CLP 400 kV Transmission Network

## 2.2 MAINTENANCE PHILOSOPHY

The increasing complexity of large electric power systems has resulted in a greater need for maintenance in order to provide a reliable supply of power. Equipment installed during the high growth periods of system expansions in previous decades may now be reaching their end-of-life and may require significant maintenance. Traditionally, the maintenance philosophy for substations has been to perform work at periodic intervals, i.e. planned maintenance, without regard to the actual in-service duty or the conditions or performance of the equipment. In order to become more efficient in the utilization of resources, there has been a growing tendency towards predictive maintenance philosophies. That is, maintenance

should only be performed when required and according to maintenance priorities [32]. In order to meet these requirements, special techniques for diagnosing the conditions of various power system components are required in order to arrive at the optimal maintenance decisions. Thus, predictive maintenance actually comes with condition based maintenance.

In most existing CLP plant equipment, there are certain amount of on-line monitoring devices or facilities that continuously monitor items such as gas pressure, CB timing, hydraulic and pneumatic system operation etc. A limited amount of data is fed to the existing SCADA system that can serve real time display only without the establishment of any database for further analysis. However, all these information is very useful in evaluating the plant performance and determining the maintenance requirement if the predictive maintenance strategy is to be adopted.

The Diagnosis & Monitoring Team was established in 93/94 whose objective was to develop a comprehensive condition monitoring information system so as to reduce the burden on preventive maintenance and to lower equipment failure rate. The implementation has gone along with the execution of the following approaches:

- a) reliability centred maintenance concept
- b) total productive maintenance concept
- c) predictive based maintenance concept
- d) **on-line condition monitoring and diagnosis**
- e) management by observation
- f) specialised and multi-skill programme
- g) on-line inspection/maintenance concept
- h) equipment failure preventive programme

Item (d) is closely related to this project. The goals are to reduce operating costs without affecting quality and reliability, to enhance the reliability level and to extend the life of equipment to an optimum. The strategies are to utilise advanced technologies where appropriate to reduce maintenance costs and improve efficiency and to enhance the approach

of condition-based maintenance. The first trial was successfully conducted in Castle Peak 400 kV substation by the author in early 1995.

### 2.3 MONITORING 400 kV SUBSTATIONS

For Castle Peak 400 kV substation, the gross floor area of the whole substation is around 76 m (L) x 43 m (W) = 3268 m<sup>2</sup>. The outlook and the floor plan of the substation are shown in Figure 2.2 and Figure 2.3 respectively in the following page. Within this area, there are totally seventy two individual CBs, three in one group by direct linkage. A protection equipment room is located in the second floor of the substation where the local control, alarm facia, protection and telecommunication equipment are housed. A typical one and a half circuit layout is used for two circuits, i.e. two generators.

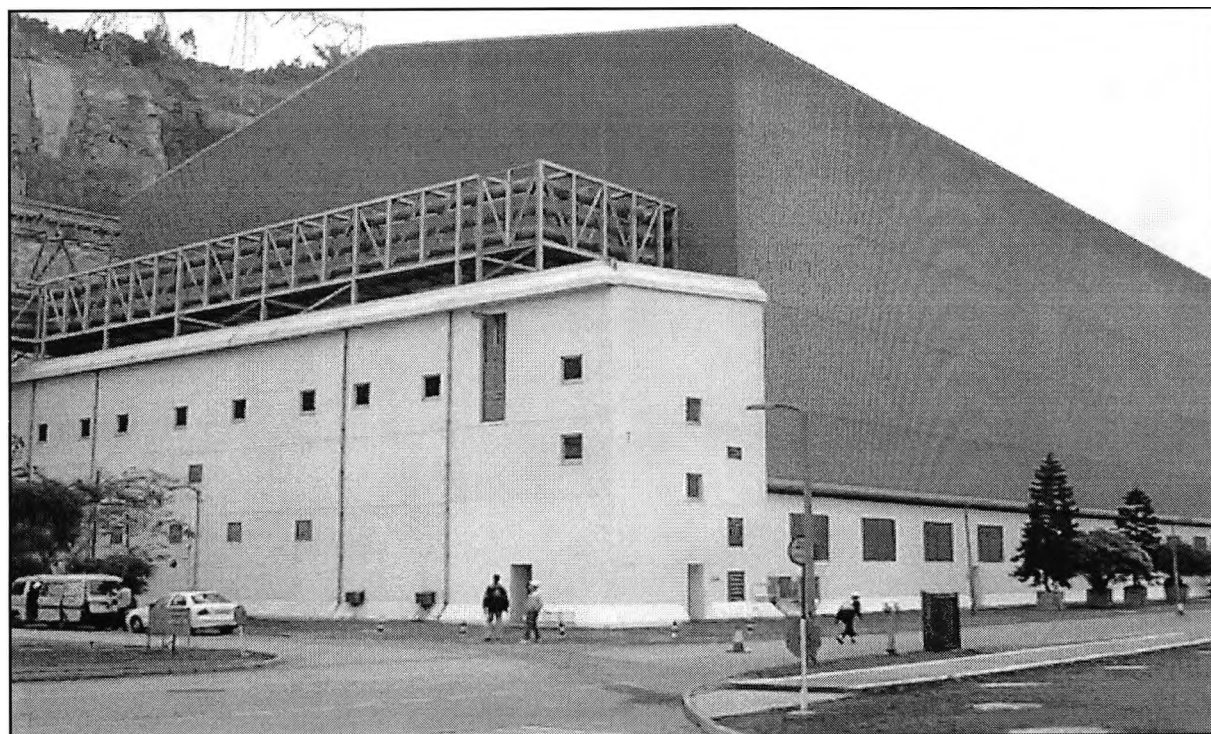


Figure 2.2 The Castle Peak 400 kV Substations

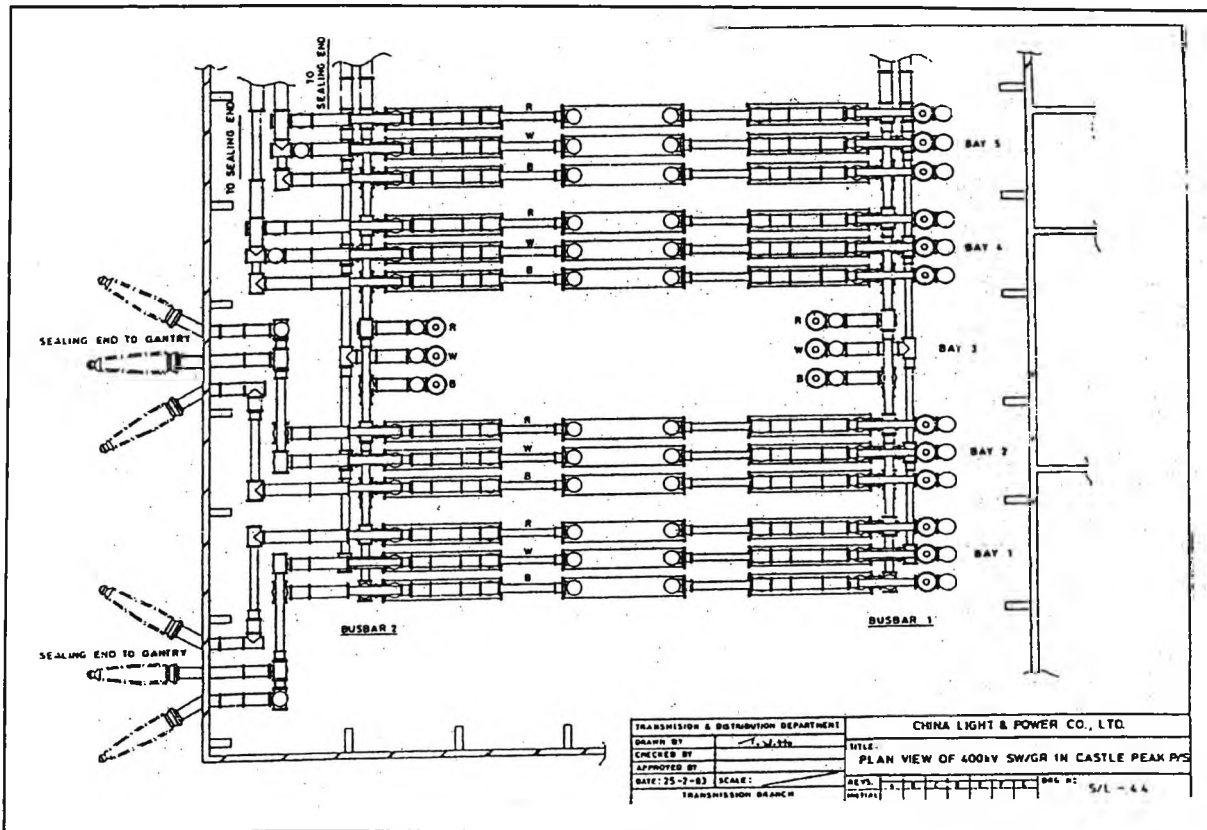


Figure 2.3 Floor Plan of Castle Peak 400 kV Substation

Three groups of CBs are responsible for serving one generator output, hence twenty four groups in total for four 350 MW generators in Castle A and four 660 MW generators in Castle B. The CB's for either Castle A or Castle B are operating in between two common 400 kV busbars.

When a group of CB is in "open" state, the actuating mechanism is operated by hydraulic systems. When a closing command of that group from Tai Po control centre arrives, a 110 V DC which is supplied by the station batteries will be applied to the closing coils of the three phases of that group and three breakers will be made instantaneously. Once the breakers are made, the voltage applied to the closing coil will be removed automatically. Similarly, when a tripping command from Tai Po arrives, a 110 V DC will be applied to the tripping coil of each phase and the breakers are opened instantaneously. Similar layout can be found in Tsz Wan Shan 400/132 kV substation.

## Chapter II

Theoretically, the operation of the breakers should be immediate right after the receipt of the 110 V DC signal and the three breakers should make or break synchronously. However, due to mechanical imperfection or fatigue, time delay in the operation after the 110 V energisation of a coil and non-uniform action of individual CB are unavoidable and this is a major problem. Other problems include nitrogen and hydraulic oil leakage and air trapped within the hydraulic circuit and misalignment of actuating mechanism etc.

A long delay in CB operation will cause instability in the 400 kV transmission system during the occurrence of a fault elsewhere in the system. The delay may cause damage to expensive equipment elsewhere as well. The asynchronous action of individual CB within a group would cause imbalance within the three phase circuits on a transient basis, resulting in power system instability. More seriously, the two events described above might be considered as a CB failure by the protection system, resulting in the tripping of another CB. This would lead to unnecessary outages at other consumer centres. The normal closing time of each CB is from 89 ms to 99 ms and the normal opening time is from 33 ms to 37 ms. The synchronisation of individual CB within a group should be within 10 ms for both closing and tripping actions. Conventionally, the CB contact travel has been timed by fitting a recording device to the accessible section of each actuator drive above the SF<sub>6</sub> shaft seal. Indications of contact position are derived from the actuator movement by the use of a reflective travel recorder based on the interaction between light emitting diodes and phototransistors. However, it is not a standard provision for all types of CB's and even not a built-in item for the CB in the substation. Hence, the particular CB needs to be switched off every time when its contact travel needs to be measured.

Apart from the operational timing of the CBs, other problems inside the substation such as leakage of SF<sub>6</sub> as indicated by the gas pressure, the operational frequency and duration of hydraulic pump and fault current etc. need to be monitored as well. The significance of detecting leakage rate of SF<sub>6</sub> gas and plotting the leakage curves can help the maintenance staff to arrange gas top up before any alarm initiation. The running time of hydraulic pump can reflect the performance of the pump motor by cross checking the system charging time. The operational count of the hydraulic pump can reflect possible oil leakage situations. Since

the operation of CB will affect both the running time and operational count, one needs to take into account the CB operation when analysing the frequency and duration of hydraulic pump operation.

Some modern CBs are fitted with on-line monitors so that the real-time condition monitoring can be done because more than half of the maintenance dollars are spent on CBs [33]. However, they are usually standalone components that need manual attention frequently for data retrieval and they could not be fitted to existing or old CBs, i.e. a huge investment would be needed to modernise the existing system. With all these aforementioned factors are considered, the distributed on-line monitoring system was developed to provide a low cost solution to condition based maintenance in high voltage substations.

### 2.4 CONCEPT OF DISTRIBUTED MONITORING

It has been mentioned that the Castle Peak 400 kV substation is quite remote and the floor area of the substation is more than 3200 m<sup>2</sup>. Also, the operational timing of each CB must be regularly monitored after routine maintenance and during normal operation. The data can be treated as important information to reveal the trend of the deterioration of the mechanism so that the goal of predictive maintenance can be attained.

Each group of CB is monitored by an individual system with data being wired back to an on-site microcomputer for secondary storage. Therefore, the failure of any one system has no effect on the normal operation of the remaining twenty three systems, hence achieving very high reliability. There are other advantages as well. The first one is the high capability of extension of the whole configuration, e.g. addition of other monitoring parameters can easily be achieved. Secondly, suitable maintenance can be arranged in advance once the CB has been found to be approaching an abnormal condition. Thirdly, sudden fault cases can be minimised and hence, forced outages become less frequent and the duration can be shortened. Maintenance cost can be reduced by putting less effort on routine inspection and data recording. Finally, the total manpower can be minimised subsequent to the successful installation of this on-line monitoring system.

## 2.5 DETAILS OF THE MONITORING SYSTEM

Each group of CBs are monitored by a standalone microcontroller. The microcontroller continuously monitors the status of each CB within a group. All microcontrollers are interconnected together and to the on-site microcomputer using a local area network with a baud rate of 9,600. Commands and monitored data are exchanged between microcontrollers and the microcomputer for configuration maintenance and secondary backup respectively. Each microcontroller is equipped with 32 kbyte of local RAM, capable of storing data for one whole year. Each microcontroller is also equipped with eight channels of analog input functions, capable of monitoring other plant parameters besides time interval measurement alone. The schematic diagram of the microcontroller is shown in Figure 2.4. Each on-site microcomputer exchanges data with a remote central microcomputer in the control centre at Tsz Wan Shan by standard telephone lines. In this way, the whole distributed on-line monitoring concept can be fulfilled where the central microcomputer at Tsz Wan Shan is able to communicate with all on-site microcomputers and also with all microcontrollers to retrieve the updated status and analog data of each CB.

### 2.5.1 System Hardware

The schematic diagram of the CB timing circuit is shown in Figure 2.5. For closing time monitoring, the voltage of the

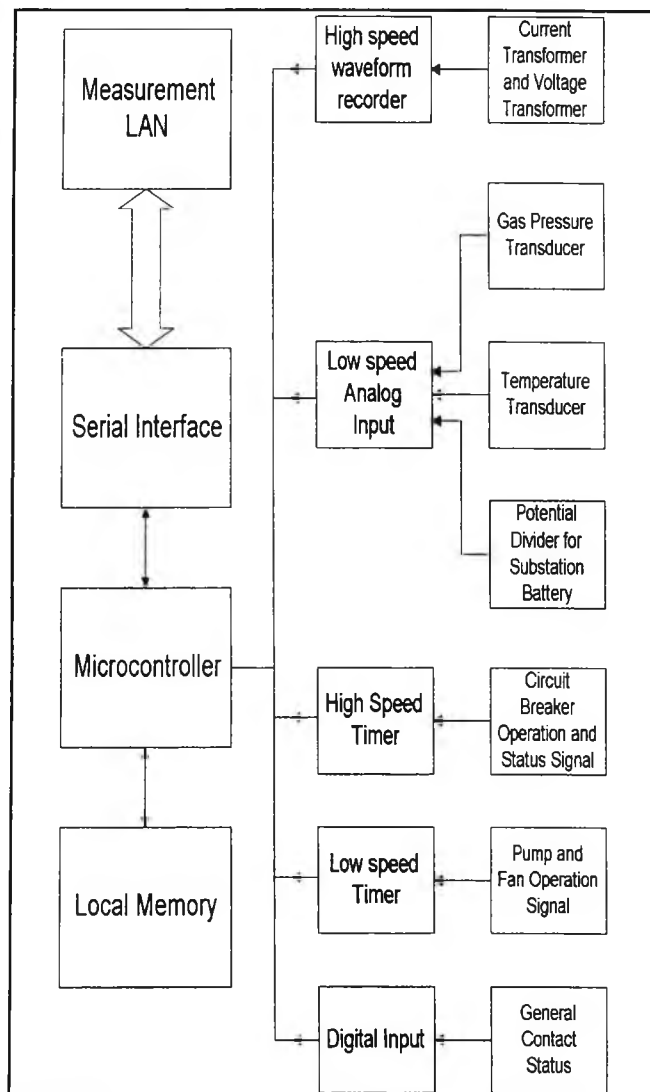


Figure 2.4 Schematic diagram of single microcontroller

## Chapter II

closing coil is sampled by an opto-coupler to provide full isolation between the CB and the microcontroller. Upon the energisation of the closing coil by the 110 V DC, three high speed digital timers inside the microcontroller are triggered on. The resolution of each timer is 5  $\mu$ s. Each CB has an auxiliary clean contact. Upon the successful closing of a breaker, its contact will be closed and its timer is halted. The count value stored inside the timer reveals the closing time of that breaker, with very high accuracy. The value is time stamped and stored inside the local RAM of the microcontroller. The microcontroller then resets the timer value to zero and switches its operating mode to the measurement of the tripping time. When the tripping coil voltage is sampled by another opto-coupler, the timer is triggered on again and then halted by the same auxiliary switch clean contact of the breaker. The tripping delay time is also time stamped and stored inside the local RAM similarly. The on-site microcomputer situated inside the protection room periodically polls each microcontroller sequentially and retrieves the useful monitored data for secondary storage and further analysis. Alarms are generated to make the maintenance personnel alert in accordance with a built-in expert system.

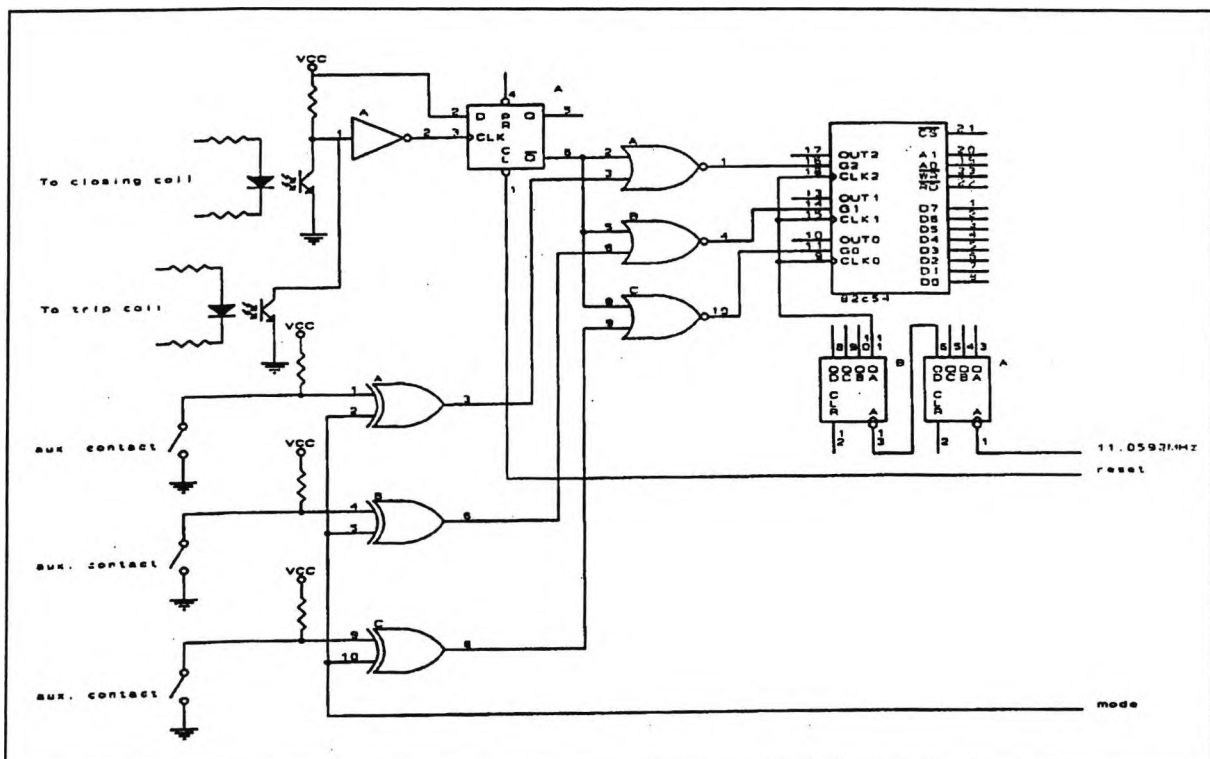


Figure 2.5 Schematic diagram of the CB timing circuit

## Chapter II

Besides, hydraulic pump running time and operational frequency being monitored with the low speed timer, the gas pressure and the substation batteries can be continuously monitored by the analog channels in each microcontroller. Other parameters that can effectively reveal the plant status can be measured as well. The wiring diagram of one monitoring unit is shown in Figure 2.6.

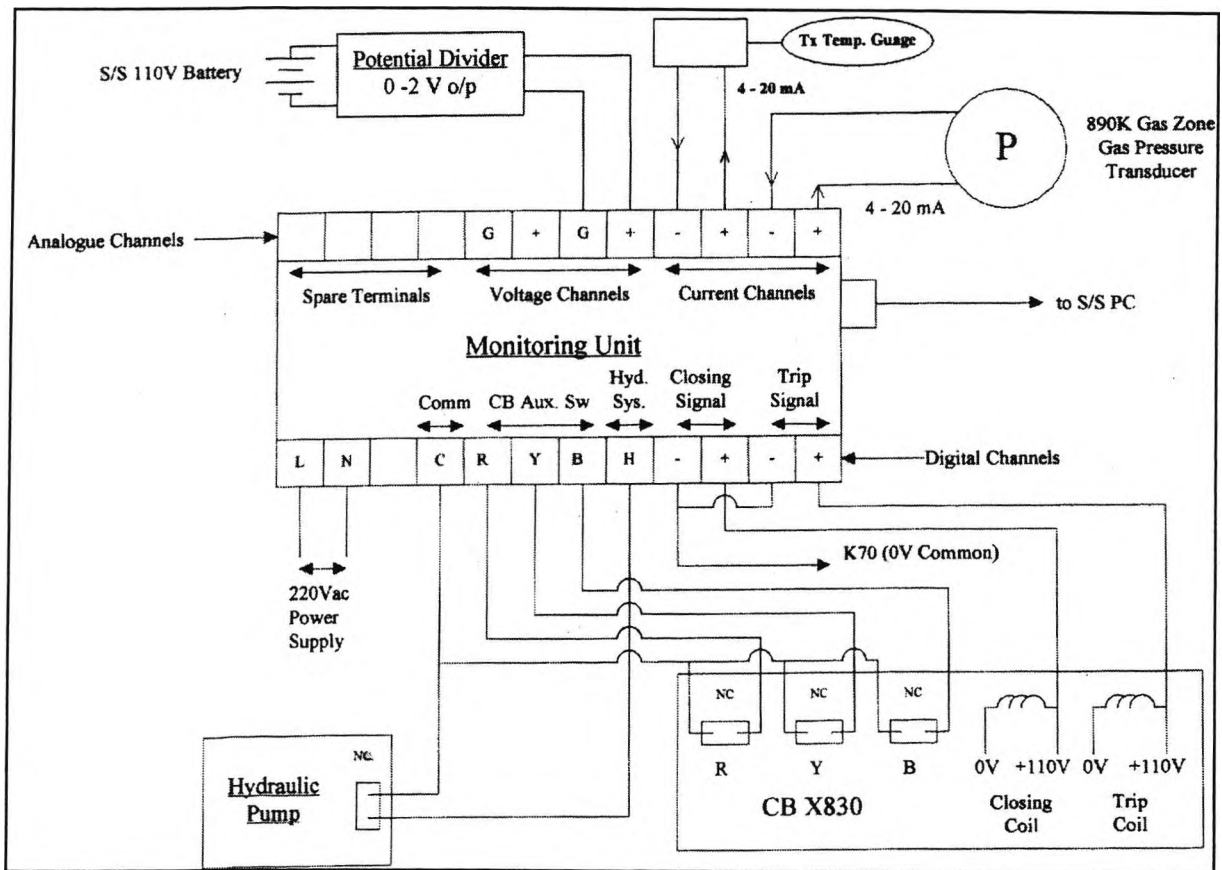


Figure 2.6 Wiring diagram of one monitoring unit

### 2.5.2 Software

Software development basically consists of three levels. The lower level is built inside each microcontroller for monitoring the plant status and for normal operation of the microcontroller. The middle level is built inside the on-site microcomputer for regular data logging and statistical functions. It also controls the communication with the central

microcomputer at Tsz Wan Shan through modems. The upper level is built inside the central microcomputer for user-friendly man-machine interface and multi-substation supervision.

## 2.6 SYSTEM PERFORMANCE

Table 2.1 shows the tripping and closing timing of the main contact of CB No. X890 in Castle Peak 400 kV substation based on the auxiliary contacts. An interesting finding is that on 15th Jan, 1996, that CB was under overhaul and the maintenance team failed to close the CB on time at 10:36:06 a.m. and that event was recorded by the system in the form of timing overflow. Overflow indicates that the CB takes more than 189.63 ms to either close or trip and that is unacceptable. In the same morning, at 10:45:10 a.m., the maintenance team failed to trip the same CB and an overflow message was recorded again. There is an individual CB for each phase in Castle Peak and thus three auxiliary contacts are available and thus the system is able to measure the operating time discrepancies among the three phases.

CB Status	Time	R (ms)	Y (ms)	B (ms)
Trip	09:39:59	34.29	37.15	41.56
Close	10:36:06	overflow	overflow	overflow
Trip	10:36:58	34.12	36.85	40.41
Close	10:38:37	108.57	107.79	108.68
Trip	10:45:10	overflow	overflow	overflow

Table 2.1 400 kV CB Operation at Castle Peak

Next, the SF<sub>6</sub> gas pressure measurement history of 4 months, from October, 1995 to January, 1996, is presented for CB No. X830 and the trend is shown in Figure 2.5. It can be found that there has been a very serious SF<sub>6</sub> gas leakage problem with the CB and the system was successful in warning the maintenance team on 17th December, 1995 and the gas topping up exercise was completed on 18th December, 1995, thus avoiding a major failure of the CB. Thanks to the on-line distribution monitoring system, a permanent damage to the CB was

prevented by an effective alarm message delivered to staff at Tsz Wan Shan office from the central microcomputer.

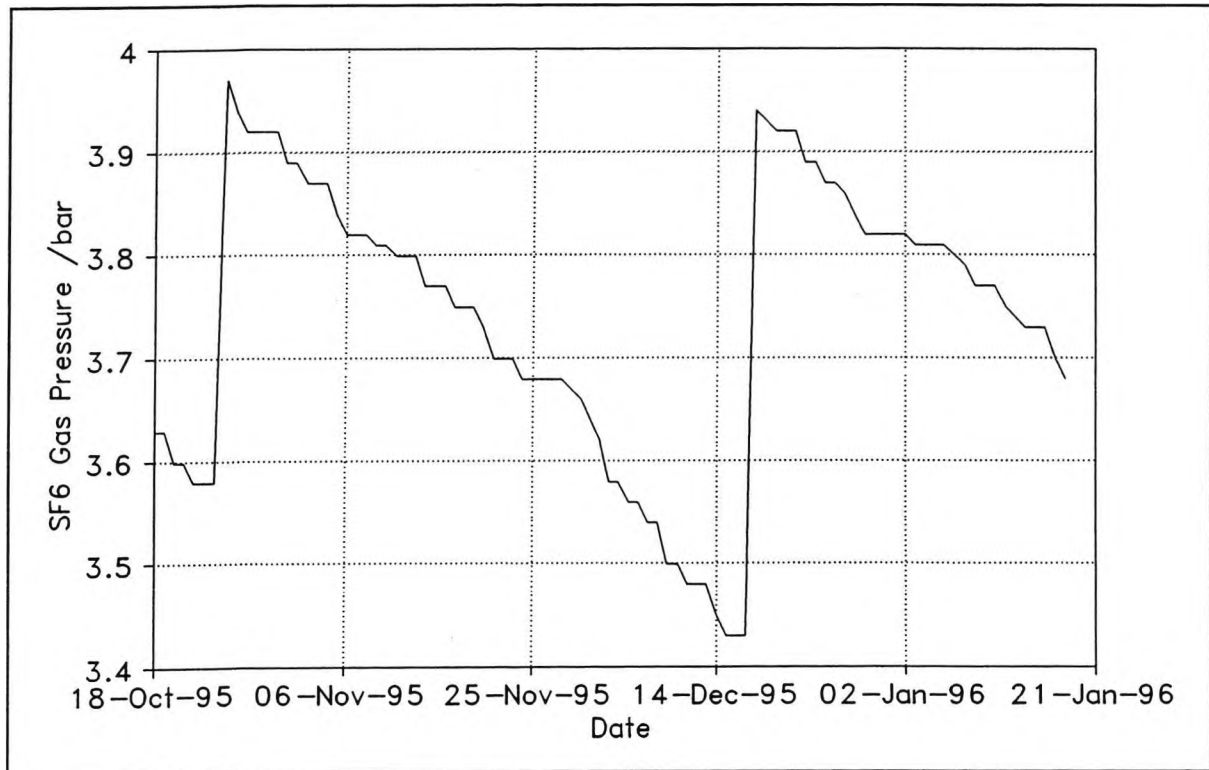


Figure 2.5 SF<sub>6</sub> gas pressure variation of CB X830

Moreover, the system is able to record the operation of each of the two compressed air pumps for all 132 kV CBs in the Tsz Wan Shan 400 kV substation. The outlook of the substation is shown in Figure 2.8. The normal starting time is around 21:00:34.46 and the stopping time is around 21:13:34.64 with an average duration of around 13 minutes. If there is any deviation from this set of data, a serious hidden fault with the CB may be implied. Table 2.2 shows the operation of a typical 132 kV CB. Since only a single auxiliary contact is available, it is not possible to obtain the 3-phase travelling data as in Castle Peak.

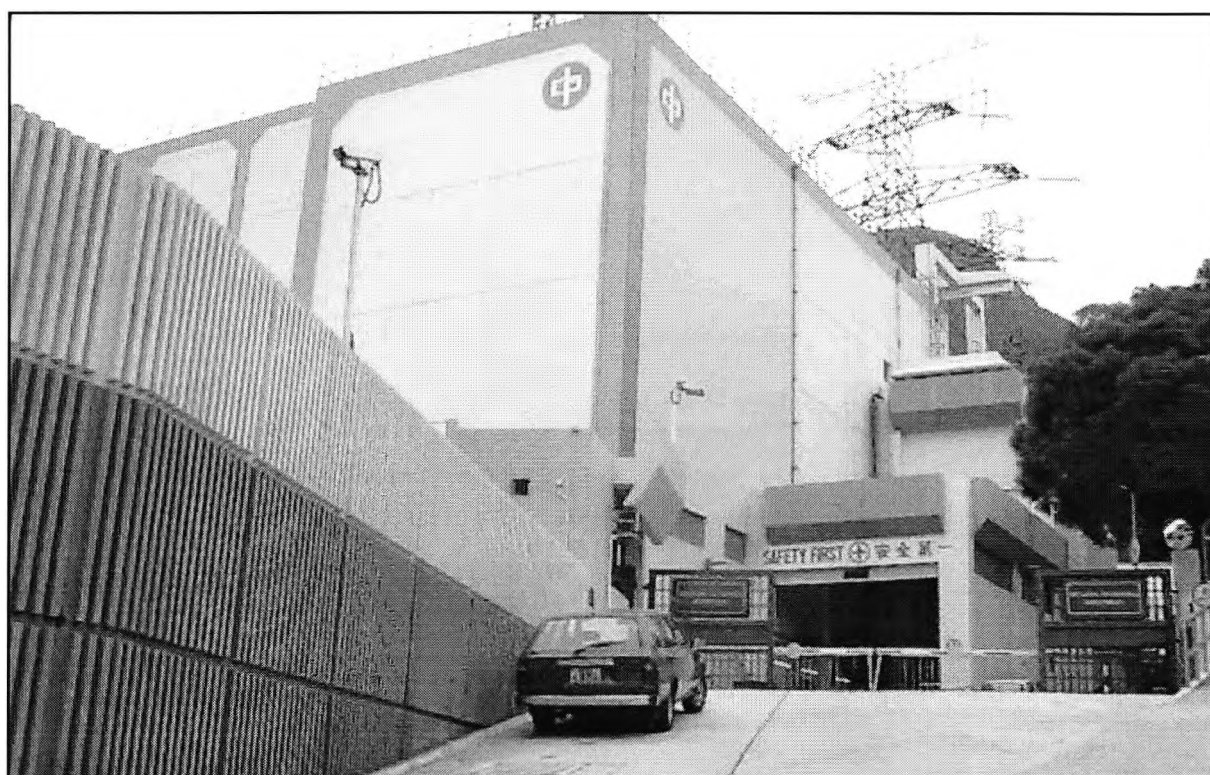


Figure 2.8 The Tsz Wan Shan 400 kV Substation

CB Status	Time	Operating Time (ms)
Close	13:57:38	86.21
Trip	13:57:56	22.77
Close	13:58:30	86.08
Trip	13:59:00	23.05
Close	13:59:23	86:07
Trip	13:59:38	23.12

Table 2.2 132 kV CB operation at Tsz Wan Shan

Another type of CBs, shown in Figure 2.9, in Tsz Wan Shan is for reactor switching. The reactor is shown in Figure 2.10. Auxiliary contacts are not accessible for this type of CBs. Therefore, a new method to measure the contact travelling of CBs based on the current waveforms has been developed. The result of measurement on a typical 132 kV CB which

is used to switch a 132 kV 80 MVA reactor is shown in Figure 2.11 and Figure 2.12.

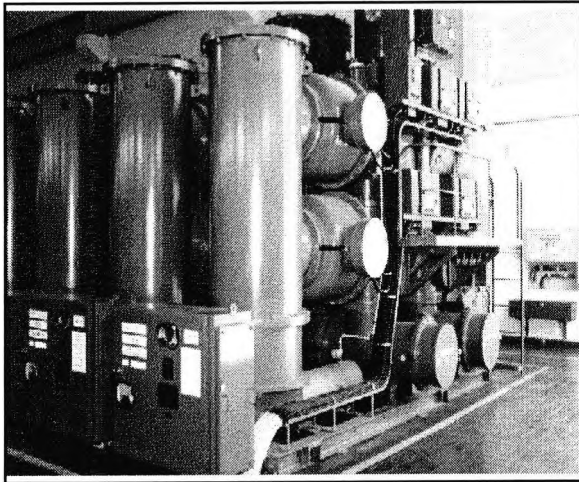


Figure 2.9 132 kV Circuit Breaker

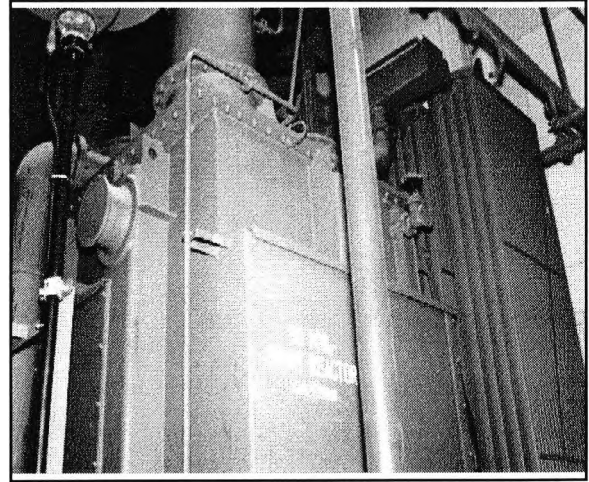


Figure 2.10 The 132 kV 80 MVA Reactor

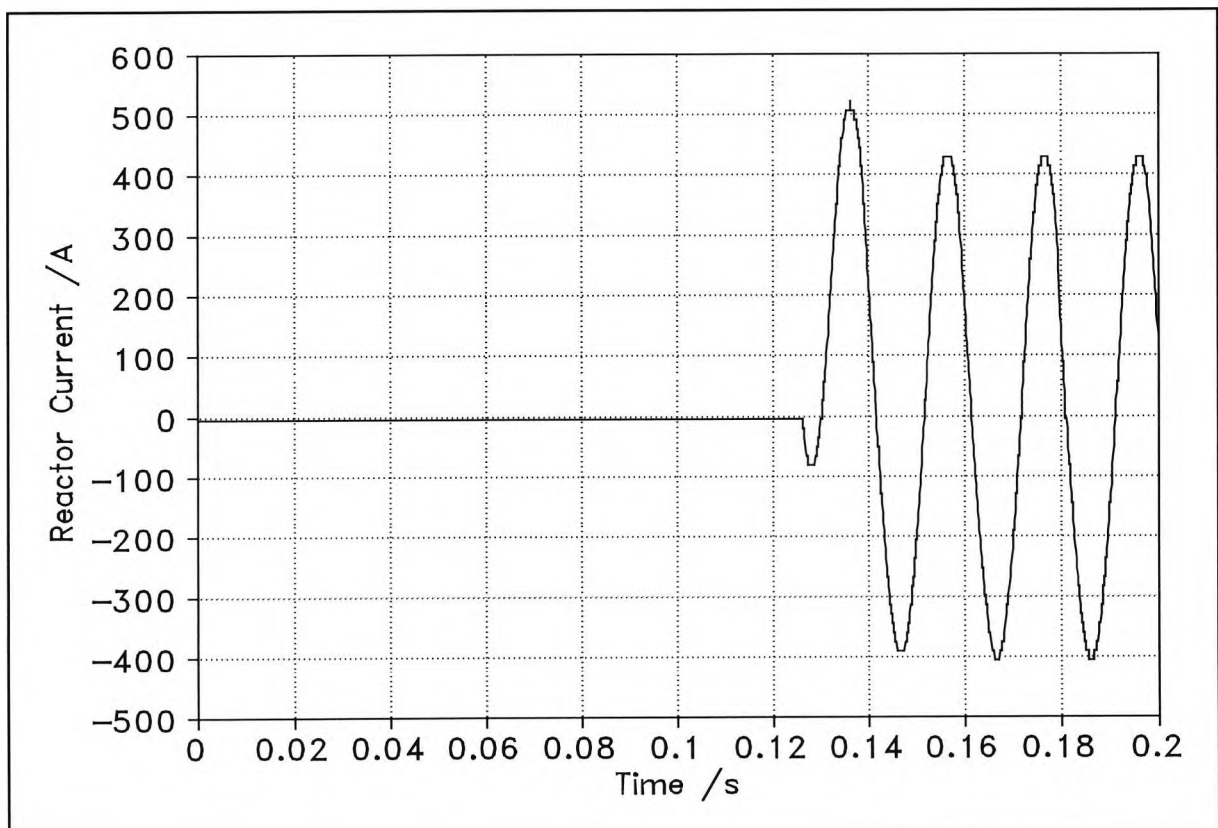


Figure 2.11 Current waveform for closing of reactor CB

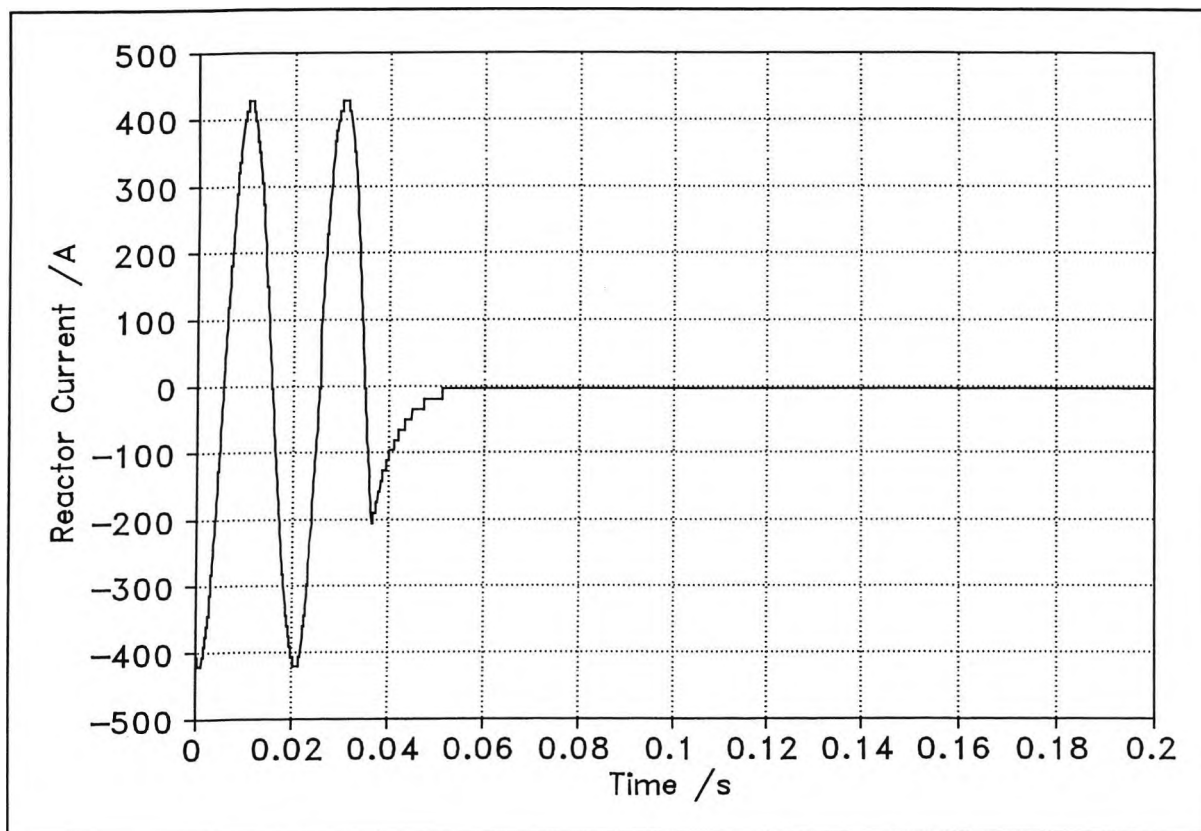


Figure 2.12 Current waveform for tripping of reactor CB

From the two figures, it is obvious that the closing time for the CB is 125 ms while the tripping time is 50 ms. This method is particularly useful for measuring the time discrepancy in the travelling action of the three CBs when auxiliary contacts are not available. This method is considered superior even when the CB is equipped with auxiliary contacts because it is the actual disruption of the current waveforms that is being measured. Figure 2.13 is the temperature profile of the reactor.

In the case of the Po Lam 132 kV substation, the measured results are described as follows. Figure 2.14 shows the typical closing and tripping waveforms. The upper ones are the transient waveforms of the main contact and the lower ones are the DC current waveforms of the corresponding actuating coil.

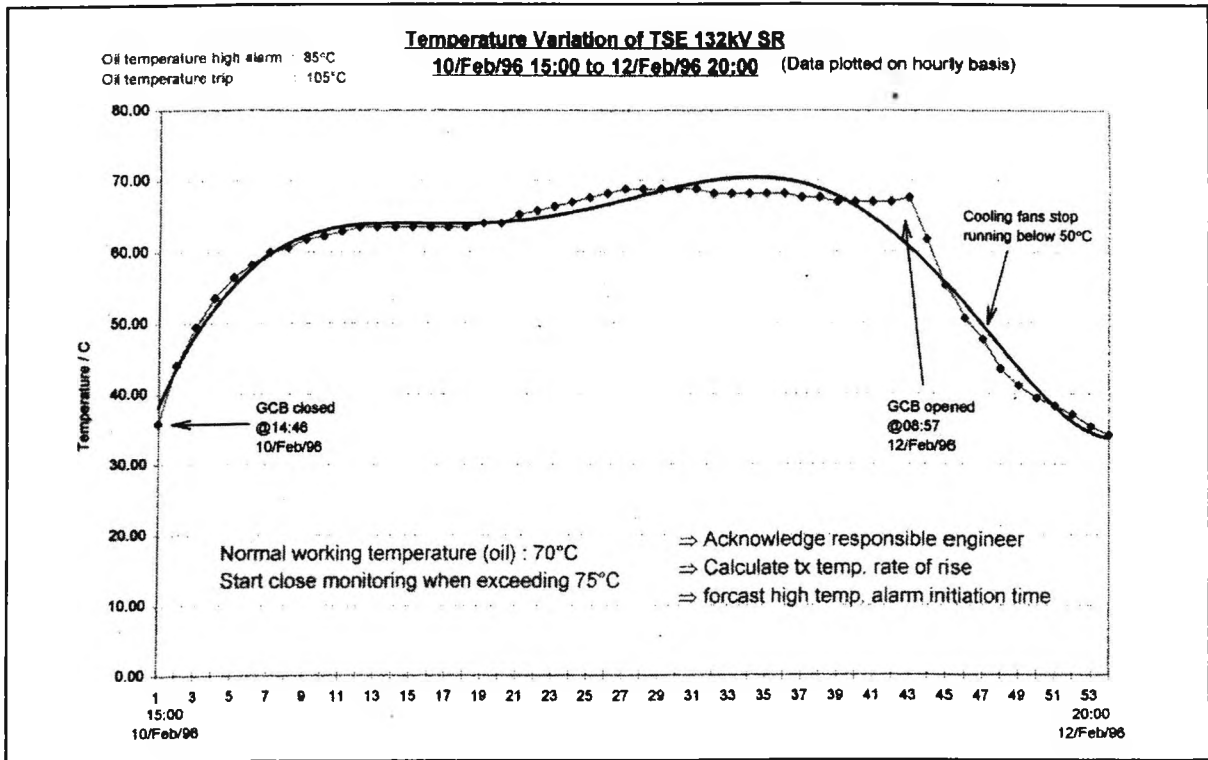


Figure 2.13 Temperature variation of a 132 kV reactor

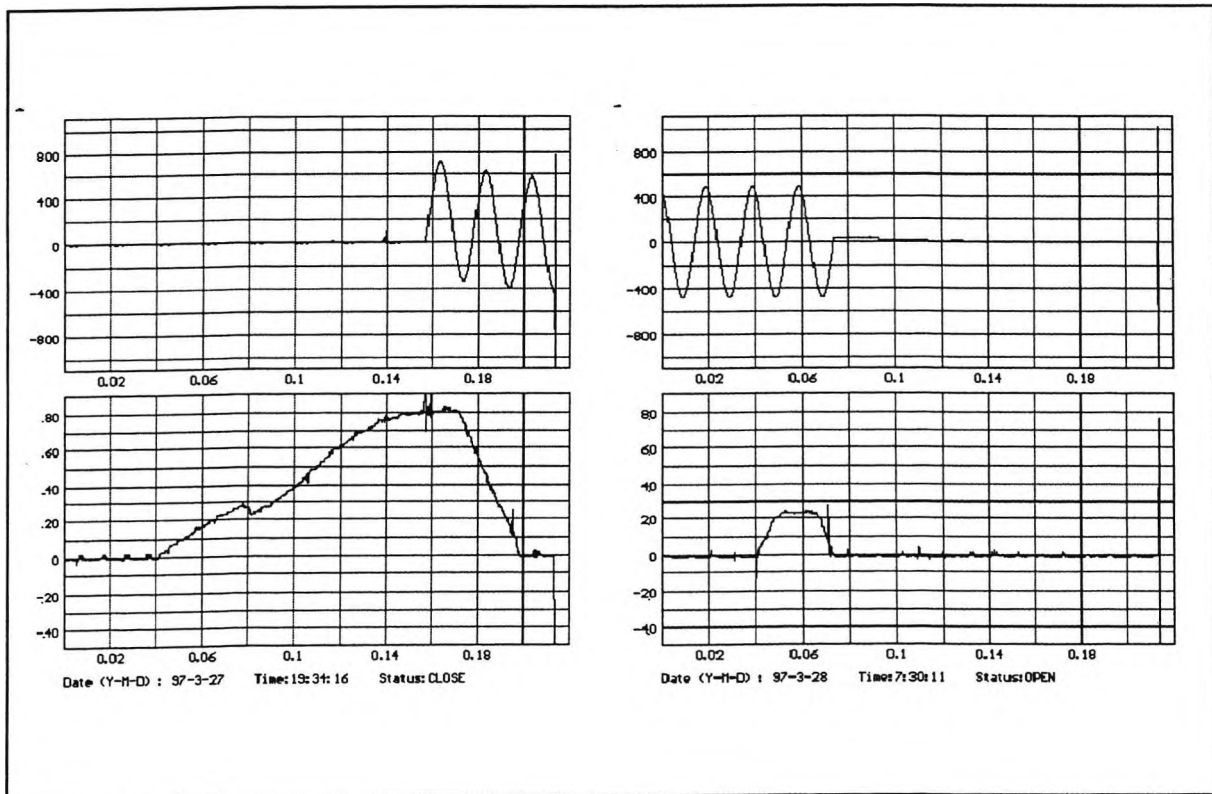


Figure 2.14 Typical circuit breaker waveforms

The circuit breaker switching timing may be determined by the time difference between the point when current is applied to the actuating coil and the point when current begins to flow through the main contact. Figures 2.15 and 2.16 show graphs of closing time and tripping time respectively of typical operations.

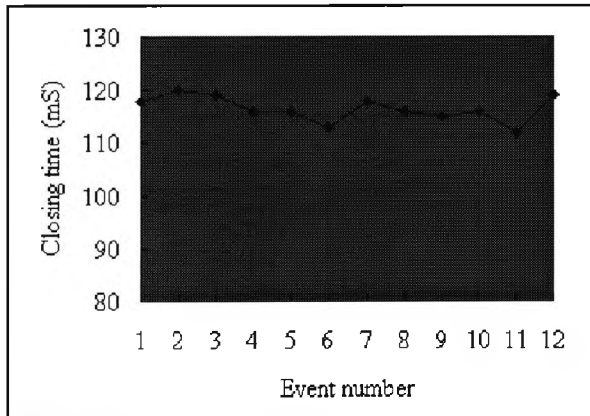


Figure 2.15 CB closing time

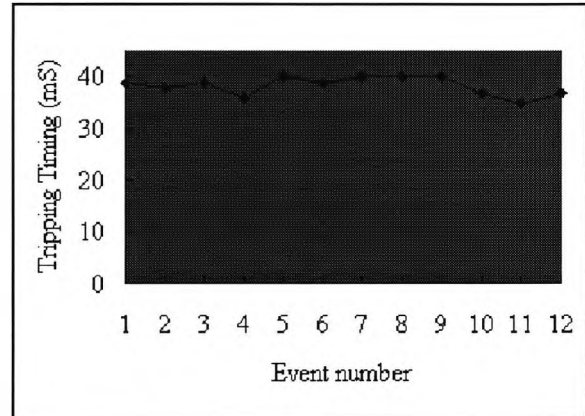


Figure 2.16 CB tripping time

The typical temperature profiles of a reactor are shown in Figure 2.17.

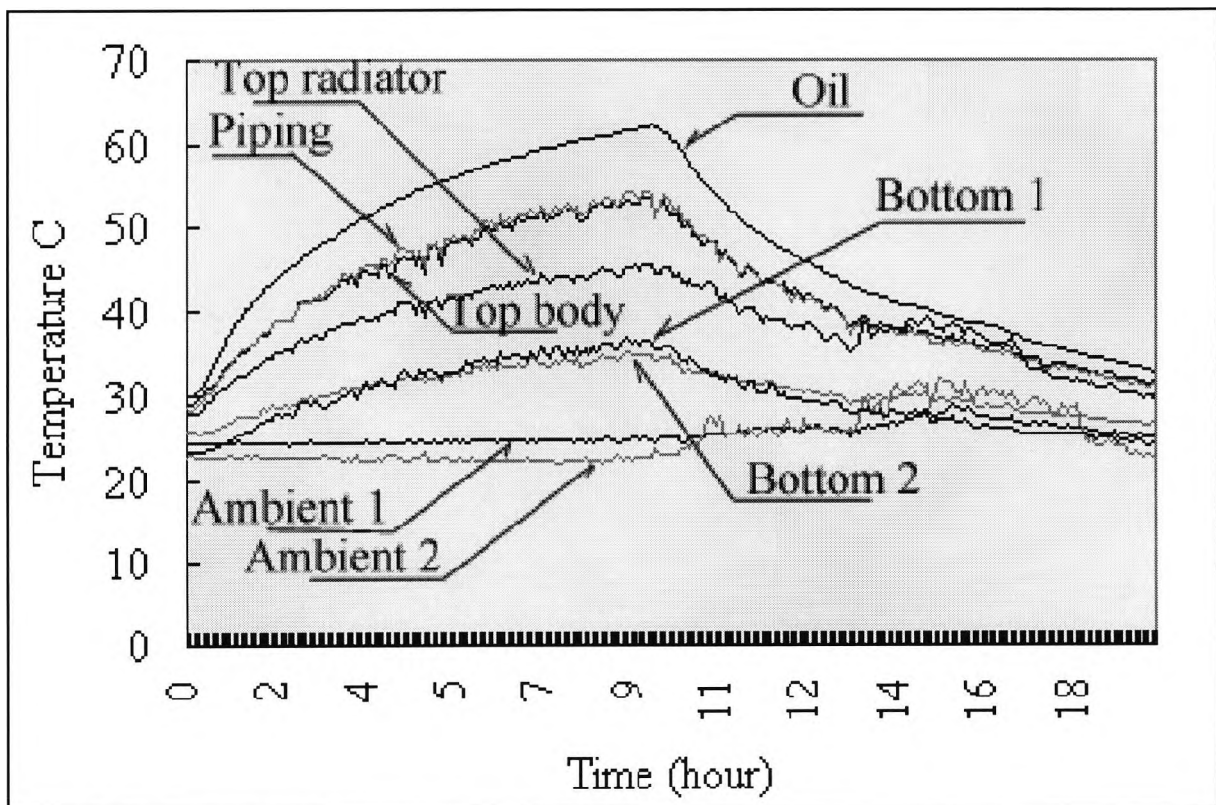


Figure 2.17 Typical temperature profiles of eight sensing points

Figure 2.18 shows the SF<sub>6</sub> gas pressure variation for two weeks.

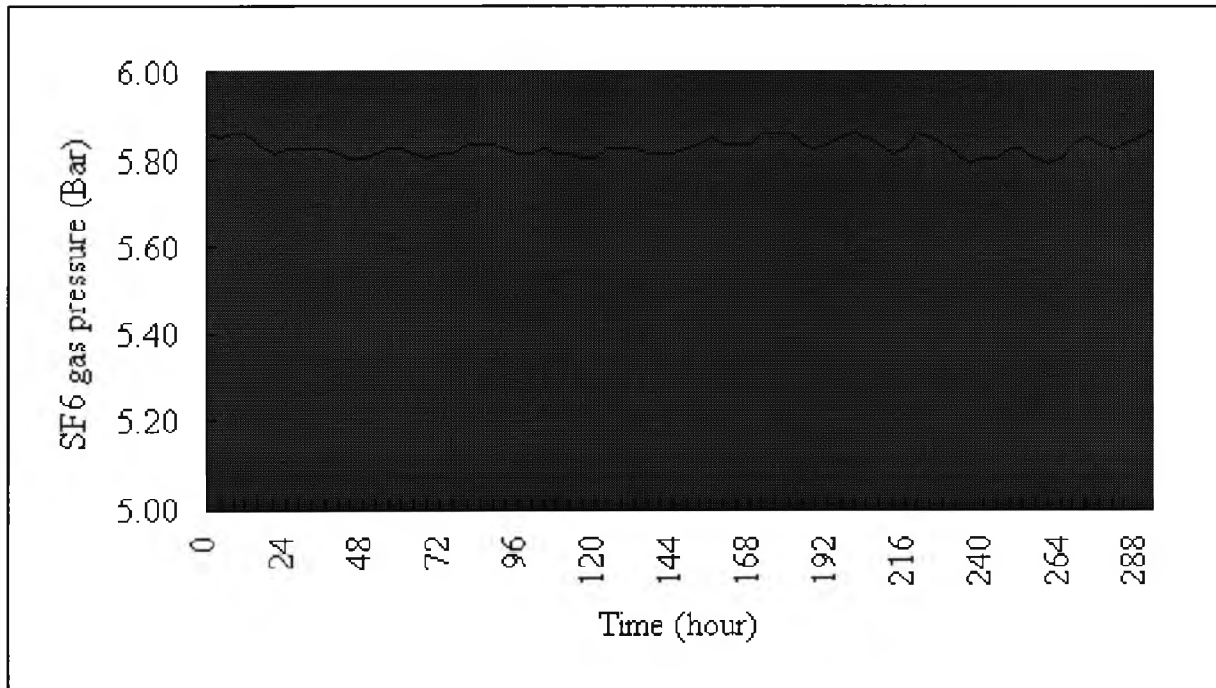


Figure 2.18 SF<sub>6</sub> gas pressure variation for two weeks

A continuous monitoring of the battery voltage can provide information on the breakdown of the charging system. Figure 2.19 shows the voltage variation within a period of two weeks.

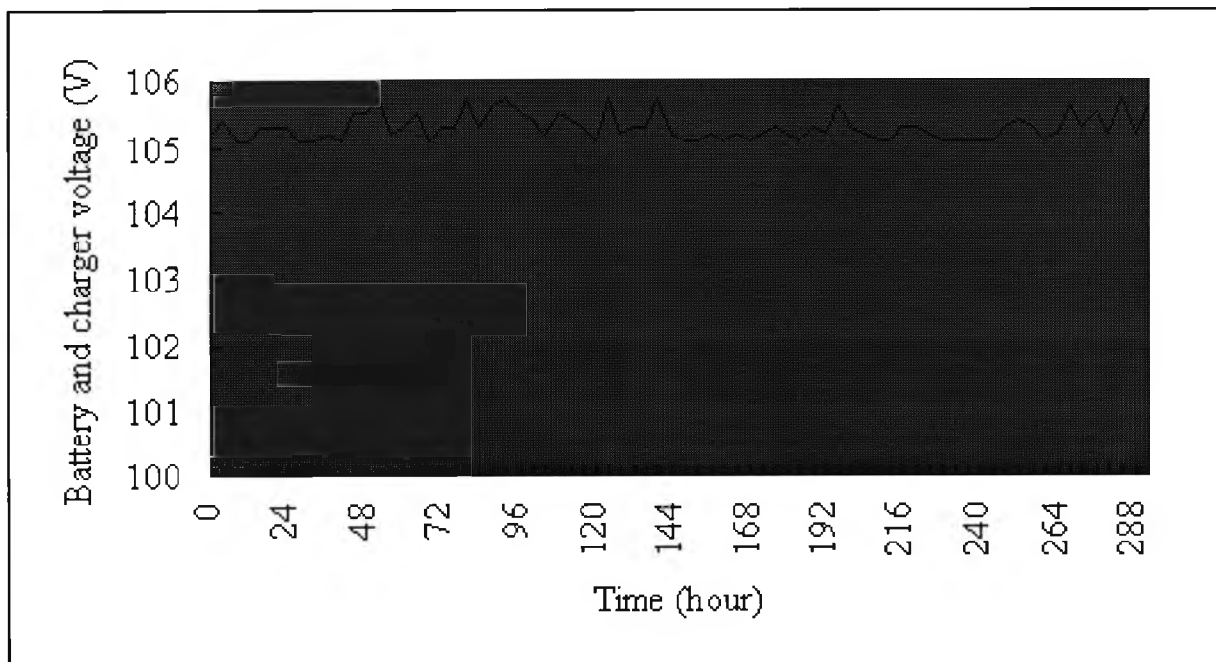


Figure 2.19 Typical battery voltage variation for two weeks

The air compressor operating time (Ton) and idling time (Toff) can be monitored as well, as shown in Figure 2.20.

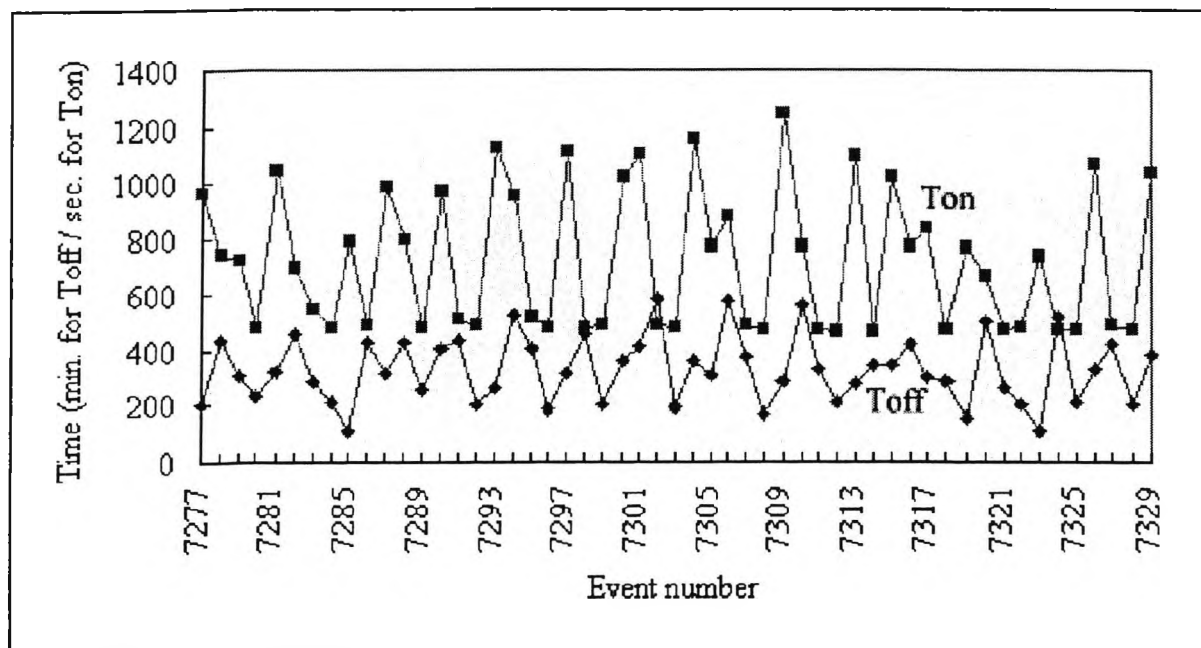


Figure 2.20 Air compressor on/off timing

If Toff time is short, the indication is that the pressure of compressed air can meet the lower limit very quickly. It may be caused by air leakage in the piping system or the storage tank. If Ton is exceptionally long, the indication is that the efficiency of the air compressor becomes poor as it takes a longer period of time to charge up the storage tank.

## 2.7 ADVANTAGES OF THE SYSTEM

An on-line distributed monitoring system has been described in this chapter. It is the basic hardware and software platform for the development of intelligent substations. The advantage of this system is that every microcontroller works independently so that the reliability of the whole system becomes extremely high when the mean time between failure of the whole system is considered. On the other hand, all microcontrollers are interconnected together by a local area network and all data monitored can be transmitted to the on-site microcomputer for secondary storage and statistical processing. This feature further improves the reliability of the system. Even if a microcontroller suddenly fails, the previous data measured by it can

## Chapter II

easily be retrieved from the harddisk of the on-site microcomputer. The processed data can be further transmitted to the remote central microcomputer for alarm generation, trend logging and multi-substation supervision. Although the concept of on-line distributed monitoring is not totally new, existing systems proposed in the western world are usually either very costly or not comprehensive enough. In this chapter, a low cost, effective and reliable design for setting up such a system has been presented and it has been implemented and tested in two major 400 kV substations of CLP Power with very satisfactory results. The system has appreciable track records since it had successfully assisted the maintenance teams many times before to identify potential faults within the 400 kV and 132 kV CBs so that immediate repair works, quite minor technically, could be carried out to prevent the occurrence of major faults. The user-friendly software packages also make this system an economical and efficient tool for predictive and condition based maintenance of these critical components of the high voltage transmission system. The system can easily be extensible to cover all high voltage substations in CLP Power as well. On top of that, it is anticipated this design concept can be employed to all existing high voltage transmission networks around the world where aged and old equipment were erected decades ago. This may be the ultimate and economically affordable solution to all power authorities in the world.

*Chapter III*

**INTERNET BASED SUBSTATION MONITORING SYSTEM**

As the new international airport in Hong Kong was completed, new power substations have to be constructed to meet the huge demand. The capacity of the distributed monitoring system described in Chapter II is considered to be inadequate and therefore, a study was carried out to arrive at a completely new design concept. The schematic block diagram of the newly developed system is shown in Figure 3.1. The design of the system is based on the additional requirements from the power utility. The engineers in charge of the transmission network in CLP, very often, need to know not only the real-time status of power equipment but also the security and fire safety of the substation. Furthermore, in consideration of a more efficient operation of the system in future, the personnel in other organisations, such as Airport Authority, Fire Services Department and other operation and maintenance departments within CLP may need to have access to these important information within the substation simultaneously. Therefore, the original information system needs to be enhanced and extended. In order to tackle fire safety and security requirements, the idea of remote vision for substation monitoring has been employed. Engineers and relevant staff must be able to see on their remote display monitors the real-time scene of the indoor environment of the substation at different office locations or at home when they are standing-by. Intruders and fire outbreak in terms of smoke emission can be detected immediately. In order to allow simultaneous access to information by numerous parties concerned, the old idea of using modem based one-to-one communication has been given up and it is upgraded by the Internet based client server concept.

**3.1 SYSTEM IMPLEMENTATION**

Existing substations are equipped with fire alarm panels that retrieve signals from smoke and heat detectors. Fire alarms are normally available to the CLP System Control Centre only while other relevant organisations are kept informed by the CLP System Control Centre. In

addition, false alarms are frequently encountered, and this is obviously wasting manpower

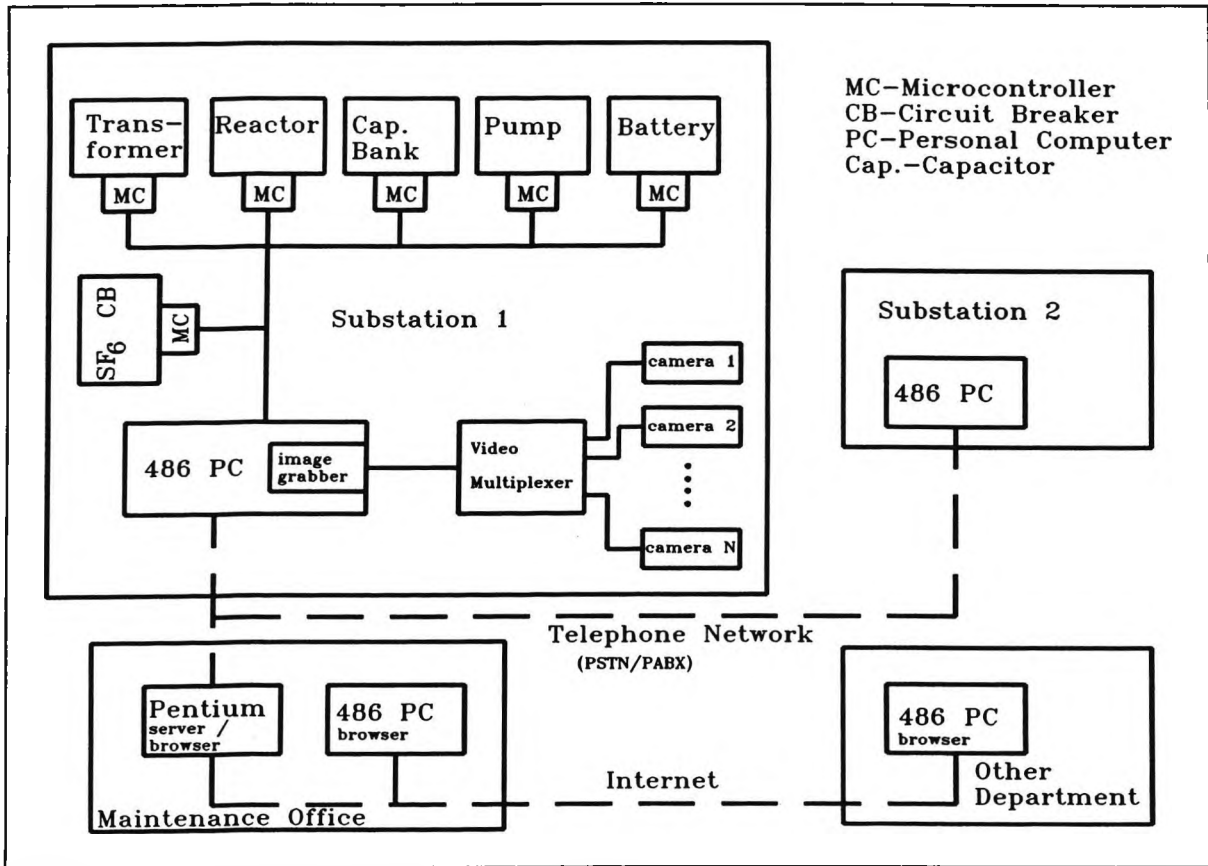


Figure 3.1 The Whole Internet Based Monitoring System

resources as the firemen could only discriminate them when they arrive physically at the remote sites. Also, the substations, though very important on the integrity and normal operation of the whole airport, are normally unmanned. Illegal intruders must be detected and prohibited from entering such substations anytime. To accomplish these aims mentioned above, a remote vision system was newly developed. The system was installed in the Airport 'A' Substation of CLP Power.

Figure 3.4 shows the whole fire panel being monitored by the developed remote vision system. The real-time image of that fire panel captured by one of the cameras is shown in Figure 3.5.



Figure 3.2 The Airport 'A' Substation

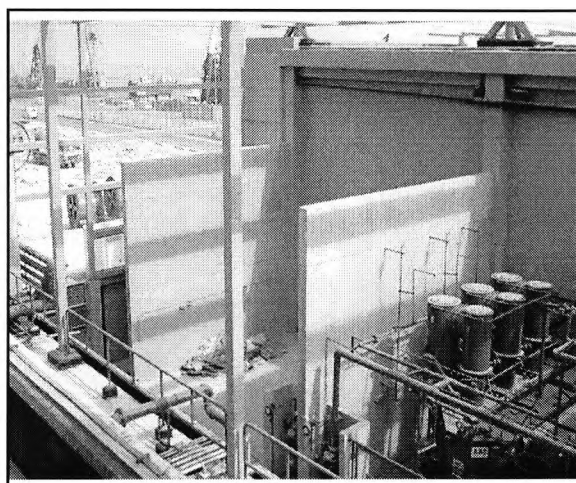


Figure 3.3 Another view of the Airport 'A' Substation

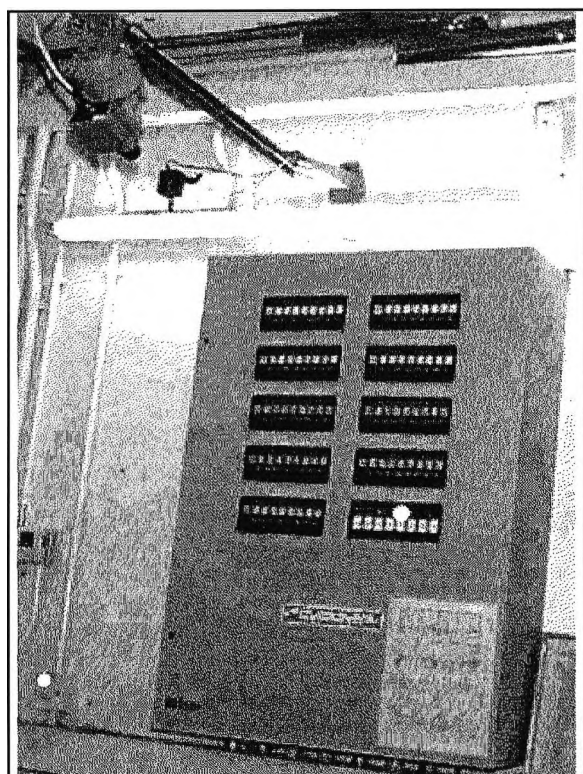


Figure 3.4 The Fire Alarm Panel monitored by Remote Vision System

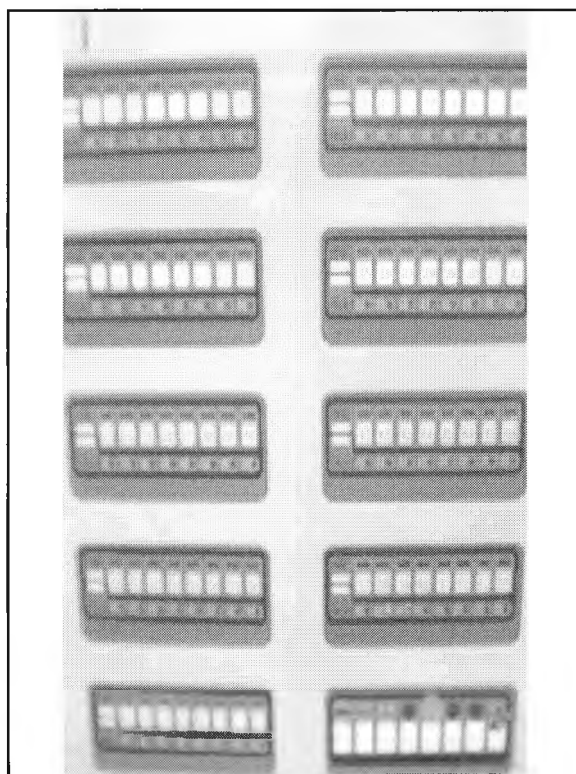


Figure 3.5 An Image of the Fire Alarm Panel

### 3.2 THE REMOTE VISION SYSTEM

Eight off-the-shelf CCTV cameras are installed at different locations in each sub-station. The

reason why eight CCTV cameras have been chosen is that there are either eight or sixteen channels within a standard multiplexer. It will be much more expensive to use a sixteen channel multiplexer as we have found only eight critical points worthy of being monitored inside the sub-station. Figure 3.6 shows the structural schematic diagram of the remote vision system. The aim is to cover all internal areas as much as possible. For example, the eight locations of the Airport Sub-station being monitored are fire panel, control room, 11 kV switchgear room, 132 kV switch gear room, sub-station entrance, 132/11 kV transformer bay, cable basement 1 and cable basement 2 respectively. Each camera is equipped with functions of panning, zooming and tilting.

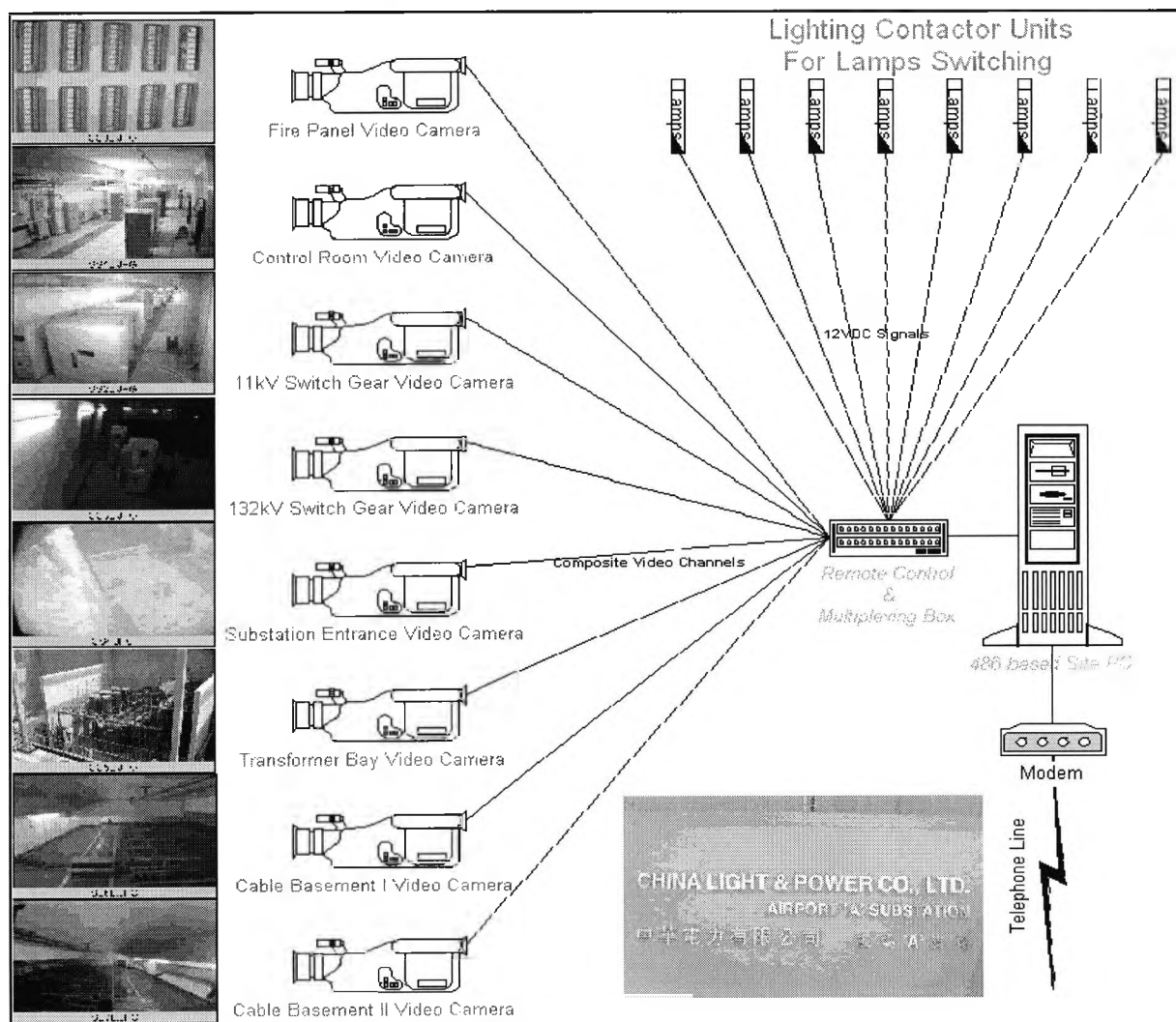


Figure 3.6 The Remote Vision System

The video signal from each camera is wired back to a tailor-made "remote control and

multiplexing box". Such box is controlled by the on-site PC via the printer port. Through this box, the lighting contactors (as shown in Figure 3.8) of the eight locations can be energised and de-energised based on commands from a remote server. This is to ensure adequate illumination level for each camera to grab a satisfactory real-time image of each location. Via this box, the video signal of any one camera can be selected to an image grabber card on a time-multiplexing basis, Video Blaster SE100, on the local 486 DX4-100 PC which is the one that communicates with all micro-controllers in the existing distributed monitoring system. On the other hand, control signals for panning and tilting each camera can be output from the box. Communication between the PC and the CLP Maintenance Centre is accomplished by a 28,800 baud rate fax modem which is being upgraded to 33,600.

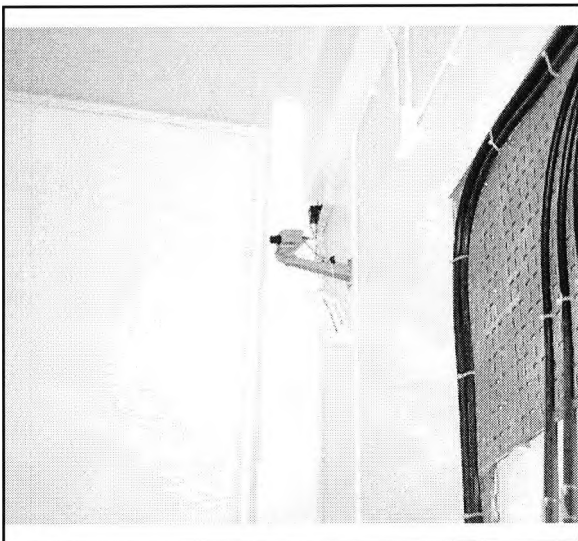


Figure 3.7 Installation of a Video Camera



Figure 3.8 Installation of a Lighting Contactor

### 3.2.1 Illumination Level Detection

On the software side, the on-site PC has two modes of operation, namely the regular mode and the real-time mode. The regular mode is active during normal operation. Images from the eight cameras are sequentially grabbed by the on-site PC at 5 seconds per frame. The effectiveness of computer vision system very much depends on the ambient illumination level. Therefore, images should be grabbed regularly to update the background illumination level for comparison and we have found that a rate of 5 seconds is more than enough. The average grey level of each image can be evaluated by equation (3.1). There are two functions to

### Chapter III

estimate the average grey level of each image. The first function is used as a threshold value for the computer to decide whether the artificial lighting system inside the sub-station should be switched on or off. The switching action is accomplished by each of the eight lighting contactor as shown in Figure 3.8. The second function is to correct the change in overall brightness for image comparison and analysis, which will be discussed later.

Let  $G(x, y)$  be grey level at  $(x, y)$

$$\text{Average grey level} = \frac{\sum_x \sum_y G(x, y)}{\sum_x \sum_y 1} \quad (3.1)$$

The value of the average grey level can be used to assess the overall illumination level of the site and the lighting system of the site can be switched in and out accordingly. For illustrative purposes, Figure 3.9 shows a view of the 11 kV switchgear room before the artificial lighting system is turned on. Figure 3.10 shows the same view after the lighting has been turned on by the on-site computer through the appropriate contactor.



**Figure 3.9** A View of the 11 KV Switchgear Room at Night



**Figure 3.10** The View of the 11 kV Switchgear Room when the Lighting Contactor is Switched on

### 3.2.2 Intruder Detection

The average grey level of this updated image is further compared with that of the previous image, which was grabbed and saved onto the harddisk 40 seconds ago, of the same camera. It is believed that if a human intruder enters the sub-station illegally, he/she will be present for a period longer than 40 seconds. Hence, a comparison between two images taken 40 seconds apart by the same camera is deemed good enough. If there is a significant change in the average grey level, the two images cannot be compared directly and the system will regard it as an error and would wait for another 40 seconds. Otherwise, the updated image is subtracted by the previous image so that any significant change in the scene can be identified. The mechanism of subtraction is shown in Equation (3.2).

$$\xi(x, y) = |G_{t-40}(x, y) - G_t(x, y)|$$

$$\Xi = \sum_x \sum_y u(\xi(x, y) - D_{TH}) \quad (3.2)$$

$$\text{where } \begin{cases} u(t) \text{ is unit step function} \\ D_{TH} \text{ is difference threshold} \end{cases}$$

If  $\Xi$  is greater than a preset value, 600 in our case, the change is considered significant and the on-site PC will firstly save the two relevant images onto the harddisk for later reference and then inform the maintenance centre by producing an alarm at the server. On top of

## Chapter III

analysing the images, the on-site PC saves the real-time images onto the harddisk at a rate of two sets per hour. Regarding the real-time mode, the communication between the maintenance centre and the on-site has to be active, and image files can be continuously transmitted through the telephone circuitry at a baud rate of 28,800. Here, there are two levels of operation being selected by the server, namely the coarse level and the fine level. Under the coarse level, images of size 320 pixels x 200 pixels are transmitted, resulting in a transmission cycle of only 48 seconds for the eight images from eight respective cameras. If the user finds anything unusual, the fine level can be switched in, resulting in a transmission rate of around 35 seconds for each image of size 640 x 400. The user is able to fix any camera "on-line" and pan/tilt/zoom that particular camera. The compression algorithm for these images is "standard JPEG format" with a quality factor set at 15% so that the file size of coarse level images is around 5 kB while that of fine level images is around 30 kB. There are two factors that govern the transmission rate, namely the quality factor and the speed of the modem. 15% for the quality factor is the optimal value based on our experimental trial and thus there is only a limited room for improvement. If an ISDN link is provided from the server to the airport sub-station, the transmission rate will at least be improved by 30 times.

### 3.2.3 Fire Alarm Zone Detection

There are a number of fire detection zones in the substation. The occurrence of fire is indicated by a number of lamps on the alarm panel. The positions of the indicating lamps represent different kinds and zones of fire occurrence. The detection alarm type and fire zone can be done automatically by the site computer. This is a very useful feature since it is too expensive to wire all the fire alarm signals back to the control centre. However, some of the non-critical alarm signals can be useful for fault detection. The detection process is very straightforward. Figure 3.11 is an image of the fire alarm panel when two alarms occurred. By subtracting the illumination level corrected image with the template image captured during the installation of the system, it is possible to generate the image as shown in Figure 3.12. The centre of the two patches is determined by the computer as (250, 233) and (119, 443). With a coordinate table which is prepared during the system installation, the

two alarm type and zone can be easily worked out.

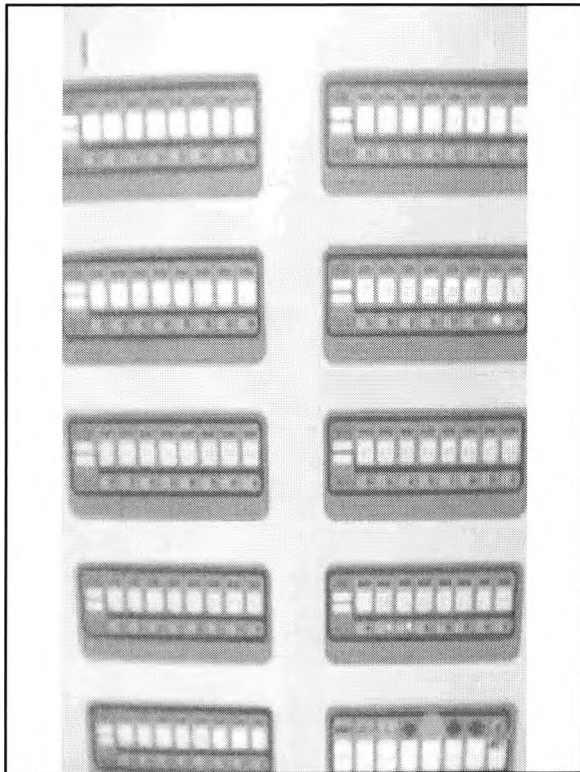


**Figure 3.11** The Image of the Fire Alarm Panel when Alarms are Occurred

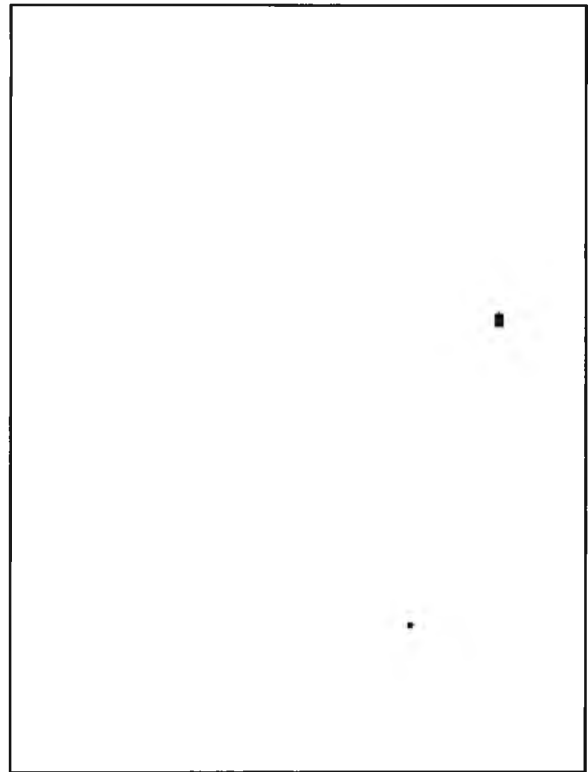


**Figure 3.12** The Threshold of the Subtracted Images

### 3.2.4 Substation Meter Reading [34]

Large number of signals that reflect the instantaneous substation conditions are wired back to the central control room and presented to the operators as chart recorders or different kinds of meters. For old installations, the duty staff is required to visit individual substation and takes down the instantaneous readings of each meter. General instrumentation measurable parameters such as temperature, current, voltage and pressure etc. are displayed inside the substation. From the readings, useful information, including trend-logging, high/low alarms and daily/monthly fluctuations etc. can be evaluated. It will be very cost effective with immediate response if we are able to upgrade the existing mode of human attendance to automatic recording. One way is to change all the old analog meters into digital devices and convey the signals back to the control room by LANs or hard wire. This would however be a very expensive project. An economical solution is to use computer vision or "image

understanding" so that the work of human duty staff will be transferred to the camera-computer system.

The system is based on two simple assumptions which could be easily justified in any substation room which is normally a controlled environment, since the position of each meter is fixed, whose coordinates are well calibrated, and the lux level of the environment does not change significantly. Moreover, all the analog meters and chart recorders make use of pointers or luminous bars to indicate the real-time value of the signal. Hence, it is good enough to get the general picture of the measured parameter by locating the instantaneous position of the pointer or bar. An off-the-shelf CCD camera, location should be fixed, is installed in the substation, such that the camera will be facing the control panel or switchboard being monitored and the output of the camera is fed to an image grabber of the on-site computer. This camera should possess functions of panning, tilting and zooming which are controllable by the computer. The aiming angle of each meter is stored inside the memory and the computer can accurately direct the camera to grab an image of each meter consequently. The gain and offset of the amplifier of the image grabber are adaptively adjusted to maintain a steady average illumination level for each picture.

During initialisation, the image of a meter with zero reading is retrieved. Another image of the same meter captured by the same camera at the same location under the same illumination will be grabbed. As shown in Figure 3.13, a "maximum" operation is carried out between the two images, resulting in an image of the meter without the pointer or the bar. This image is treated as a reference and stored inside the memory of the computer. During normal operation, a real-time image of the meter is grabbed and an "image subtraction" algorithm is then executed to compare this real-time image and the reference image stored in the computer memory. The operation is shown in Figure 3.14. Hence, a pointer is then highlighted as shown in Figure 3.15. "Hough Transform" is then carried out to locate the most probable position of the pointer and those noisy points can be eliminated. A "robust line fit" algorithm is employed to identify the optimal position and orientation of the pointer. Once the orientation is known, the real-time reading can be obtained by referring to the table within the database kept in the memory of the computer. The time-stamped value is then

stored for trend logging and statistical analysis. The flowchart of the method is shown in Figure 3.16.

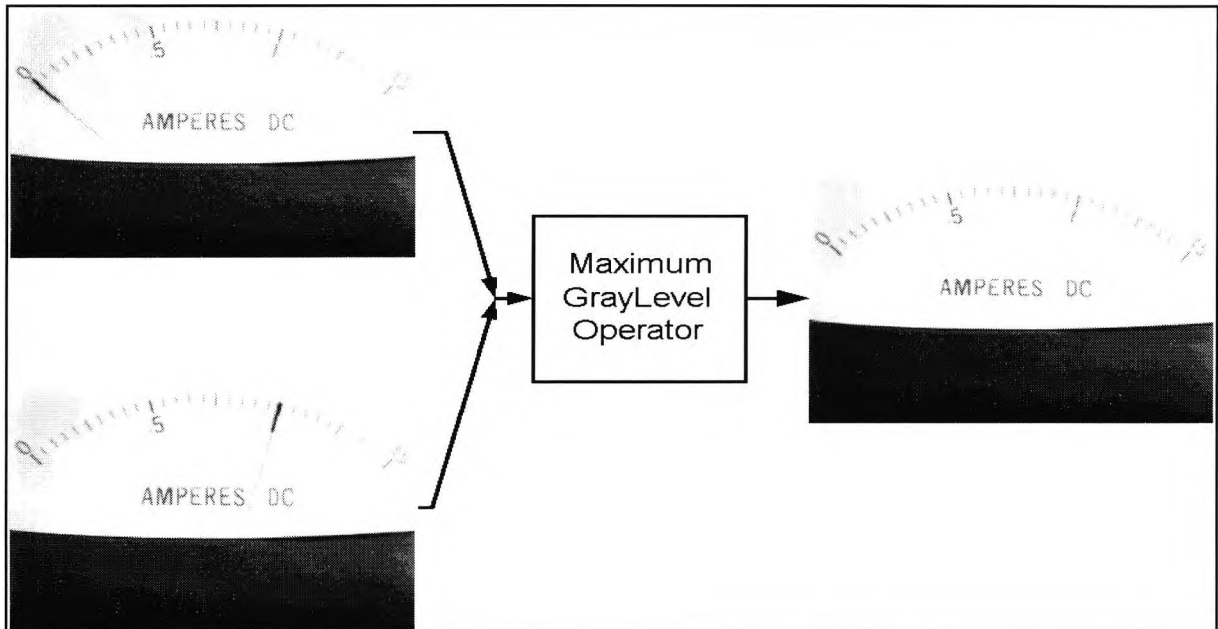


Figure 3.13 An illustration of the "maximum" operation

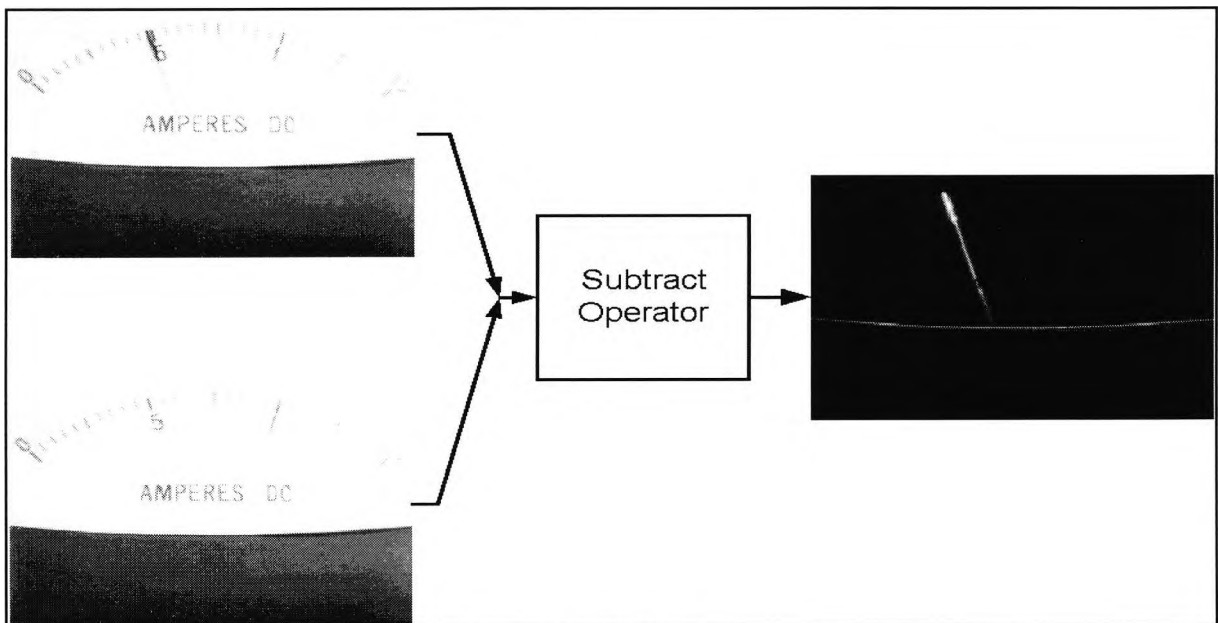


Figure 3.14 An illustration of the Subtraction Operator

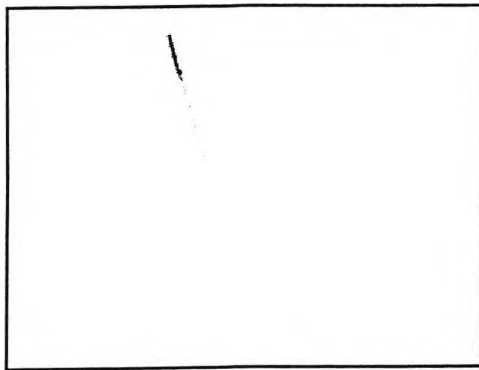


Figure 3.15 The Extracted Meter Pointer

For Hough Transform, a straight line can always be written as:

$$x \cos \theta + y \sin \theta = r$$

where  $\theta$  is the angle that a normal to line makes with the x-axis and  $r$  is the length of this normal. Any point,  $(x_i,$

$y_i)$  on this line must satisfy the straight line equation while the equation can be interpreted as a sinusoidal curve in the  $(r, \theta)$  space. If a number of points are collinear in the  $(x, y)$  space, their Hough transform curves must intersect in the same point in the  $(r, \theta)$  space. Each point  $(x_i, y_i)$  will contribute a count to the cells given by the equation and the cells with high counts will give the desired lines. The value  $\theta$  gives an approximate position of the meter pointer. To refine the meter reading, the optimal line that represents the point can be obtained by means of robust fit of the useful pixels. The line fitting is based on minimisation of the squared deviation of all useful pixels from the optimal line which has the equation "y = a + bx".

$$a = \frac{\sum (y_i - b x_i)}{\sum 1} ; 0 = \sum x_i (y_i - a - b x_i)$$

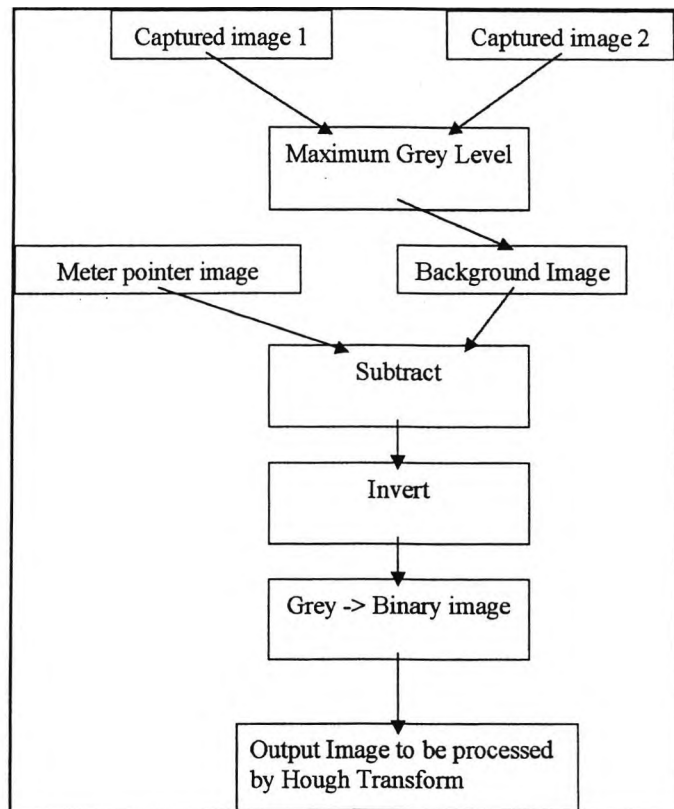


Figure 3.16 The Flowchart of the Method

### 3.2.5 Other Useful Features

The remote vision system requires no spare contact nor additional transducer. It can be used to prevent theft as well. General inspection of the sub-station can be carried out, such as checking cleanliness and the work quality of maintenance work. The alarm indicators on the fire panels can be grabbed as images so that the user at the central operation and maintenance office can confirm whether the alarms are false or genuine by selecting the relevant camera to see the existence of smoke or fire in the activated zone. Further to these functions, the remote vision system can be used to monitor external contractors working on site. No manning by the CLP staff in the sub-station is deemed necessary. Equipment in hazardous areas or areas without adequate clearance, such as confined space or equipment room with live conductors, can be monitored by this system. During major overhaul or fault handling, the maintenance manager is able to visualise the equipment status through the display monitor to give direct instructions to the site engineers so that site problems encountered can be efficiently solved with the joint co-operation between site staff and central management staff.

### 3.3 INTEGRATION WITH INTERNET

In order to accomplish the goal of sharing information related to the integrity of the electric power system with other utilities and organisations who are responsible for the smooth operation of the new international airport of Hong Kong, communication by Internet was employed in our system to be described. A homepage was developed, which can serve, in principle, a large number of approved users at the same time. In this way, there is no need for standby staff to return to office to gain access to the plant status outside office hours as communication is ready anywhere and anytime. Using Internet will be very helpful when the plant is under emergency situation because all parties concerned are eager to look at the plant data simultaneously. This feature was impossible in the old system using modems. By doing so, time for trouble shooting can be shortened and thus the time for system restoration to normal can be shortened as well. Before the details of implementation is described, the state-of-art of Internet technology is introduced. The Internet is becoming an integral part of life and a comprehensive review can be found in various documents [35-38]. In fact, an Internet

## Chapter III

based building automation system [39,40] was developed and the idea of global campusless university by an Internet based degree course [41] was also explored. With all these advantages, it is extremely fruitful for us to put the distributed on-line monitoring system onto the Internet.

A Pentium 166 based PC equipped with LAN service connected to Internet has been installed to be the Internet server as shown in Figure 3.1 by executing the program entitled "Windows httpd V1.4c Worldwide Web Server". This system will soon be upgraded to "Linux OS" which is more reliable and can support more flexible communication modes. Figure 3.17 and Figure 3.18 show the typical homepages. The server periodically "polls" each on-site PC by modems. Site information, including images and plant parameters, is collected and saved onto the harddisk of the server. Plant parameters include most updated plant status with respect to SF<sub>6</sub> switchgears, power transformers, capacitor banks, batteries and signals from the building systems such as air-conditioning, fire alarms and lighting systems. Unlimited number of ordinary users can retrieve site information from any sites without restriction while authorised users are able to instruct the server to connect itself to a particular sub-station and retrieve real-time images and plant status on an ad-hoc basis. Hence, passwords are categorised into two levels for ordinary and authorised users respectively. Figure 3.19 shows the password page of the homepage. As an example, the program for automatic image updating of each polled sub-station is attached herewith for illustrative purpose. The program is in form of a "HTML 3.0" text file, which is easily executable under an environment of Netscape, Internet Explorer and Mosaic. This program is automatically executed every 35 seconds to upload images.

```
<HTML>
<HEAD>
<TITLE>Fire Protection Panel, New Airport 'A'</TITLE>
<META HTTP-EQUIV="REFRESH" CONTENT="35">
</HEAD>
<BODY>
<CENTER>
<A HREF="nod.htm"> <H3>Substation On-Line Monitoring System</H3> </A>
```

```

<P>
<A HREF="airport/airport.htm"> <H3>New Airport 'A' 132 kV
Substation</H3> </A>
<P>
<A HREF="airport/rvis.htm"> <H3>Remote Vision</H3> </A>
<P>
<H3>Fire Protection Panel</H3>
<IMG SRC="cgi-win/update.exe?a2">
</CENTER>
</BODY>
</HTML>

```



Figure 3.17 Front Page of the Monitoring Homepage

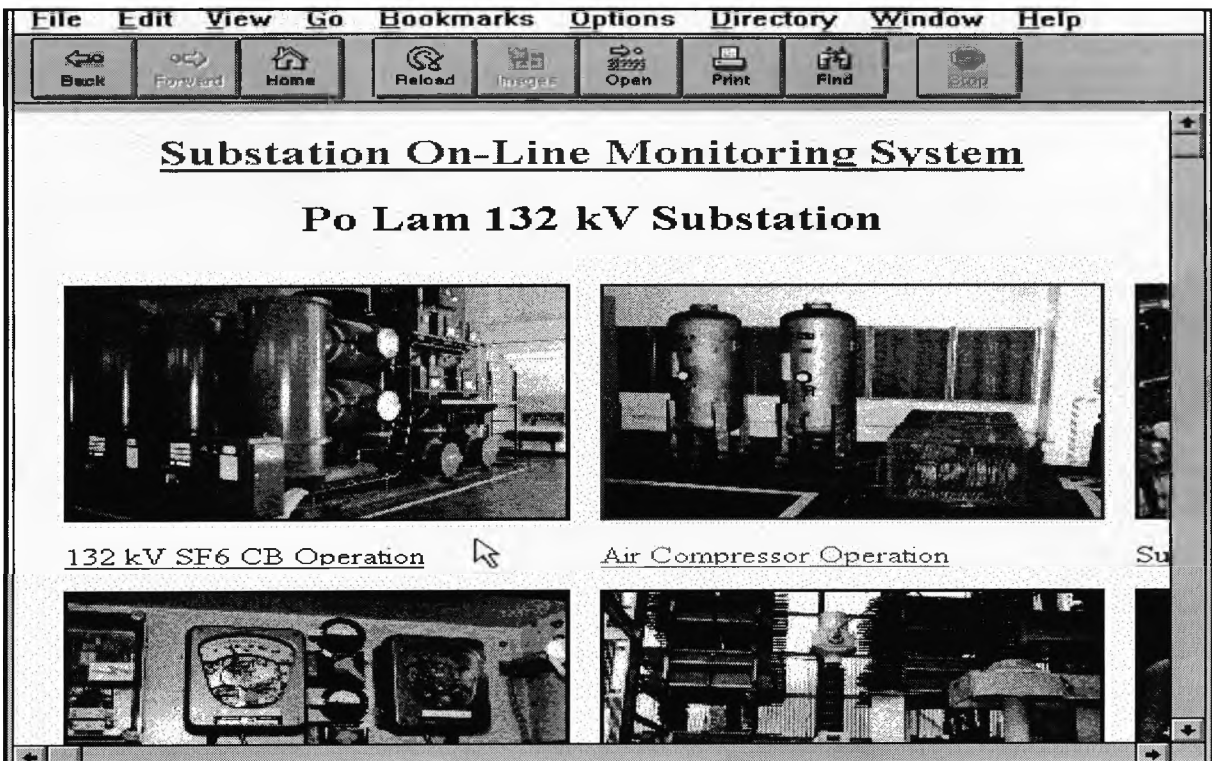


Figure 3.18 Monitoring Homepage for Po Lam Transmission Sub-station

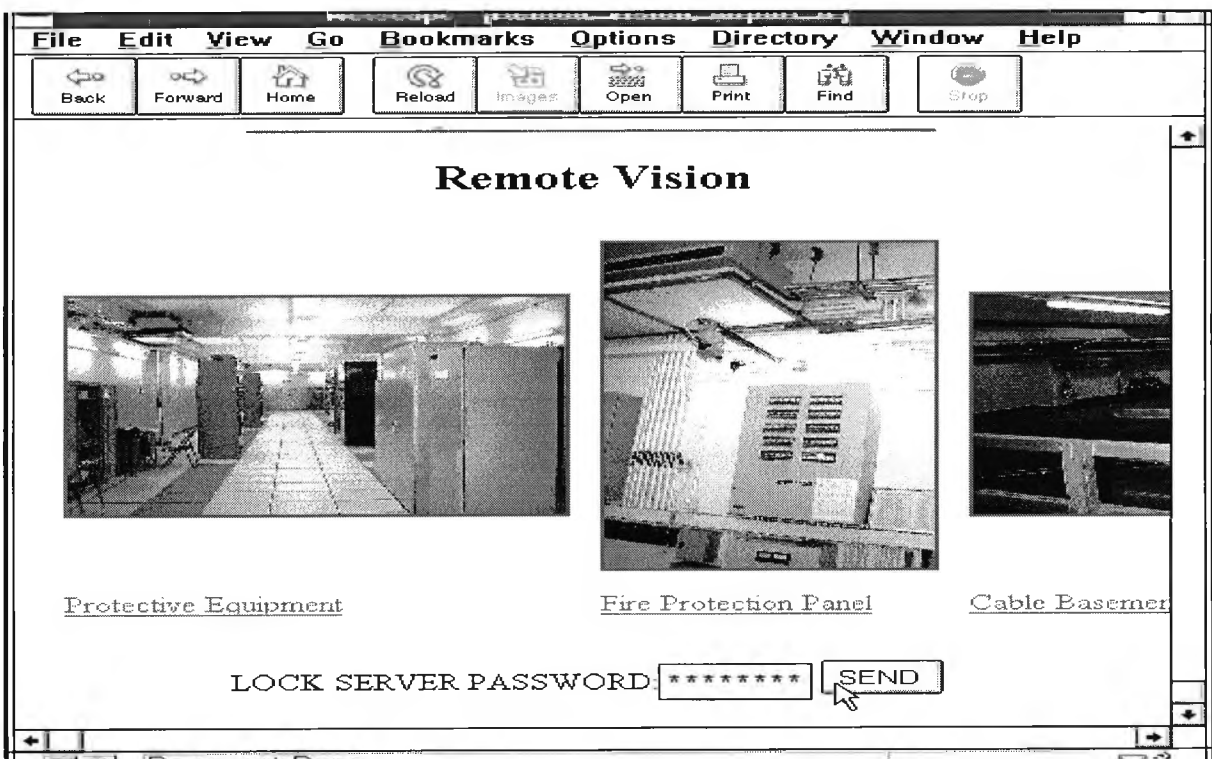


Figure 3.19 Layout of Authorised User's Page

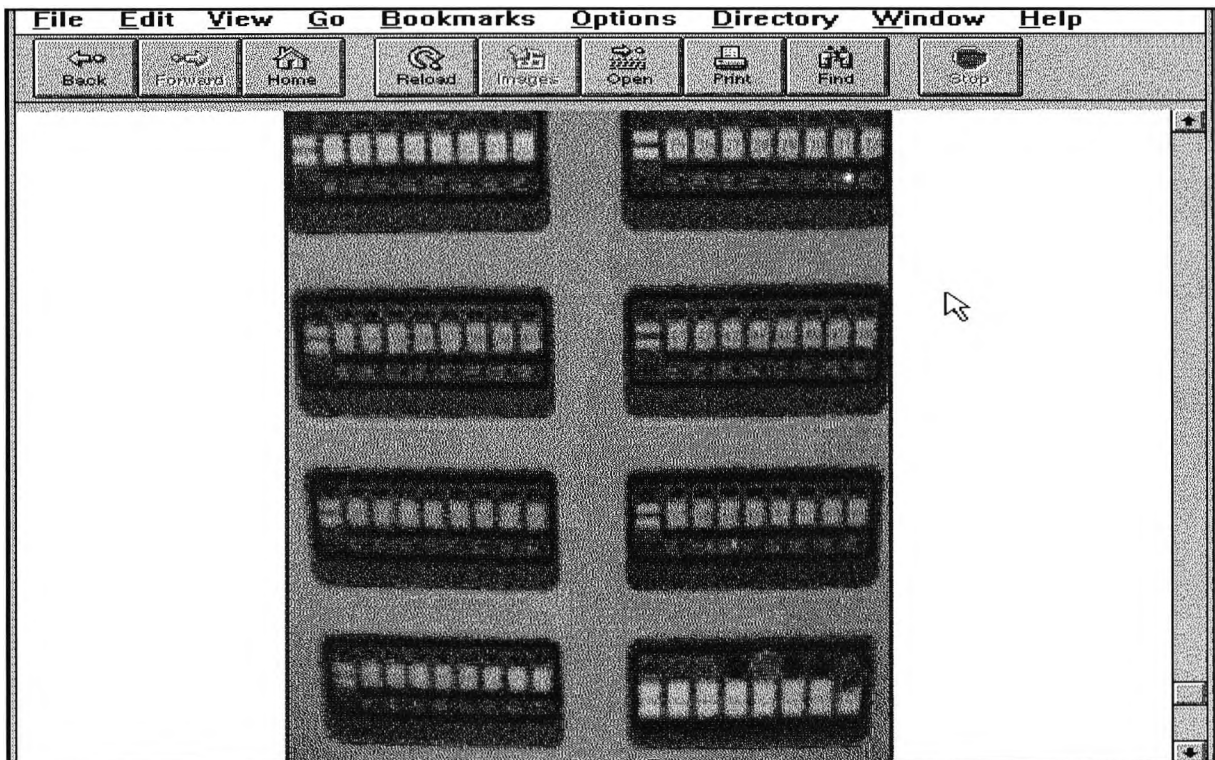


Figure 3.20 Image of Fire Alarm Panel on Homepage

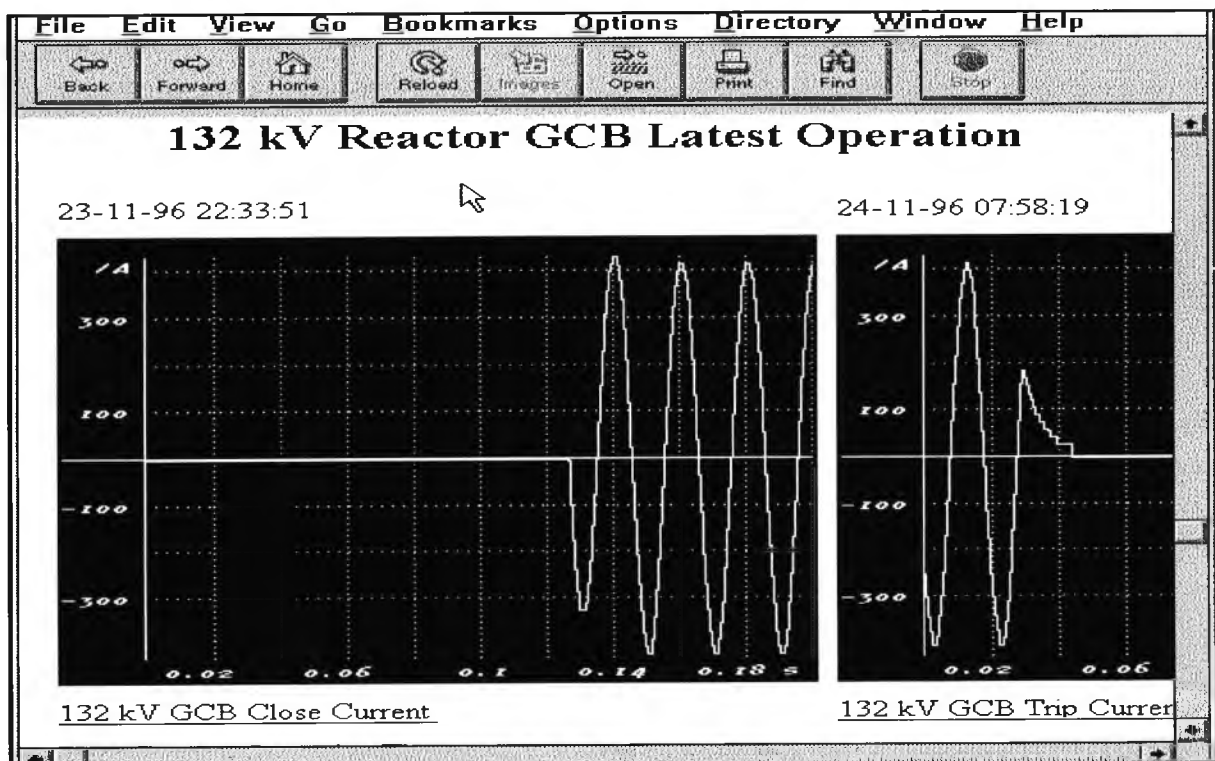


Figure 3.21 Homepage showing Current Waveforms of Latest 132 kV SF<sub>6</sub> GCB Operation

### Chapter III

Figure 3.20 is the page for displaying the real-time image of the fire alarm panel. Besides images and digital plant parameters, the homepage offers other features, such as the analog signals that record current waveforms at the SF<sub>6</sub> Gas Circuit Breakers, as shown in Figure 3.21.

Subject to the additional requirements at newly constructed power substations for the new international airport of Hong Kong, two new features have been incorporated into the existing system. Such requirements are mainly due to the isolated environment and the large number of parties responsible for operating the airport. Remote vision is included so that users are able to see the scenes of different important locations within the sub-stations on a real-time manner. The employment of Internet technology to produce a world-wide homepage allows simultaneous multiple access from all parties concerned. This feature is particularly helpful under emergency conditions.

*Chapter IV*

**FUZZY LOGIC APPLICATIONS IN SUBSTATIONS**

As discussed in Chapter I, fuzzy theory is one of the building blocks of modern intelligent systems. In fact, fuzzy logic techniques are very useful for substation applications and such applications are very important for the intelligent substations implementation. In this chapter, two fuzzy logic applications in power substations are reported. The first is the application of fuzzy controller for the switching of 11 kV capacitor banks in power substations. This chapter describes the design and algorithms of a new fuzzy controller for reactive power compensation and power factor control. The controller is universal for any type of actuation scheme and is not limited to discrete capacitor banks. It can also be used for low voltage building services application as well. The performance of the controller is good and it is extremely robust. It is also highlighted in this chapter that besides the conventional way of using power factor as the control variable, reactive power is also a necessity. In addition to the control application, the other application is the harmonic load recognition using fuzzy equations. Equations involving fuzzy numbers are unavoidable in the real world and in fact, they appear frequently in different disciplines of engineering. A new method of power harmonics pattern recognition based on solving equations with fuzzy numbers is presented. There are two reasons of introducing fuzzy numbers in this application, one being the slight variation of harmonics spectrum of the customer loads due to the variation of power consumption and another being the intrinsic errors built in any measuring equipment. Before the discussion of the applications, a brief introduction of fuzzy theory is presented first.

**4.1 FUZZY SETS AND PROPERTIES**

The conventional quantitative techniques of system analysis are unsuitable for dealing with humanistic systems and other comparable complex systems, because, as the complexity increases, the ability to make precise and yet significant statements diminishes until a

## Chapter IV

threshold is reached beyond which precision and significant relevance become almost mutually exclusive characteristics. This, in accordance with Zadeh [42], is known as the 'principle of incompatibility'. It is in this sense that precise quantitative analyses of the behaviour of humanistic systems are not likely to have much relevance to the real world where societal, political, economic and other types of problems are generated in natural and social sciences. Fuzzy approach is based on the premise that the key elements in human thinking are not just numbers but can be approximated to tables of fuzzy sets, or, in other words, classes of objects in which the transition from membership to nonmembership is gradual rather than abrupt. By relying on the use of fuzzy linguistic variables, and fuzzy algorithms, this new approach provides an approximate and yet effective and more flexible means of describing the behaviour of systems which are too complex or too ill-defined for a precise mathematical analysis by classical methods and tools.

A fuzzy set (A) in a space of points  $X = \{x\}$  is a class of events with a continuum of grades of membership and is characterised by a membership function  $\mu_A(x)$  which associates with each point in X a real number in the interval [0, 1] with the value  $\mu_A(x)$  at x representing the grade of membership of x in A. Formally, a fuzzy set A with its finite number of supports  $x_1, x_2, \dots, x_n$  is defined as a collection of ordered pairs:

$$A = \{ (\mu_A(x_i), x_i), i=1,2, \dots, n \}$$

where the support of A is

$$S(A) = \{ x, x \in X \text{ and } \mu_A(x) > 0 \}$$

$\mu_i$ , the grade of membership of  $x_i$  in A, denotes the degree to which an event  $x_i$  may be a member of A or belongs to A. When X is finite, the fuzzy subset A can be denoted by:

$$A = \sum_{x_i \in X} \mu_i/x_i, \quad i = 1, 2, \dots, n$$

When X is infinite, the fuzzy subset A can be denoted by:

$$A = \int_X \mu_A(x)/X$$

## Chapter IV

There are some basic operations related to fuzzy subsets A and B of X having membership values  $\mu_A(x)$  and  $\mu_B(x)$ ,  $x \in X$  respectively.

(a) A is equal to B ( $A=B$ ) implies

$$\mu_A(x) = \mu_B(x), \quad \forall x \in X$$

(b) A is a complement of B ( $A=B'$ ) implies

$$\mu_A(x) = 1 - \mu_B(x), \quad \forall x \in X$$

(c) A is contained in B ( $A \subseteq B$ ) implies

$$\mu_A(x) \leq \mu_B(x), \quad \forall x \in X$$

(d) The union of A and B ( $A \cup B$ ) is given by

$$\mu_{A \cup B}(x) = \bigvee (\mu_A(x), \mu_B(x)), \quad \forall x \in X$$

where  $\bigvee$  denotes maximum

(e) The intersection of A and B ( $A \cap B$ ) is given by

$$\mu_{A \cap B}(x) = \bigwedge (\mu_A(x), \mu_B(x)), \quad \forall x \in X$$

where  $\bigwedge$  denotes minimum or product

Consider a universe of three girls,  $X = \{\text{Mary, Jean, May}\}$ , the fuzzy set 'pretty' may be defined as  $P = 0.8/\text{Mary} + 0.3/\text{Jean} + 0.7/\text{May}$ , while the fuzzy set 'rich' may be defined as  $R = 0.5/\text{Mary} + 0.8/\text{Jean} + 0.4/\text{May}$ . The fuzzy set 'pretty and rich' can be obtained from these two sets. That is,

$$P \text{ AND } R = 0.5/\text{Mary} + 0.3/\text{Jean} + 0.4/\text{May}$$

The operations listed above satisfy many classical properties of crisp set operations, i.e. commutativity, associativity, distributivity, identity, absorption, De Morgan's laws, involution, equivalence and symmetrical difference etc.

## 4.2 FUZZY EXPERT SYSTEMS

A popular class of expert systems uses if-then rules to represent knowledge. Such systems are known as rule-based systems. The basic fuzzy expert system operates in three stages: converting input variable values to fuzzy set values (fuzzification), rule instantiation and converting from fuzzy set values back to crisp output values (defuzzification). A fuzzy if-then rule assumes the form:

**IF**            x is A  
**THEN**        y is B

where A and B are linguistic values defined by fuzzy sets on universes of discourse U and V, respectively. 'x is A' is called the antecedent, while 'y is B' is called the consequence. A fuzzy if-then rule can be defined as a binary fuzzy relation R on  $U \times V$ .

$$R = A \rightarrow B = \int_{U \times V} T(\mu_A(x), \mu_B(y)) / (x, y)$$

Regarding fuzzification of inputs, each fuzzy system is associated with a set of inputs which can be described by linguistic terms like high, medium and small called fuzzy sets. Fuzzification is the process of determining a value to represent an input's degree of membership in each of its fuzzy sets. In order to express relationships between imprecise concepts and model the system's behaviour, a fuzzy system designer develops a set of fuzzy if-then rules in consultation with the domain expert. Fuzzy reasoning (approximate reasoning) is an inference procedure that derives conclusions from a set of fuzzy if-then rules. Let A, A', and B be fuzzy sets of U, U, and V, respectively. If the fuzzy implication  $A \rightarrow B$  is expressed as a fuzzy relation R on  $U \times V$ , the set B' ( $B' = A' \circ (A \rightarrow B)$ ) induced is defined by

$$\mu_{B'}(y) = \max_x \min\{\mu_{A'}(x), \mu_R(x, y)\}$$

The fuzzy inference system is a computing framework based on the concept of fuzzy set theory. The system is known by numerous names, like fuzzy-rule-based system, fuzzy expert system, fuzzy model, fuzzy associate memory and fuzzy logic controller. The basic structure

of a fuzzy inference system consists of three conceptual components: a rule base (if-then statement); a database (membership functions) and a reasoning mechanism. With crisp inputs and outputs, a fuzzy inference system implements a nonlinear mapping from its input space to output space. The mapping is accomplished by a number of fuzzy if-then rules, each of which describes the local behaviour of the mapping. In the case of Mamdani model, defuzzification refers to the way a crisp value is extracted from a fuzzy set as a representative value. The most widely adopted strategy is the centre of mass method:

$$z = \frac{\int_U x\mu_F(x)dx}{\int_U \mu_F(x)dx}$$

An example of defuzzification in Mamdani model is shown in Figure 4.1.

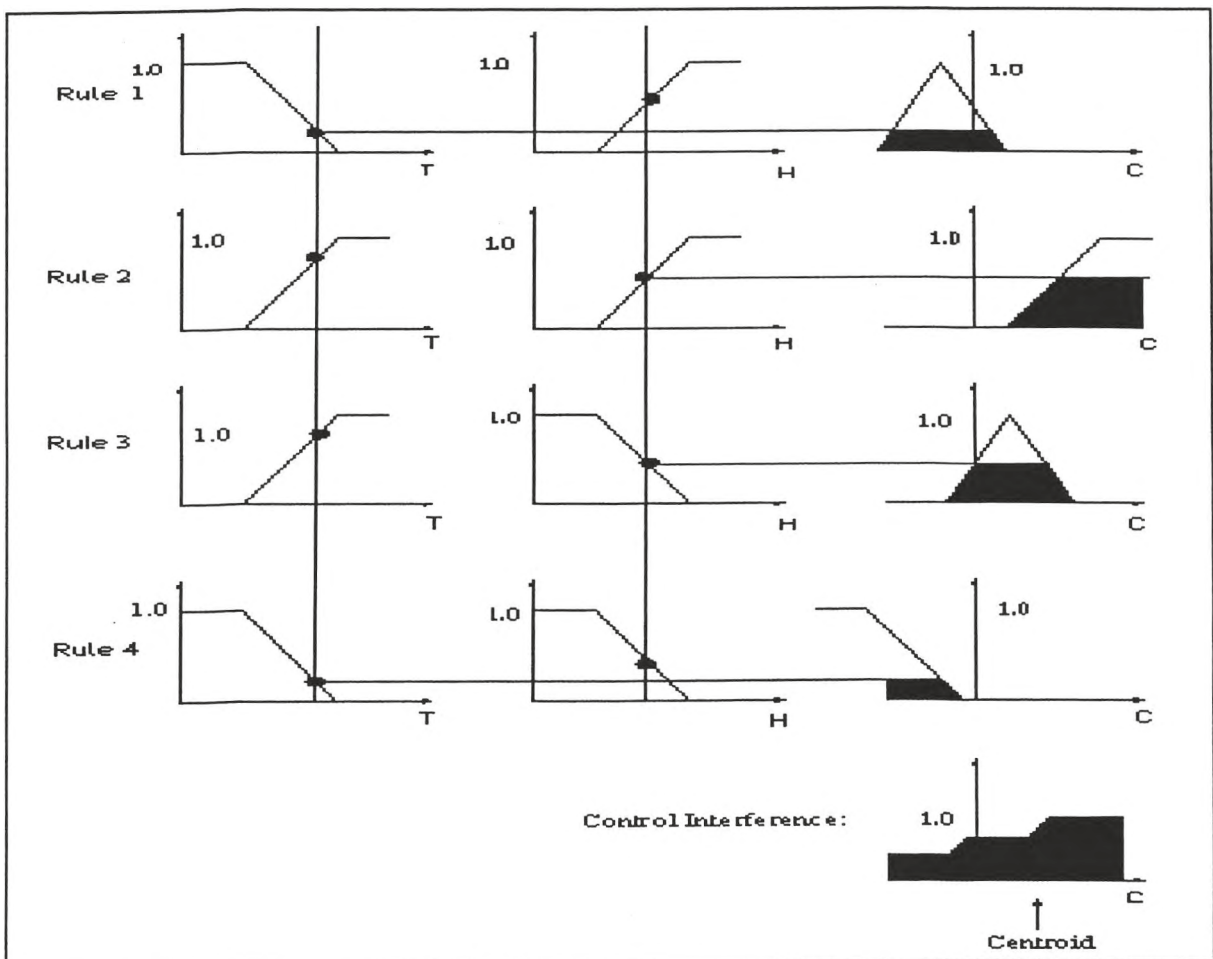


Figure 4.1 An Example of Defuzzification

### 4.3 APPLICATION IN CAPACITOR SWITCHING

In the Hong Kong power system, over a hundred of 5 MVA 11 kV capacitor banks have been installed in the primary substations for reactive power compensation. With the import of nuclear energy from China in 1993, it is expected that the total installation of capacitor banks will be very much increased over the next ten years. Such large quantities of capacitors will raise difficulties in system operation because the time of capacitor switching always coincides with the busy hours for the control engineers to pick up generation in the morning or to reduce generation in the evening. Such phenomenon does not solely happen in Hong Kong, but it is quite common everywhere in the world. At present, capacitors in different substations are divided into groups and each group can be remotely switched in/out via the SCADA system. However, during the busy hours, it is impractical, though not totally impossible, for a control engineer to look up the SCADA system to check which group is most appropriate to be switching in/out. Moreover, as different substations have different load demand patterns, over-compensation in some substations and under-compensation in others (within the same group) are inevitable during switching. To relieve the heavy burden of daily routine switching of a control engineer and to optimise the system performance, it is highly desirable to employ automatic and also intelligent switching, instead of the conventional 'manual' operation. This urgently calls for the idea of fuzzy control.

#### 4.3.1 Choice of Control Variable

Normally, capacitors are switched in when load increases in the morning. However, the time to switch out the capacitors is very much dependent on the loading. For instance, the capacitors are switched out after the morning peak in winter, but would remain until midnight during the summer peak load period. In some cases, when the demand is extremely low, such as the Chinese New Year holidays in Hong Kong, capacitive compensation appears to be unnecessary at all. Hence, the control strategy adopted and the choice of control parameter(s) should be consistent with the load demand. Conventionally in reactive power control, power factor has been utilized as the control parameter. However, the recent research [43] has revealed that it is insufficient to employ power factor as the only parameter

when the load characteristics are taken into account. In reactive power control, either MVAR or power factor can be utilized as the control parameter. Let pf, P and Q denote power factor, active power and reactive power respectively and their relationship is governed by:

$$pf = \frac{P}{\sqrt{P^2 + Q^2}}$$

$$\Rightarrow 1 = pf^2 \left( 1 + \frac{Q^2}{P^2} \right)$$

By applying small perturbation to the system, the following equation is obtained:

$$0 = 2pf\Delta pf \left( 1 + \frac{Q^2}{P^2} \right) + pf^2 \left( \frac{2Q\Delta Q}{P^2} - \frac{2Q^2\Delta P}{P^3} \right)$$

$$= \frac{\Delta pf}{pf^3} + \frac{Q^2}{P^2} \left( \frac{\Delta Q}{Q} - \frac{\Delta P}{P} \right)$$

$$\Rightarrow \Delta pf = K \left( \frac{\Delta P}{P} - \frac{\Delta Q}{Q} \right) \quad \text{where } K = pf^3 \frac{Q^2}{P^2}$$

Hence, the variation of power factor depends on both the relative changes of P and Q. In a standard transmission and distribution system as shown in Figure 4.2, the following equations are obtained:

$$P = P_{load} + \sum P_{loss}$$

$$= P_{load} + \sum I^2 R$$

and

$$Q = Q_{load} + \sum Q_{loss}$$

$$= Q_{load} + \sum (I^2 X - V^2 B)$$

Hence,  $\Delta P = \Delta P_{load} + 2 \sum I R \Delta I$

and  $\Delta Q \approx \Delta Q_{load} + 2 \sum I X \Delta I$

where  $R = \text{circuit resistance}$   
 $X = \text{circuit reactance}$   
 $B = \text{circuit susceptance}$

The system voltage variation,  $\Delta V$ , is usually very restricted and can be ignored. It can be seen that the losses are closely related to the load current(I) and the circuit parameters(R,X).

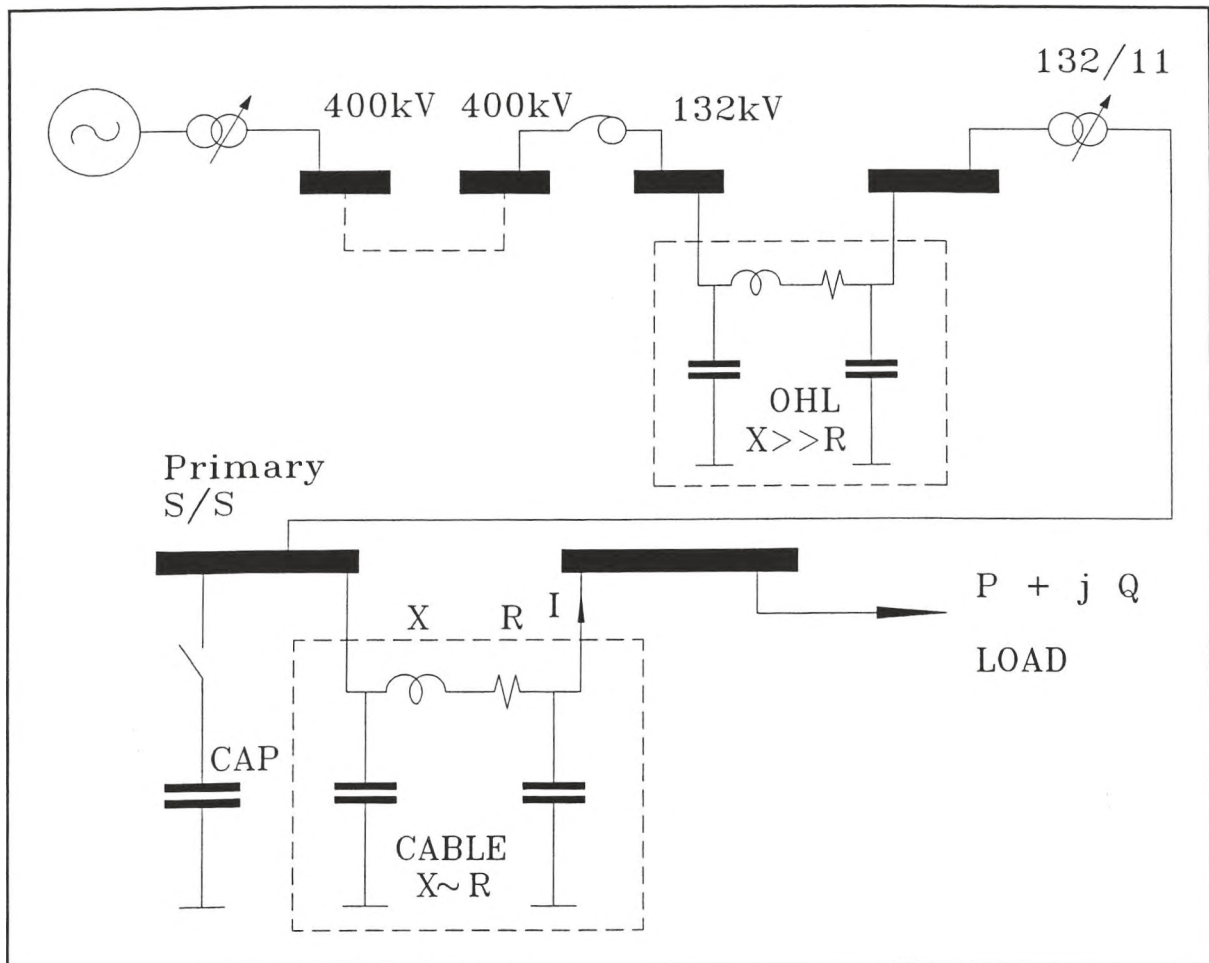


Figure 4.2 A Simplified Single Line Diagram

In the transmission network,  $Q_{\text{loss}} \gg P_{\text{loss}}$  because  $X \gg R$  for the transformers and the HV lines. Therefore, the power factor of generator output usually decreases as load increases. However, in the 11 kV distribution network,  $R$  and  $X$  of the cables are of comparable magnitude and the difference between circuit  $Q_{\text{loss}}$  and  $P_{\text{loss}}$  is practically insignificant. As a result, the variation of power factor in the primary substation with respect to load variation is dominated by the load characteristics rather than by the losses. For example, power factor  $f$  increases with real power consumption, say heating load, because  $\frac{\Delta P}{P} > \frac{\Delta Q}{Q}$ . On the contrary,  $f$  decreases as reactive power consumption, say due to an increase in motor load.

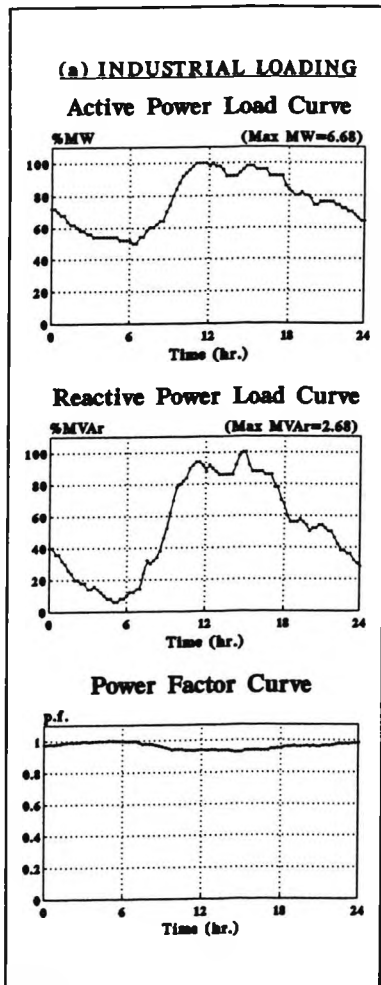


Figure 4.3(a)

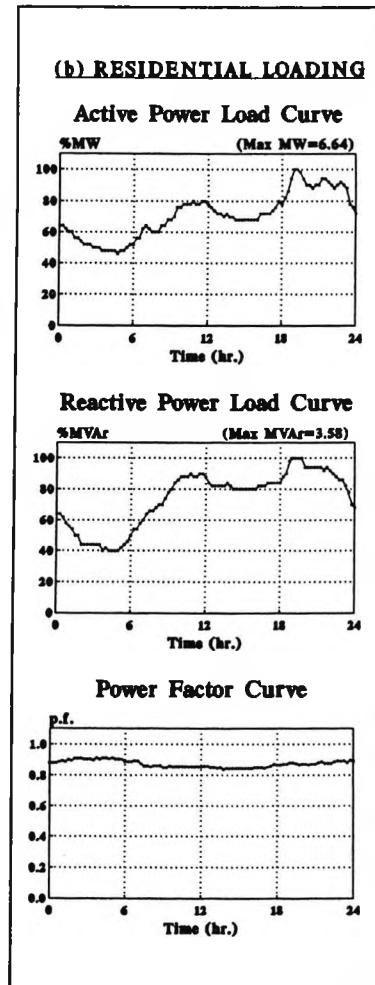


Figure 4.3(b)

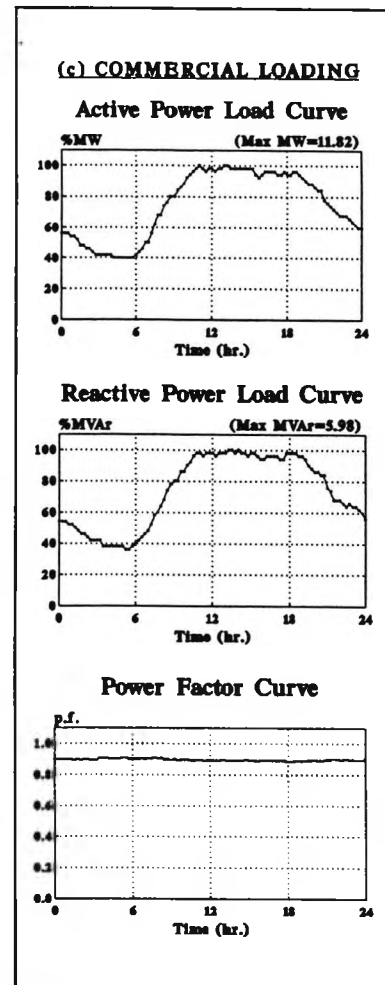


Figure 4.3(c)

It is essential to examine the load characteristics in order to determine the most suitable control parameter(s). In a primary substation, the loading is a mixture of all types - heating, lighting and motor etc. However, based on the supplying district and the major consumers, the load pattern can be roughly classified into three categories: industrial, residential and commercial. For industrial load, the power factor increases with decrease in MW, or vice versa, probably due to the dominating motor load, as shown in Figure 4.3(a). For residential load, when the MW is minimum at 5:00 or maximum at 19:00, the power factor increases in either case, i.e. inconsistent with MW changes, as shown in Figure 4.3(b). For commercial load, the power factor curve has little variation, which may be attributed to that the rates of change of P and Q are more or less the same, as shown in Figure 4.3(c). Judging from the above investigation, the power factor is much influenced by the types of

connected load and their combination, which do not bear a fixed relationship with the load demand. Owing to the uncertainty on the trend of load power factor, it is therefore considered inappropriate to use power factor as the *only* control parameter.

From the above figures, it can be seen that the MVAR demand is fairly consistent with the MW demand irrespective of the load type. Therefore, 'MVAR' seems to be quite suitable to be a control parameter as well since:

- a) it is a direct measurement of reactive demand;
- b) since the capacitor rating is also in terms of MVAR, a simple but global control strategy of, say, achieving zero MVAR can be applied to the controller;
- c) the sharp changes of MVAR demand in the morning and after the daily peak will facilitate stable control and setting design.

Thus, both the "power factor" and the reactive load "MVAR" are used as the control parameters.

### 4.3.2 Discrete and Continuous Actuation

Currently, there are two types of reactive compensation control methods, namely the step control and continuous control. For step control, each capacitor or inductor is rated at 5 MVAR and they are switched in/out depending on the instantaneous power factor and reactive power consumption. For continuous control, static shunt compensators are used. There are basically two types of commonly used compensators, namely the thyristor-controlled reactor (TCR) and thyristor-switched capacitor (TSC) [44,45]. For TCR, two way thyristors which conduct on alternate half-cycles of the supply frequency would connect the reactor onto the bus bar. If the thyristors are gated into conduction precisely at the peaks of the supply voltage waveform, full conduction results in the reactor, and the current is the same as though the thyristors are short-circuited, resulting in a current which is nearly 90° lagging. Phase control of the gating signals can result in an adjustable fundamental-frequency susceptance. For TSC, the susceptance is adjusted by controlling the number of parallel capacitors in

conduction. Each capacitor always conducts for an integral number of half-cycles. Therefore, with  $k$  capacitors in parallel, the total susceptance can be equal to that of any combination of the  $k$  individual susceptances taken 0,1,2, ... , or  $k$  at a time. The total susceptance thus varies in a stepwise manner. As a conclusion, the reactive power consumption or generation of a TSC/TCR combining system can be freely adjusted in a continuous manner.

### 4.3.3 Fuzzy Control

In this project, the aim is to develop a universal controller which must be adaptable to both the step and continuous control strategies. Definitely, the PID control is not applicable. The modern adaptive control will still be problematic in identifying the model of the system in real time whenever different control modes are employed. Rule based control relies on a limited number of decision levels which certainly oversimplifies the complex situation. Fuzzy control has the merit that it does not require real-time model identification. The advent of fuzzy control systems has dramatically transformed the control problem from one of exact mathematics, to the encoding of inexact, commonsensical inference rules. This approach, besides being intuitive, has the rewards of flexibility, ease of implementation and elegance. Rules based on the experience of the control engineers are incorporated into the inference engine and the two parameters, namely power factor and reactive power, are first of all fuzzified and manipulated by the rules. Finally, the decision is based on a centre-of-gravity algorithm to determine whether more reactive power should be generated or consumed.

### 4.3.4 Fuzzification

For each input parameter, six fuzzy subsets are created. A target power factor,  $f_o$ , is chosen, say 0.95 lagging. The real time power factor is read in and substituted into the curves shown in Figure 4.4. The membership functions of the six fuzzy subsets, namely very lagging (VLA), medium lagging (MLA), slightly lagging (SLA), slightly leading (SLE), medium leading (MLE) and very leading (VLE), can then be compiled. Once  $f_o$  is fixed, the target reactive power,  $Q_o$ , can easily be calculated if the real time active load,  $Q_r$  is known, as

shown below:

$$P_{rt} = \frac{pf_{rt} Q_{rt}}{\sqrt{1 - pf_{rt}^2}}$$

$$Q_o = \frac{P_{rt}}{pf_o} \sqrt{1 - pf_o^2}$$

where  $rt$  denotes real time

Once  $Q_o$  is fixed, the membership functions of the six fuzzy subsets for reactive power, namely, very positive (VP), medium positive (MP), slightly positive (SP), slightly negative (SN), medium negative (MN) and very negative (VN), can be compiled. Here, a positive reactive power means consumption of reactive power by the load while a negative value refers to the generation of reactive power by the load.

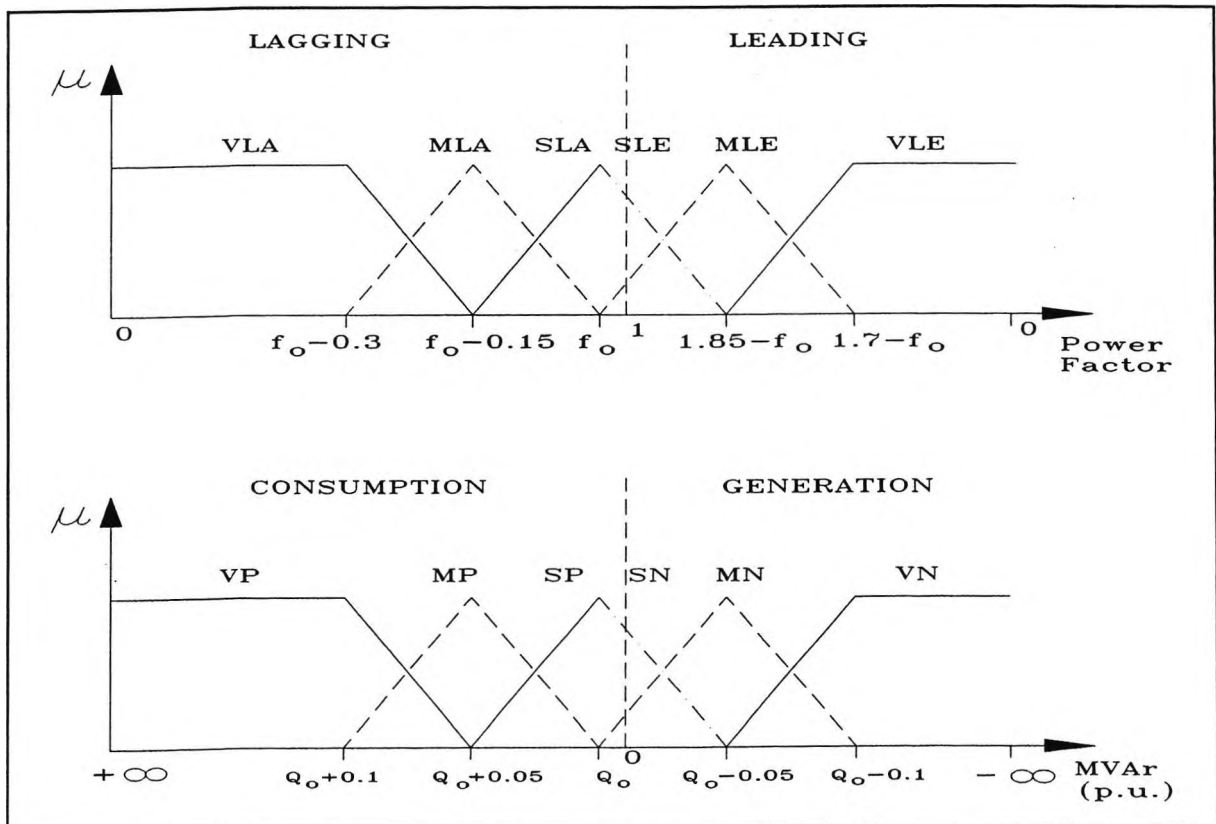


Figure 4.4 Membership Function of the Input Variables

## 4.3.5 The Rule Base

Six actuation actions have been defined, namely large increase (LI), medium increase (MI), slightly increase (SI), slightly decrease (SD), medium decrease (MD) and largely decrease (LD) respectively. Here, "increase" means an increase in reactive power generation or a reduction in reactive power consumption by the compensation system while "decrease" is the contrary. For the case of discrete actuation, if inductors have already been connected to the system, an "I" signal will always result in a disconnection of inductors before a switching in of capacitors. Similarly, if capacitors have already been connected to the system, a "D" signal will always imply a switching out of capacitors before the real connection of inductors. For the case of continuous actuation, TSC and TCR are working in parallel with one another and there should be no other problem. Since there are totally six fuzzy subsets for each input variable, there are in principle thirty six rules to be prepared. They are listed in the following table:

		Power Factor					
Q	OUTPUT	VLA	MLA	SLA	SLE	MLE	VLE
	VP	LI	LI	E	E	E	E
	MP	LI	MI	MI	E	E	E
	SP	MI	MI	SI	SI	E	E
	SN	E	E	SD	SD	MD	MD
	MN	E	E	E	MD	MD	LD
	VN	E	E	E	E	LD	LD

The abbreviation "E" means an error which indicates something is wrong with the data acquisition system. Since we are using two transducers, one for measuring power factor and the other for measuring reactive power flow, there are from time to time errors occurring in the system, resulting in unreasonable situations. Whenever the resultant membership function of the fuzzy subset "E" is larger than 0.5, an alarm is triggered on to imply the hardware should be checked and maintenance is to be carried out.

### 4.3.6 The Inference Engine and Defuzzification

During real time operation, the power factor is read in from the power factor transducer while the reactive power is read in from the reactive power transducer. They are then put under the evaluation according to the thirty six rules for evaluation by using the standard max-min operation. One rule is used as an example for illustration, which is "If  $Q$  is  $MP$  and  $pf$  is  $MLA$  then Output is  $MI$ ". The membership function of  $MI$  is given by:

$$\mu_{MI} = \min \{ \mu_{MP} ( Q_r ) , \mu_{MLA} ( Pf_r ) \}$$

After the evaluation process, one will obtain thirty six membership functions from all the rules. Any membership function for "E" larger than 0.5 should be treated as an alarm for attendance. In order to defuzzify the output, each actuating action is assigned a MVAR value, as shown below:

LI : + 0.1 p.u.

MI : + 0.05 p.u.

SI : + 0.01 p.u.

SD : - 0.01 p.u.

MD : - 0.05 p.u.

LD : - 0.1 p.u.

Only eighteen rules are involved in the defuzzification process. The final actuation signal is given by:

$$\begin{aligned} \text{Output} &= \frac{A}{B} \text{ where } A = 0.1 * \sum_{i=1}^3 \mu_{LI}(i) + 0.05 * \sum_{i=1}^4 \mu_{MI}(i) \\ &\quad + 0.01 * \sum_{i=1}^2 \mu_{SI}(i) - 0.01 * \sum_{i=1}^2 \mu_{SD}(i) \\ &\quad - 0.05 * \sum_{i=1}^4 \mu_{MD}(i) - 0.1 * \sum_{i=1}^3 \mu_{LD}(i) \\ B &= \sum_{i=1}^3 \mu_{LI}(i) + \sum_{i=1}^4 \mu_{MI}(i) + \sum_{i=1}^2 \mu_{SI}(i) \\ &\quad + \sum_{i=1}^2 \mu_{SD}(i) + \sum_{i=1}^4 \mu_{MD}(i) + \sum_{i=1}^3 \mu_{LD}(i) \end{aligned}$$

Here,  $i$  stands for the number of rule with the related actuation result. For continuous actuation, the output signal is used to control the TSC/TCR combination to fulfil the required MVar generation/consumption. However, for discrete actuation, the unit step of each capacitor or inductor is 5 MVar, or 0.05 p.u. Therefore, the actuator will only take action if the signal is larger than 0.025 p.u. for one step and 0.075 p.u. for two steps.

### 4.3.7 Hardware Design

With reference to Figure 4.5, the hardware design basically consists of three parts: controller, substation model and other electronic circuits. A standard PC is the core component of the controller. The VAr and power factor signals are received from the transducers and sampled by the A/D converters. Graphics display is available for monitoring the real time system performance. The capacitors, inductors, TSC and TCR are controlled by the driving/switching circuit based on the digital commands through the 8255 interfacing card.

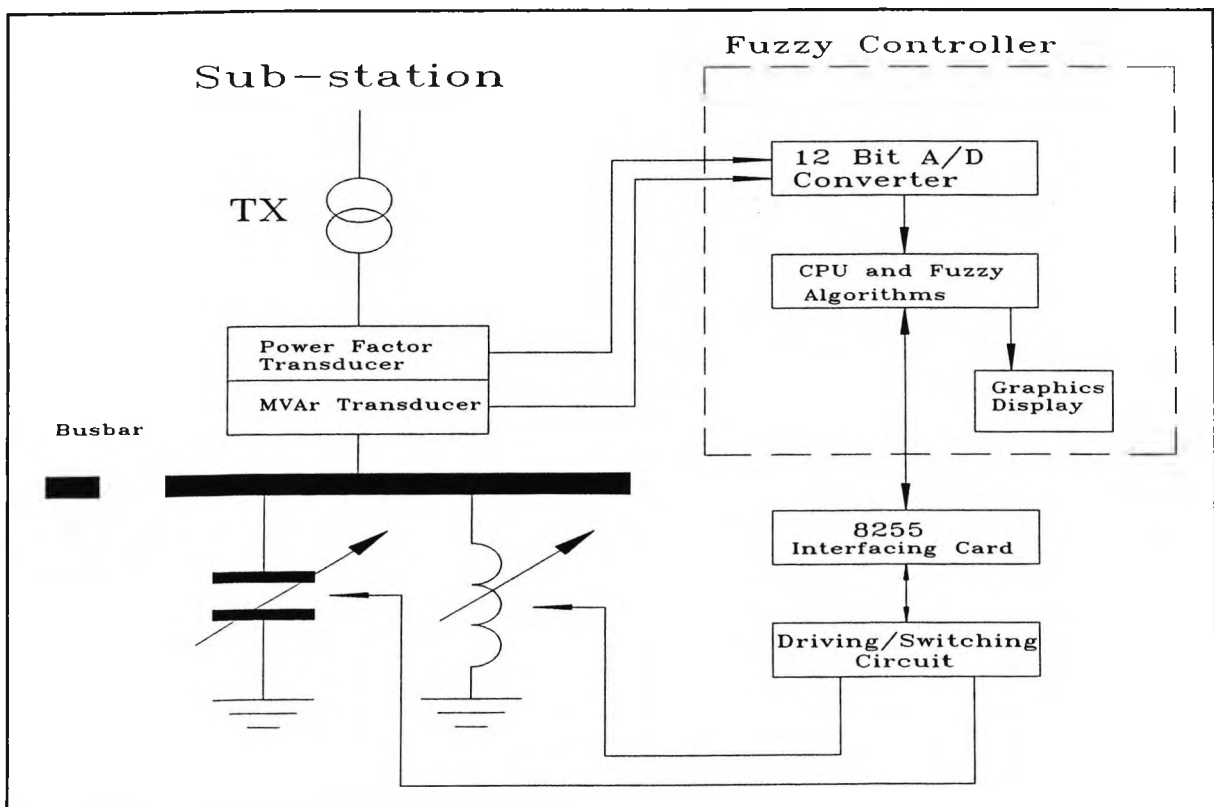


Figure 4.5 Block Diagram of the Controller

4.3.8 Performance of Controller

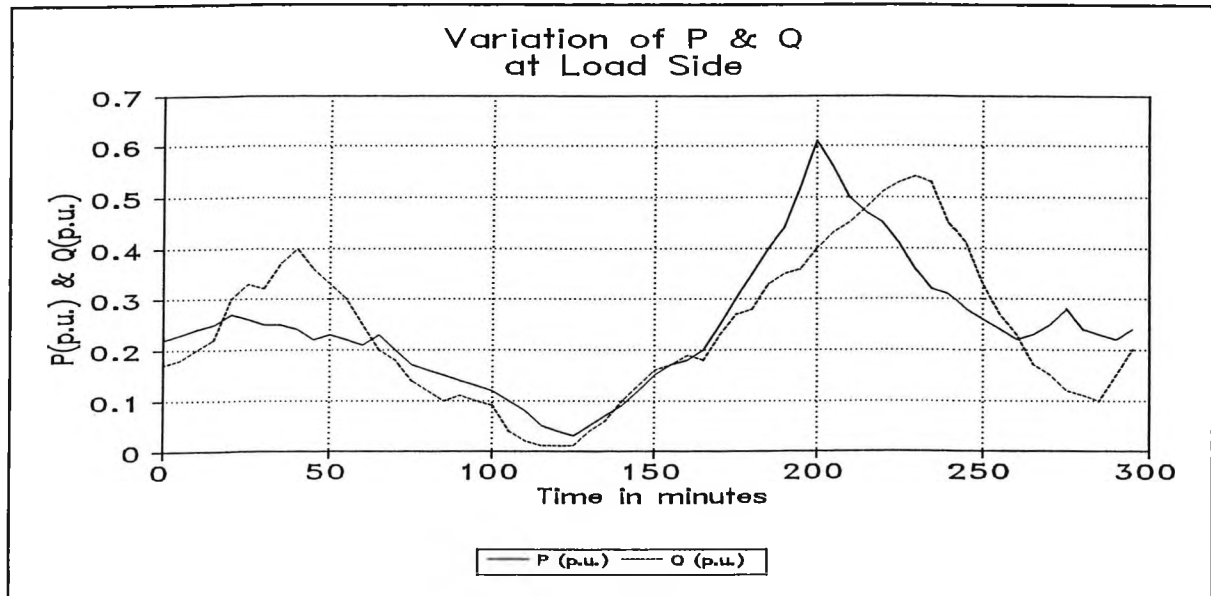


Figure 4.6 Variation of P and Q

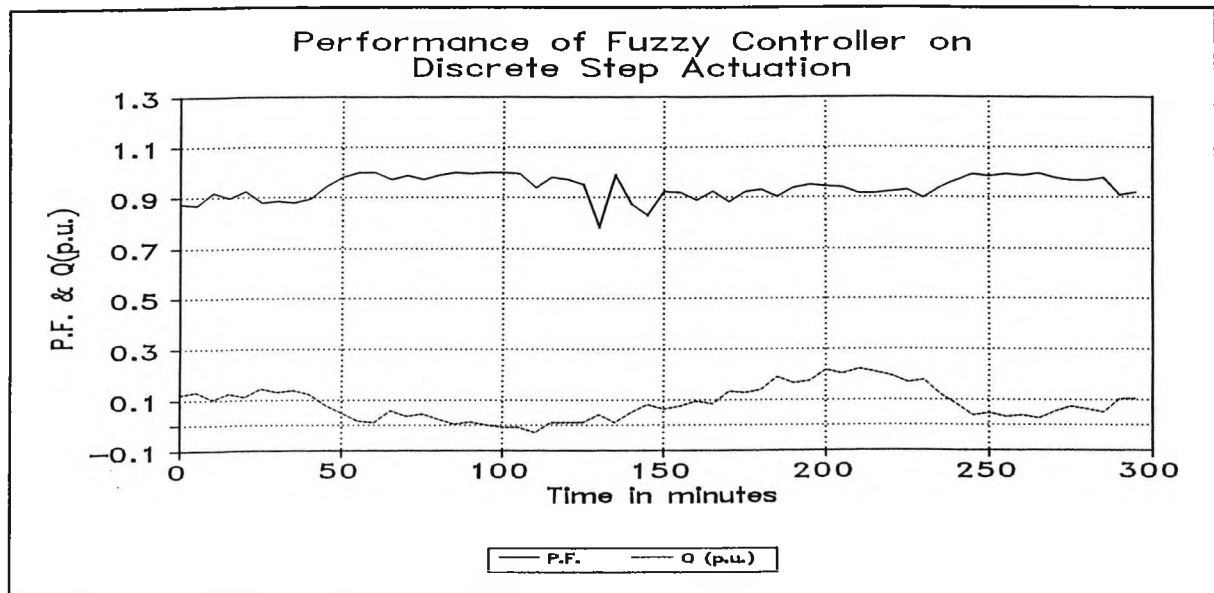


Figure 4.7 Variation of Power Factor and Q

Figure 4.6 shows the variation of active and reactive power of the load side throughout a period of five hours. Figure 4.7 shows the variation of power factor and reactive power at the substation when the discrete actuation scheme is employed under the fuzzy controller.

Figure 4.8 shows the variation of the same parameters when the continuous actuation scheme is employed under the fuzzy controller.

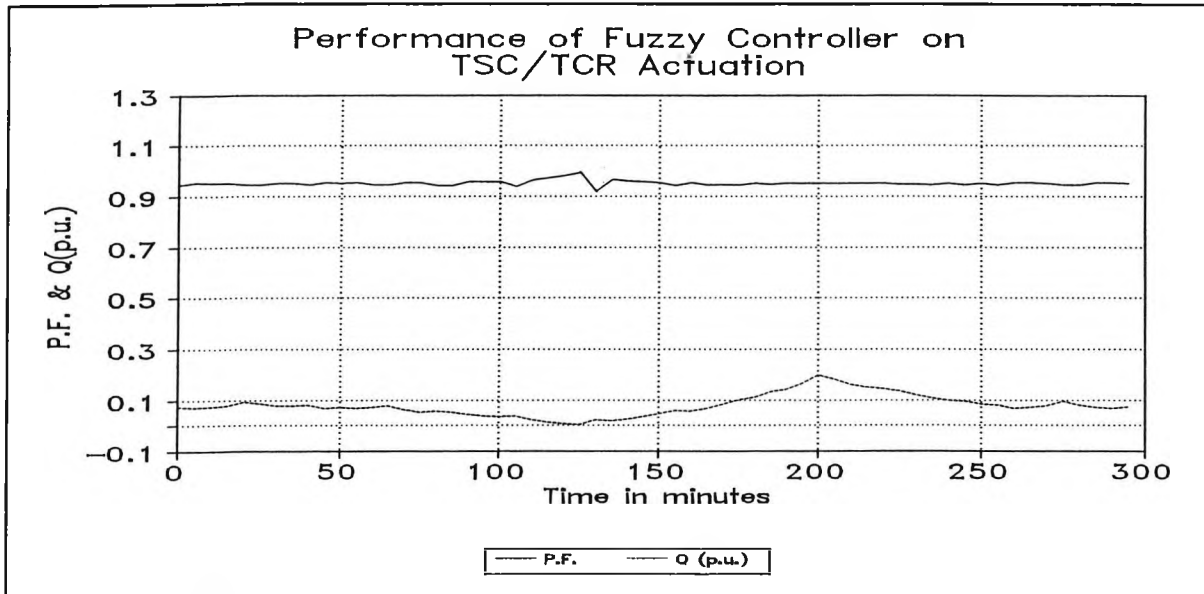


Figure 4.8 Variation of Power Factor and Q

#### 4.4 APPLICATION IN HARMONIC LOAD RECOGNITION

Equations with fuzzy numbers appear frequently in our daily life in many disciplines [46-48]. An analytical solution for such equations is generally very difficult to obtain due to the nature of high non-linearity among other problems. Optimisation is one way to handle such a problem and it can be very efficient. In particular, when one is handling problems with power system harmonics signature recognition, one might come across the existence of equations involving fuzzy numbers. Harmonics levels on the power distribution system are receiving increasing attention as the number of distorting loads are increasing. The harmonics performance of the distribution system depends on four major components of the system, namely the line characteristics, the source characteristics, the power factor correction capacitors and most important, the load. While the individual performance of each of the first three of these groups is generally understood, the load performance is not well understood, and has received little attention so far. Past studies of distribution system harmonics have tended to focus on systems with a single point source of harmonics [49,50], with the loading neglected or represented by passive impedances. The author has successfully

built up a distributed harmonics monitoring network [51,52] to record harmonics patterns for different loads. It is based on this measuring system that this project is handled. First of all, harmonics patterns of different types of loads are measured and recorded, forming the templates of signature recognition in future. However, there are, from time to time, measurement errors due to the imperfection of the measuring equipment and the intrinsic variations of load characteristics. Actually, the laboratory measurements on several types of typical customer loads have also revealed that the spectrum of the same type changes slightly with both the magnitudes and phase angles in accordance with the real time power consumption and the particular characteristics of the individual load model. Thus, it will be very useful if the templates can be represented in fuzzy numbers. When an unknown harmonics pattern is obtained (such pattern is also fuzzy in nature), the contribution from each type of load can be restored by solving a set of fuzzy linear equations with constants and coefficients represented in fuzzy numbers and unknown variables that are crisp.

### 4.4.1 Harmonics Patterns of System Loads

In order to gain an understanding of the harmonics characteristics of common customer loads, measurements of individual devices were performed. Measurements of some distorting loads such as electronic devices, fluorescent lighting and single phase motors had been carried out before to produce star diagrams showing the harmonics phasors [53]. In the case being studied, the measurements involve four general types of load which the author believes are the major sources of harmonics pollution, namely the full wave rectifiers (e.g. switched mode power supplies etc.), phase controlled devices (e.g. light dimmers), iron cores (e.g. transformers and motors etc.) and fluorescent tubes. Of course, there are other types of load such as discharge lamps etc. They are either of low power ratings or not included in this study for the time being. It is assumed that the voltage waveforms have not been distorted considerably and that means only current harmonics need to be considered. Figure 4.9(a) and Figure 4.9(b) show the harmonics patterns belonging to a typical PC/486 (i.e. full wave converter typed switched mode power supply) with respect to both magnitudes and phase angles while Figure 4.10(a) and Figure 4.10(b) show similar patterns belonging to another PC/486. Only odd harmonics up to the 27th harmonics are presented here. It can be seen

that the patterns are more or less identical but minor differences actually exist.

It has been found that most harmonics sources are in synchronism with the power supply voltage. However, subject to the fact that measurement is not exact and also there are often slight variations between different loads of the same type, no matter what the magnitudes or the phase angles as shown in Figure 4.9's and 4.10's, the harmonics patterns are actually fuzzy in nature. At the same time, site measurement of any supply point involves uncertainty as well and therefore the harmonics distribution is best represented by fuzzy numbers.

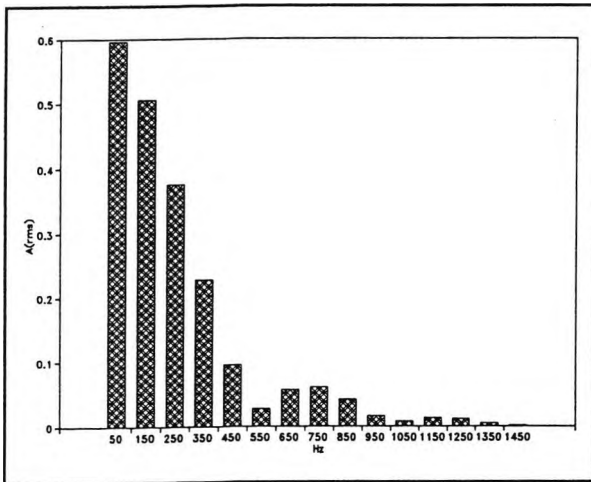


Figure 4.9(a) Magnitude Spectrum of PC1

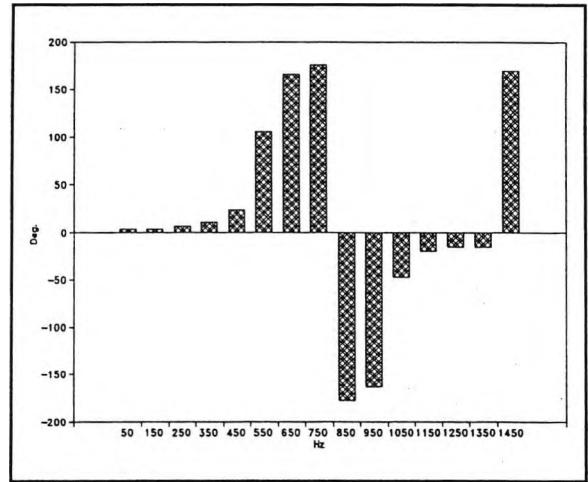


Figure 4.9(b) Phase Spectrum of PC1

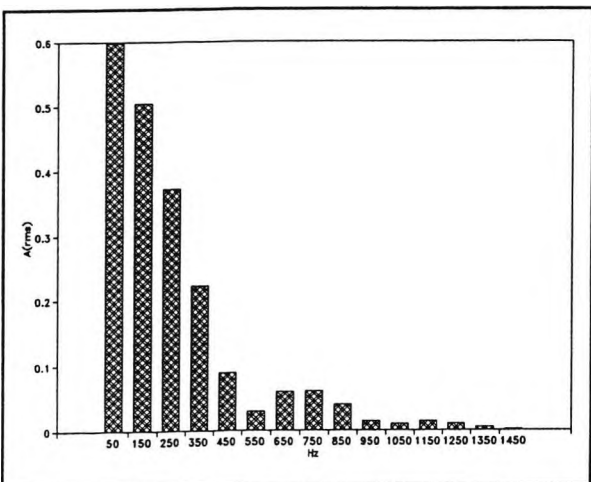


Figure 4.10(a) Magnitude Spectrum of PC2

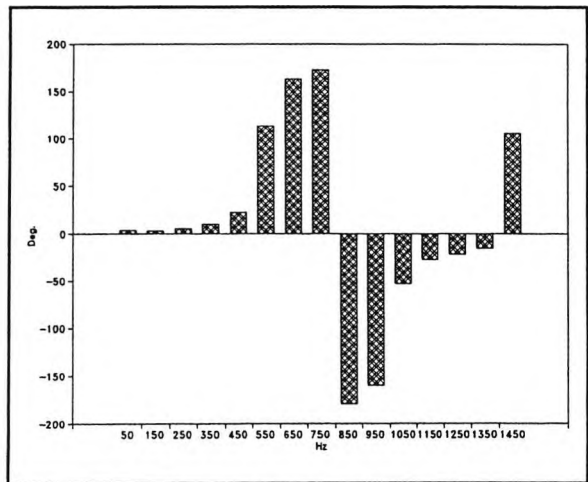


Figure 4.10(b) Phase Spectrum of PC2

## 4.4.2 Concept of Fuzzy Numbers [54]

The concept of uncertainty or fuzzy numbers may be presented in many ways. In this chapter, a fuzzy number is considered an extension of the concept of the interval of confidence, which is familiar to anyone who has computed using imprecise data in simple or complex systems. The interval of confidence is considered at several levels and more generally at all levels from 0 to 1, the maximum of presumption being at level 1 and the minimum of presumption being at level 0. A level of presumption  $\alpha$ ,  $\alpha \in [0, 1]$  gives an interval of confidence  $A_\alpha = [a_1^{(\alpha)}, a_2^{(\alpha)}]$ , which is a monotonically decreasing function of  $\alpha$ , i.e.

$$\begin{aligned}
 (\alpha' > \alpha) &\Rightarrow (A_{\alpha'} \subset A_\alpha) \\
 &\text{or} \\
 (\alpha' > \alpha) &\Rightarrow ([a_1^{(\alpha')}, a_2^{(\alpha')}] \subset [a_1^{(\alpha)}, a_2^{(\alpha)}]) \\
 \forall \alpha, \alpha' &\in [0, 1]
 \end{aligned}$$

These are actually alternative representations of the well-known  $\alpha$ -cuts so that the intervals can be clearly defined. The expressions level of presumption or presumption level are well suited to the concept of fuzzy numbers. With the concept of presumption level, two fuzzy numbers A and B with levels of presumption  $[a_1^\alpha, a_2^\alpha]$  and  $[b_1^\alpha, b_2^\alpha]$  are considered so that certain simple operations on these two fuzzy numbers can be defined below:

**Addition:**

$$(A + B)_\alpha \triangleq [a_1^\alpha + b_1^\alpha, a_2^\alpha + b_2^\alpha]$$

**Subtraction:**

$$(A - B)_\alpha \triangleq [a_1^\alpha - b_2^\alpha, a_2^\alpha - b_1^\alpha]$$

**Multiplication:**

$$(A (\cdot) B)_\alpha \triangleq [a_1^\alpha b_1^\alpha, a_2^\alpha b_2^\alpha]$$

**Division:**

$$(A \text{ ( : ) } B)_\alpha \triangleq \left[ \frac{a_1^\alpha}{b_2^\alpha}, \frac{a_2^\alpha}{b_1^\alpha} \right]$$

In crisp cases, the distance between two real numbers,  $a$  and  $b$ , can easily be defined as  $|a-b|$ . For two fuzzy numbers,  $X$  and  $Y$ , the distance  $d(X,Y)$  to be defined between  $X$  and  $Y$  should have the following properties:

*For any three fuzzy numbers*

$X, Y, Z$  :

$$d(X, Y) \geq 0$$

$$(X = Y) \Rightarrow (d(X, Y) = 0)$$

$$d(X, Y) \equiv d(Y, X)$$

$$d(X, Z) \leq d(X, Y) * d(Y, Z)$$

*where \* is an operator*

*associated with notion of distance*

It should be noted that although  $X$  and  $Y$  are fuzzy in nature,  $d(X,Y)$  is *non-fuzzy*. For any two fuzzy numbers,  $X$  and  $Y$ , two values, namely  $\beta_1$  and  $\beta_2$ , are chosen as convenient values that can surround all  $X_{\alpha=0}$  and  $Y_{\alpha=0}$ . The distance between  $X$  and  $Y$  is known as the dissemblance index, or  $\delta(X,Y)$  of  $X$  and  $Y$ , as given below:

$$\delta(X, Y) \triangleq \frac{1}{2(\beta_2 - \beta_1)} \int_{\alpha=0}^1 \Delta(X_\alpha, Y_\alpha) d\alpha$$

$$\text{where } \Delta(X_\alpha, Y_\alpha) \triangleq |x_1^{(\alpha)} - y_1^{(\alpha)}| + |x_2^{(\alpha)} - y_2^{(\alpha)}|$$

$$\beta_1 \geq x_2^{(0)} - x_1^{(0)}$$

$$\beta_2 \geq y_2^{(0)} - y_1^{(0)}$$

#### 4.4.3 The Harmonics Templates

For each type of customer load, a comprehensive measurement at the laboratory is taken to find out the full harmonics spectrum, up to a certain practical limit, which is chosen to be 27 in this project. The on-site experience has revealed that it is rare to have frequency

## Chapter IV

components higher than the 25th harmonics in a real power distribution system. For each frequency component, the  $n$ th harmonics, two parameters can be obtained, namely the r.m.s. magnitude,  $I_n$  and the phase angle relative to the supply voltage,  $\theta_n$ . Thus, the harmonics spectrum of the total current waveform of the  $p$ th type of load,  $I_p$ , can be represented below as:

$$I_p = \sum_{n=1}^{\infty} I_{np} \sin ( n\omega t + \theta_{np} ) \quad \text{where } \omega = 2 \pi f$$

In order to provide computational convenience, the complex plane is employed to represent the spectrum and a representation of it is known as the star diagram, i.e.

$$\text{For the } p\text{th type of load , } I_p = \sum_{n=1}^{\infty} [ I_{rnp} + j I_{inp} ]$$

$$\text{where } \begin{cases} I_{rnp} = \text{Re} ( I_p ) = \text{real part of } n\text{th harmonic component} \\ I_{inp} = \text{Im} ( I_p ) = \text{imaginary part of } n\text{th harmonic component} \end{cases}$$

However, due to the errors and uncertainty associated with the measuring equipment and also the slight differences between different loads of the same type,  $I_n$  and  $\theta_n$  should best be

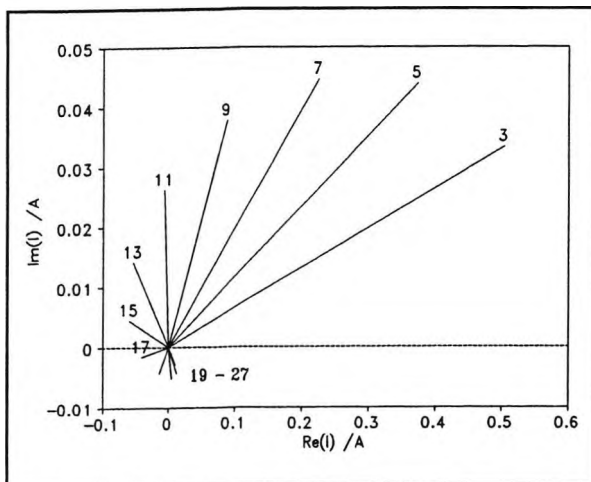


Figure 4.11(a) Harmonics Pattern of PC1

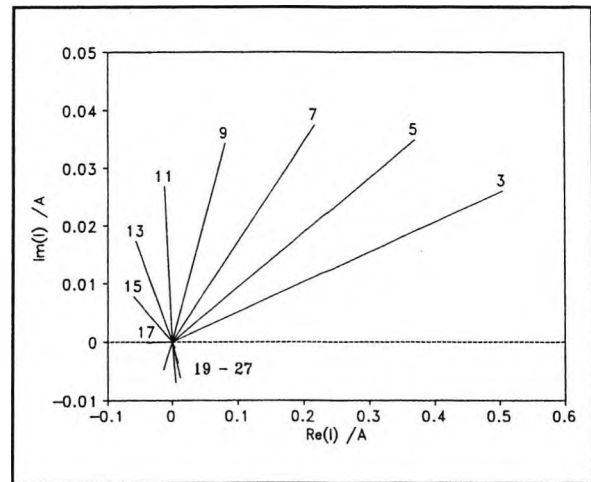


Figure 4.11(b) Harmonics Pattern of PC2

represented by fuzzy numbers and hence  $I_{rn}$  and  $I_{in}$ . Figure 4.11(a) and Figure 4.11(b) show the harmonics patterns, star diagrams, of the two typical full wave converters as shown in Figure 4.9's and Figure 4.10's, i.e. switched mode power supplies (200W) of two typical

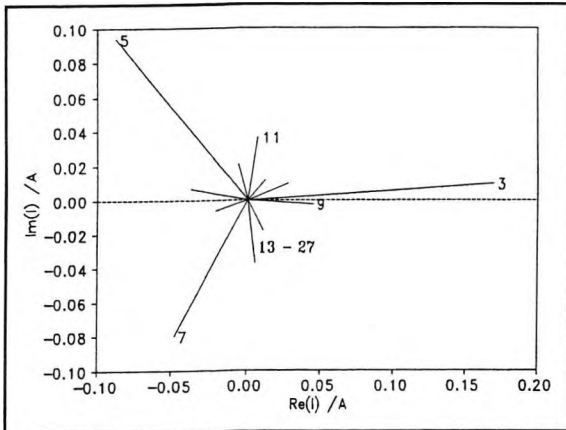


Figure 4.12 Harmonics Pattern of 200W Dimmer

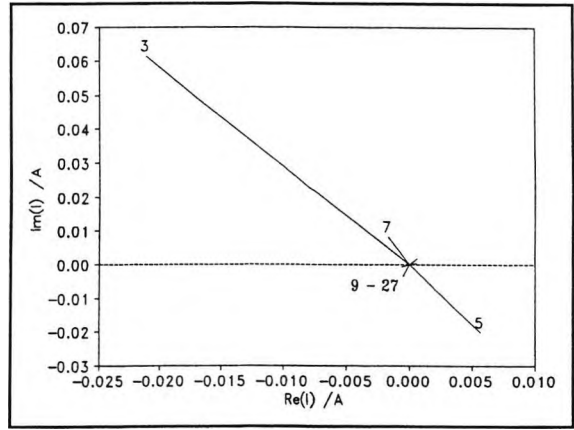


Figure 4.13 Harmonics Pattern of 200kVA Transformer

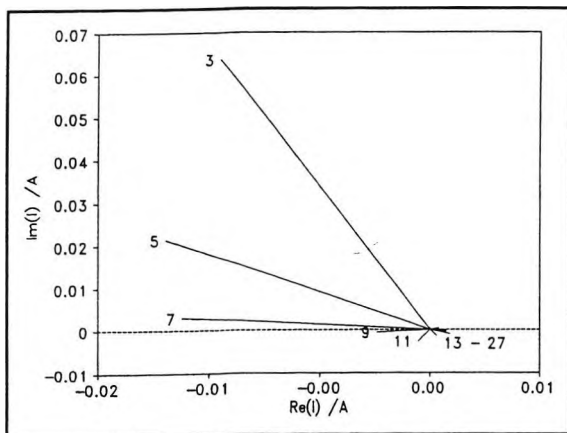


Figure 4.14 Harmonics Pattern of Fluorescent Tubes (120W)

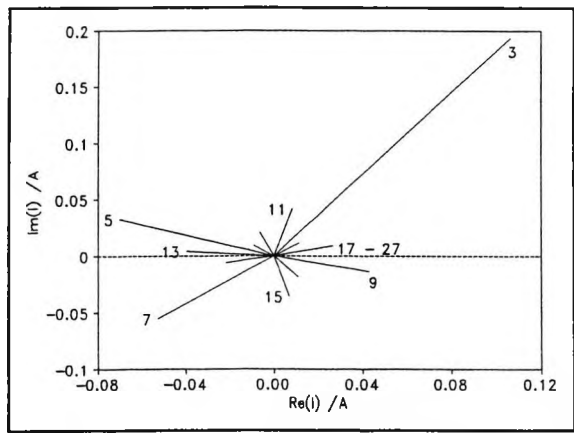


Figure 4.15 Star Diagram of 3 Transformers Plus 1 Dimmer

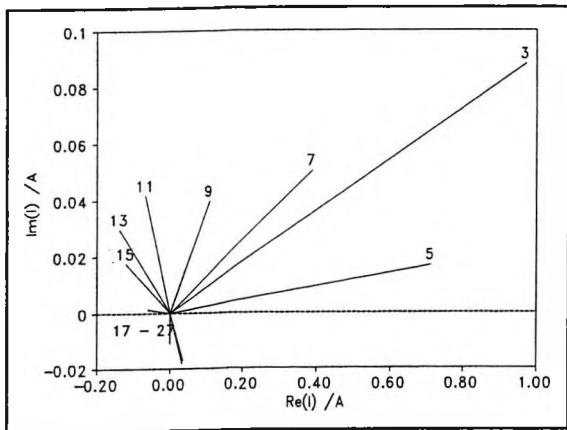


Figure 4.16 Star Diagram of 1 Transformer Plus 2 PC's

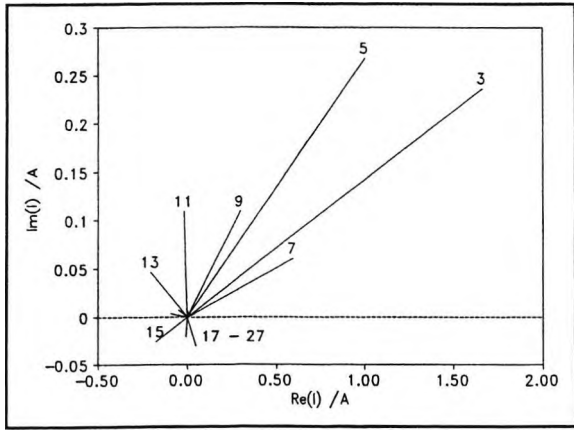


Figure 4.17 Star Diagram of Mixture of Fluorescent Tubes, Personal Computers and Dimmer

PC/486. Figure 4.12 shows the star diagram of a typical incandescent light dimmers (200W); Figure 4.13 belongs to a typical power transformer (5kVA); Figure 4.14 belongs to a series

of fluorescent tubes (120W). A point that is worthy to note is that it is sufficient enough to consider the odd harmonics only due to the symmetrical nature of the majority of the power system waveforms.

#### 4.4.4 Fuzzy Number Representation of Harmonics Spectrum

As it has been explained before, two sources in the real world would make the measurement inaccurate for each type of load. The first one is associated with the intrinsic characteristics and error inside the measurement equipment. The second one is associated with the slight deviation from the rated values of each load even of the same type. An example can be given here. The author has carried out some measurements on 17 different personal computers of the same brand and model, including PC1 and PC2 mentioned above. It has been found that there are slight variations in the results and the 3rd harmonics of them are shown in Figure 4.18(a) for the real part and Figure 4.18(b) for the imaginary part as an illustration. Of course, more measurement samples will enhance the statistics obtained and thus improve the result of fuzzification. It can be seen that they are actually fuzzy in nature and each can be represented by a triangular fuzzy number (TFN) subject to computational simplicity where Figure 4.19(a) shows the real part and Figure 4.19(b) shows the imaginary part. A TFN is completely represented by a triplet such as:

$A = (a_1, a_2, a_3)$ . At the level  $\alpha$ , the interval of confidence is given by:

$$\begin{aligned} A_\alpha &= [ a_1(\alpha) , a_3(\alpha) ] \\ &= [ a_1 + \alpha (a_2 - a_1) , a_3 - \alpha (a_3 - a_2) ] \end{aligned}$$

It can easily be shown that the addition, subtraction and multiplication by an ordinary number of TFN's will produce TFN.

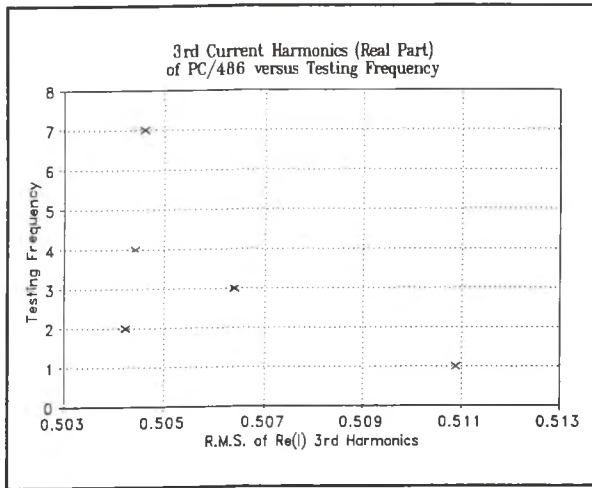


Figure 4.18(a) 3rd Harmonics Measurement (Real Part)

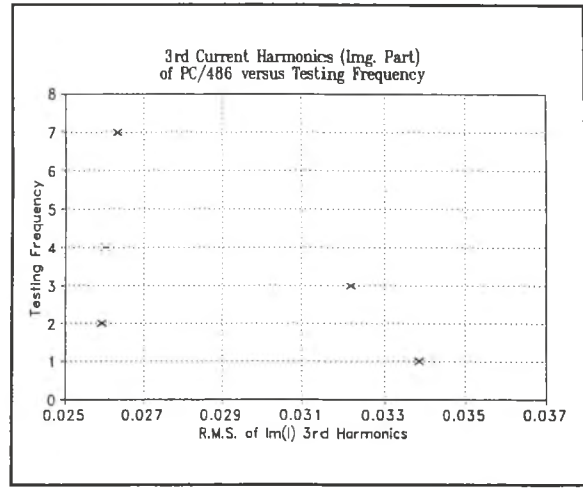


Figure 4.18(b) 3rd Harmonics Measurement (Imaginary Part)

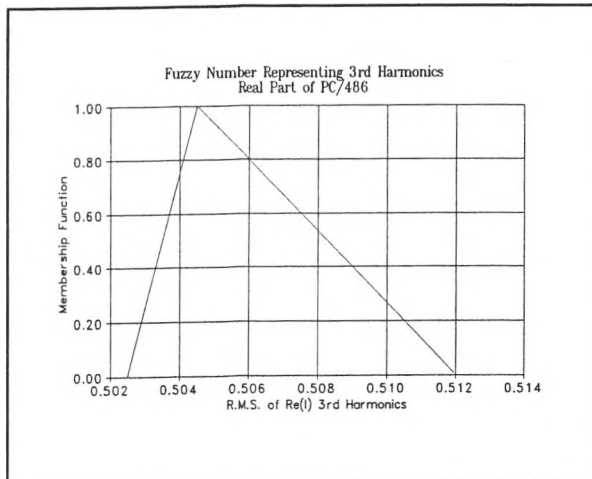


Figure 4.19(a) Fuzzy Number Representing Real Part

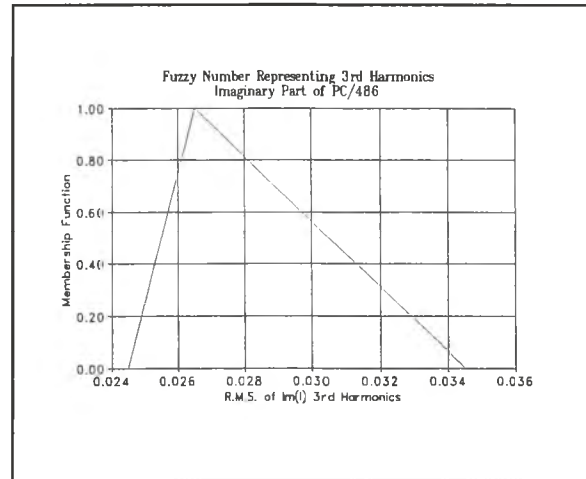


Figure 4.19(b) Fuzzy Number Representing Imaginary Part

#### 4.4.5 Setting up the Fuzzy Linear Equations

After the templates are well prepared in the format of fuzzification of each frequency component, site measurement of total current,  $I_s$ , at any load point can be carried out and a full harmonics spectrum is obtained, i.e.

$$I_s = \sum_{n=1}^{\infty} (I_{rms} + j I_{ins}) \quad \text{where } s \text{ implies site measurement}$$

It should be noted that  $I_{rms}$  and  $I_{ins}$  are fuzzy numbers as well due to the uncertainty in the

measuring devices. It is reasonable to assume that such measured spectrum on site is actually a combination of various templates in appropriate ratios,  $a_p$  ( $p$  stands for the  $p$ th type of template and  $p$  runs from 1 to  $K$ ). Here,  $K$  is the total number of templates available in the data base. The following approximate equality thus holds:

$$\sum_{n=1}^{\infty} ( I_{rms} + j I_{ins} ) \approx \sum_p \left[ a_p \left\{ \sum_{n=1}^{\infty} I_{rnp} + j I_{inp} \right\} \right]$$

In fact,  $a_p$  specifies the contribution or significance of the  $p$ th type of customer load within the measured harmonics spectrum and  $a_p$  is non-fuzzy. The objective is to estimate each  $a_p$  as the remaining variables in the approximate equality are all known. Since the complex expression is a representation of the time domain expression, approximate equality should hold for each frequency component, i.e.

$$\left( I_{rms} - \sum_p a_p I_{rnp} \right) + j \left( I_{ins} - \sum_p a_p I_{inp} \right) \approx 0 + j 0 \quad \forall n \in \mathbb{N}$$

A way to handle this set of equations with fuzzy  $I_{rms}$ ,  $I_{rnp}$ ,  $I_{ins}$  and  $I_{inp}$  and crisp  $a_p$ , that is appropriate in this setting, is the minimisation of the weighted summation of total distance  $d_n$  (i.e. the dissemblance index) between the two fuzzy numbers in both the real and imaginary parts for all the frequency components and  $d_n$  is defined below as:

$$d_{n1} \triangleq \delta \left( I_{rms}, \sum_p a_p I_{rnp} \right) ; \quad d_{n2} \triangleq \delta \left( I_{ins}, \sum_p a_p I_{inp} \right)$$

$$d_n \triangleq d_{n1} + d_{n2} ; \quad \text{Task : Minimise } D = \sum_{n=1}^{\infty} w_n d_n$$

where  $w_n$  is a weighting factor for each frequency component in order to adjust the degree of importance of each component.

#### 4.4.6 Solving the Fuzzy Equations by Optimisation

It can be seen that the problem has now been converted from a fuzzy nature into a non-fuzzy

## Chapter IV

nature of cost function minimisation. The method of Steepest Descent [55] is adopted as a numerical approach to the problem. For each iteration, the direction of searching is opposite to the direction with greatest local increase in function value and a small step given by  $\lambda$  is used. The searching direction is in fact the negation of the gradient of the cost function that needs minimisation, i.e.  $-\nabla D$ . Let  $X$  be the vector that includes all  $a$ 's, i.e.  $a_p$  for  $p = 1$  to  $K$ , where there are totally  $K$  number of templates available.

$$X = \begin{bmatrix} a_1 \\ \cdot \\ \cdot \\ a_p \\ \cdot \\ a_K \end{bmatrix}$$

Let  $X_m$  be the resultant vector after the  $m$ th iteration that is defined below as:

$$X_m = X_{m-1} - \lambda \nabla D = X_{m-1} - \lambda \begin{bmatrix} \frac{\partial D}{\partial a_1} \\ \cdot \\ \cdot \\ \frac{\partial D}{\partial a_p} \\ \cdot \\ \frac{\partial D}{\partial a_K} \end{bmatrix}$$

Iteration will end when  $\|X_m - X_{m-1}\|$  is smaller than a predefined value, 0.1% in our case.

### 4.4.7 Measurements On Site and Recognition

The fundamental frequency component is not considered as harmonics and thus, we start from  $n = 3$  until  $n = 27$ . Only odd harmonics are included due to the reason mentioned in 4.4.3.  $\lambda$  is chosen to be a constant equal to 0.005 throughout the iteration process.  $w_n = 1$  for  $n=3$  until  $n=27$ . As an illustrative example, four typical customer loads have been chosen for the

templates, i.e.  $K = 4$  where  $p=1$  for PC;  $p=2$  for transformer;  $p=3$  for dimmer and  $p=4$  for fluorescent tube.

**Case I**

Figure 4.15 shows a harmonics spectrum of an on-site measurement consisting of three transformers and one dimmer. The results are summarised below:

$$\begin{aligned} a_1 &= 0.002 ; & a_2 &= 2.890 ; \\ a_3 &= 0.981 ; & a_4 &= 0.112 . \end{aligned}$$

**Case II**

Figure 4.16 shows another site measurement consisting of one transformer and two personal computers and the results are summarised below:

$$\begin{aligned} a_1 &= 1.892 ; & a_2 &= 0.713 ; \\ a_3 &= 0.031 ; & a_4 &= 0.001 . \end{aligned}$$

**Case III**

Figure 4.17 shows a more comprehensive measurement consisting of two sets of fluorescent tubes, three personal computers and one dimmer where the results are summarised below:

$$\begin{aligned} a_1 &= 2.993 ; & a_2 &= 0.022 ; \\ a_3 &= 1.004 ; & a_4 &= 1.971 . \end{aligned}$$

**4.4.8 Harmonics Pollution Indicator**

In order to have an understanding of the seriousness of harmonics pollution at any load point, a power harmonics pollution indicator,  $\mu$ , is established and defined below:

$$\mu \triangleq \frac{\sum_p a_p^2 \left\{ \sum_{n=2}^{\infty} \left( I_{rnp(\alpha=1)}^2 + I_{inp(\alpha=1)}^2 \right) \right\}}{I_{LP}^2}$$

where  $I_{LP}$  is the total r.m.s. current measured at the supply point and  $I_{\alpha=1}$  is the value of  $I$  when a cut-set operation at  $\alpha=1$  is operated on the fuzzy number  $I$ . Obviously, a value of

$\mu$  approaching 0 is returned when the system is comparatively free from harmonics whereas a value of 1 is returned if the fundamental component does not exist at all. For our illustrative examples,  $\mu = 0.1104$  for Case I;  $\mu = 0.5011$  for Case II and  $\mu = 0.0276$  for Case III.

### 4.5 RELATIONSHIP WITH INTELLIGENT SUB-STATIONS

One of the required features of an intelligent sub-station as pointed out in section 1.3 of Chapter 1 is power quality analysis. It is understood that the power quality is getting poorer and poorer due to the increasing utilisation of power electronics equipment of high efficiency for energy conservation. The method of harmonics signature recognition can help the automatic devices inside an intelligent sub-station to carry out remedial actions, such as automatic filtering and compensation etc. Such measures will not just be beneficial to the power distribution system but to the consumers as well.

*Chapter V***NEURAL NETWORK APPLICATIONS IN SUBSTATIONS**

Artificial neural networks are simplified models of the nervous system. They are networks of highly interconnected simple computing elements (neuron) that have the ability to respond to input stimuli and to learn to adapt to the environment. Each neuron implements a local computation and its output is determined by its input and its interconnection to other neuron. The useful properties include parallelism, high level of interconnection, self organisation, learning, distributed processing, fault tolerance and graceful degradation. ANN have been shown to be effective for various applications including pattern recognition, associative recall, classification, data compression, modelling and forecasting. In supervised learning the training data set is composed of input and target output patterns. In unsupervised learning the training data set is composed solely of input patterns. The network learns the underlying features of the data and reflects them in its output. In this chapter, an Hopfield type neural network is used for the supply frequency and harmonic evaluation. A curve fitting approach is employed and the curve fit error is mapped to the energy function of the neural network. The neural network will be settled to a very low energy state automatically and the outputs of the neural network are the supply frequency and the harmonic components. The second part of this chapter reports the development of a new type of neural network which employ complex number operations. At present, most ANNs are built upon the environment of real numbers. However, it is well known that in computations related to electric power systems, such as load flow analysis and fault level estimation etc., complex numbers are extensively involved. The reactive power drawn from a substation, the impedance, bus bar voltages and currents are all expressed in complex number. Therefore, ANNs in the complex domain must be adopted for these applications although it is possible to use ANNs in the conventional way by breaking up a complex number into two real numbers representing both the real and imaginary parts. The application of this newly developed ANN on load flow analysis in a simple 6-bus electric power system is used as an illustrative example to show the merits of incorporating "complex" ANNs in power system analysis.

## 5.1 REAL-TIME FREQUENCY AND HARMONIC EVALUATION

The electrical power system has been increasing in complexity at a rapid rate in the last few decades. Many measures have been introduced to improve its reliability and security. However, the system is more and more polluted owing to the increasing use of power-electronic converters and controllers for industrial processes and drives, among other types of disturbing loads [56]. The effect is the contamination of the 50 Hz supply by a wide range of frequencies up to the radio frequencies, and thus power system monitoring becomes a necessity to check the state of health of the power network [57]. Well-proven techniques have been devised to monitor various significant quantitative measures such as RMS voltage, RMS current, power factor, active and reactive power, etc., under both steady and transient states. On the other hand, there has been difficulty in tracking the frequency if the signals are not clean. Harmonics monitoring is still considered not well developed [58]. Discrete Fourier Transform (DFT) has been a well known method for frequency spectra evaluation [59]. The main reason for the success of the DFT-based techniques for spectral analysis is the low computational requirement. The use of the FFT algorithms reduces the computational time required for evaluation of the DFT by several orders of magnitude. The method achieves this efficiency by eliminating redundancies appearing in the evaluation of different DFT coefficients. However, there are several inherent performance limitations in the DFT approach and they are due to the implicit windowing of the data that occurs when processing blocks of data with FFT. Windowing manifests itself as 'leakage' in the spectral domain [60]. Spectral leakage occurs when the time record data used by the FFT algorithm does not contain an exact integral number of power-frequency cycles or if it contains frequency components which do not correspond to one of the spectral lines. Since the power system frequency is subject to small random deviations, some degree of spectral leakage inevitably occurs. Moreover, DFT techniques for spectral analysis are inherently limited in terms of resolution (or the extent to which individual frequency components may be resolved) [60] and the fundamental frequency needs to be pre-assumed. These two performance limitations of the DFT approach are particularly evident when analysing short data sequences.

Recent studies have reported improvements on DFT based procedures which first estimated

the frequency and then applied the DFT using a window which was a multiple of the estimated period. A variety of numerical algorithms dedicated to frequency measurement have been published in the last decade. Use of zero crossing detection and calculation of the number of cycles that occur in a predetermined time interval is a simple and well-known method [61,62]. Though the use of zero crossing is simple and quite reliable even under low-level noise contamination [62], the accuracy will deteriorate in cases of very high-level harmonics distortion and the estimation time period is quite long since a multiple number of full cycles must be available before any estimation can be carried out. One method made use of the Taylor series technique and digitised samples of voltage at a relaying point [63]. Such a method suffers the same problems as with the zero crossing method. Another method made use of DFT as the starting point to estimate the fundamental phase angle recursively and then the fundamental frequency was fine-tuned based on the changes in the shifting of phase angles [64,65]. This method will only be successful if the fundamental frequency drift is very small. Otherwise, the spectral leakage has already imposed a very large error on the initial estimation of phase angles. The methods of linear least-square approach [66] and the utilisation of Kalman filtering [67] were developed. In most cases, the methods only considered the fundamental component and hence the existence of higher harmonics would seriously affect the results. The latest approach made use of non-linear curve fitting to estimate both the fundamental frequency and the higher harmonics [68,69]. By applying iterative Newton's procedure combined with an ordinary least-square technique, high measurement accuracy over a wide range of frequency changes and very fast algorithm convergency can be achieved. However, the computation work is intensive and demanding and thus, parallel computers must be employed for real-time calculation. This is the major reason why an artificial neural network is called in.

The implementation of neural network in harmonics monitoring is not a new concept [70,71]. This chapter proposes to apply the least-squares technique to harmonic extraction in time-varying situations with significant advantages together with the implementation of artificial neural networks. This system is real-time with very fast response and it can handle situations where information is not complete.

### 5.1.1 Non-linear Least-squares

The application of the least-squares approach to time-varying frequency and harmonic extraction is examined below. The least-squares approach is basically fitting the sampled waveform to a harmonic equation under the minimum total squared error criterion. Consider the following Fourier expansion of a current or voltage wave in the power system with  $n$  harmonic terms:

$$\begin{aligned} y(t) &= \sum_{k=0}^n A_k \sin(2\pi kft + \theta_k) \\ &= \sum_{k=0}^n (a_k \sin 2\pi kft + b_k \cos 2\pi kft) \end{aligned} \quad (5.1)$$

Assume that there are  $m$  measuring samples,  $(t_i, y_i)$  where  $i = 0$  to  $m-1$ . The objective is to estimate the values of  $a_k$ ,  $b_k$  and  $f$  in (5.1) so as to minimise the total squared error,  $E$ :

$$E = \sum_{i=0}^{m-1} \left( y_i - \sum_{k=0}^n (a_k \sin 2\pi kf t_i + b_k \cos 2\pi kf t_i) \right)^2 \quad (5.2)$$

By applying the Taylor's series expansion on  $E$ , Newton's method [72] can be used to solve the optimization problem. Let  $\mathbf{x} = [b_0 \ a_1 \ b_1 \ \dots \ a_n \ b_n \ f]^T$  be the vector of variables of the system being monitored. The iterative algorithm is then given as follows:

$$\mathbf{x}_{r+1} = \mathbf{x}_r - \mathbf{H}(\mathbf{x}_r)^{-1} \mathbf{g}(\mathbf{x}_r) \quad (5.3)$$

Newton's method offers high rates of convergence. If the functions are quadratic, it is possible to arrive at the minimum in a single step. However, the excessive computational requirement for obtaining the inverse of the Hessian matrix  $\mathbf{H}(\mathbf{x})$  and the gradient vector  $\mathbf{g}(\mathbf{x})$  makes the algorithm rather unsuitable for real-time applications. Therefore, the parallel operational capability of neural networks has to be used to speed up the applications.

### 5.1.2 Neural Network Formulation

As mentioned in the previous section, the computation of the Hessian matrix is very intensive. So, the dynamic gradient approach is employed with the aid of neural networks as it is not required to estimate  $\mathbf{H}(\mathbf{x})$ . It is possible to find the minimum of  $E$  by optimising on all variables but that will also be time-consuming and global convergence cannot be guaranteed. In this way,  $\mathbf{x}$  is segmented into two parts, i.e. the amplitude vector,  $\mathbf{m}$ , and the frequency scalar,  $f$ ;  $\mathbf{x} = [ \mathbf{m}^T, f ]^T$ . Therefore, the energy function,  $E(\mathbf{x})$ , can be minimised with respect to the vector  $\mathbf{m}$  and scalar  $f$  along the optimisation time scale,  $t$ , by implementing a dynamic gradient system [73,74], as shown:

$$\frac{d\mathbf{m}}{dt} = - \boldsymbol{\mu}_m \nabla E(\mathbf{m}) ; \frac{df}{dt} = - \mu_f \nabla E(f) \quad (5.4)$$

where  $\boldsymbol{\mu}_m$  = diagonal step size matrix  
 $\mu_f$  = frequency step size

For illustrative purpose, three typical elements of  $\nabla E$  are derived as shown:

$$\begin{aligned} \frac{\partial E}{\partial a_k} &= 2 \mu_{a_k} \sum_{i=0}^{m-1} (y_i - \sum()) \sin 2\pi kft_i \\ \frac{\partial E}{\partial b_k} &= 2 \mu_{b_k} \sum_{i=0}^{m-1} (y_i - \sum()) \cos 2\pi kft_i \\ \frac{\partial E}{\partial f} &= 4\pi \mu_f \sum_{i=0}^{m-1} (y_i - \sum()) R \end{aligned} \quad (5.5)$$

where

$$\begin{aligned} \sum() &= \sum_{k=0}^n (a_k \sin 2\pi kft_i + b_k \cos 2\pi kft_i) \\ R &= t_i \sum_{k=0}^n k [ -b_k \sin 2\pi kft_i + a_k \cos 2\pi kft_i ] \end{aligned}$$

The constants, 2 and  $4\pi$ , can be absorbed into the corresponding step size parameters. From (5.4), it can be seen that optimisation comes with two major blocks, the first block handling  $\mathbf{m}$  while the second block handling  $f$ . The first block is actually a linear optimisation by

assuming  $f$  is given. Initially,  $f$  is set to the nominal line frequency, i.e. 50 Hz. With the given  $f$ ,  $m$  is evaluated in the first block and the estimated  $m$  is fed to the second block for evaluating  $f$ .  $t_i$  is continuously increasing with the measured samples,  $y_i$ , and the two neural network based blocks are exchanging  $m$  and  $f$  and the process is repeating until the optimised value of  $m$  and  $f$  are obtained. The self-explanatory block diagram of the whole neural network is shown in Figure 5.1.

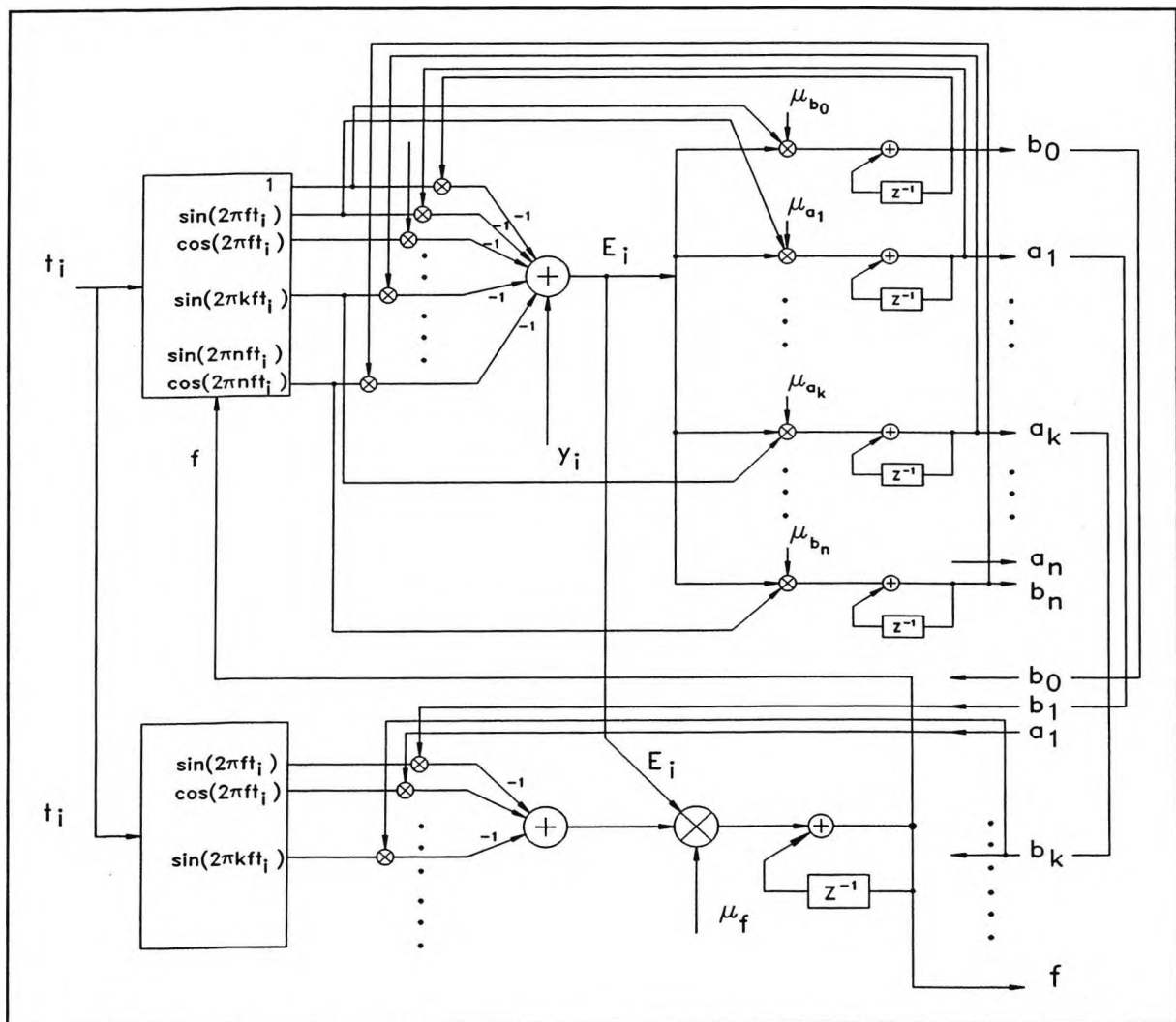


Figure 5.1 The Neural Network System for Frequency and Harmonic Evaluation

The  $z^{-1}$  module is a time delay operator for handling numerical integration; the  $\otimes$  module serves as a multiplier; the  $\oplus$  module serves as an adder while the two rectangular blocks are identical, preparing the updated sine and cosine tables. All  $\mu$ 's, in the neural network,

though different from one another, are kept constant throughout the whole learning and optimisation process. The general neural network consists of two sub-neural networks. The first sub-neural network has  $(2n+1)$  output nodes and 3 input nodes. The second sub-neural network has 1 output node and  $(2n+3)$  input nodes. Initial values are application specific, e.g.  $b_0 = 1$ ,  $a_1 = 220\sqrt{2}$  and other a's, b's = 0 for cases in voltage evaluation.

### 5.1.3 Model Validation by Simulation

In order to show the capability of the proposed system, a frequency modulated (with  $f$  fluctuating sinusoidally at 2 Hz between 46 Hz and 54 Hz), fundamental amplitude varying (amplitude exponential decaying) and harmonic amplitude changing (step change in the 15th harmonic amplitude at 0.25 s from 1 unit to 2 units) waveform is arbitrarily generated. The instantaneous waveform with a 4.8 kHz sampling rate is shown in Figure 5.2(a) and the results of monitoring are shown in Figure 5.2(b) - 5.2(f). The specifications are shown below:

*f fluctuating sinusoidally at 2 Hz between 46 Hz and 54 Hz;*

*$A_1$  decreasing from 300 V peak according to  $e^{-2t}$ ;*

*$A_{15}$  abruptly changing from 1 to 2 V peak values;*

*30 ms measurement window;*

*$k = 1, 3, \dots, n = 21$ .*

The trends are accurately reproduced provided that the 15th harmonic component is taken into account. It can be seen that the neural network system can accurately and efficiently trace the variations in fundamental frequency, which can never be done by conventional DFT as well as the variations in amplitude of each harmonic content. If only DFT is employed to detect the fundamental and 15th harmonic amplitude, Figure 5.2(e) and 5.2(f) will be produced, indicating a tremendous error in identifying the fundamental and 15th harmonic.

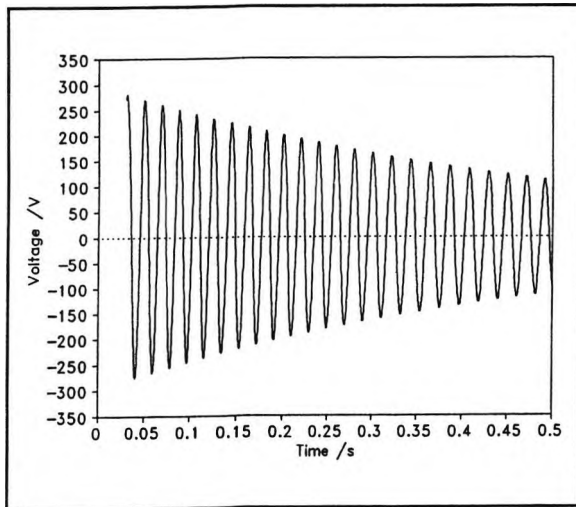


Figure 5.2(a) Instantaneous waveform by simulation

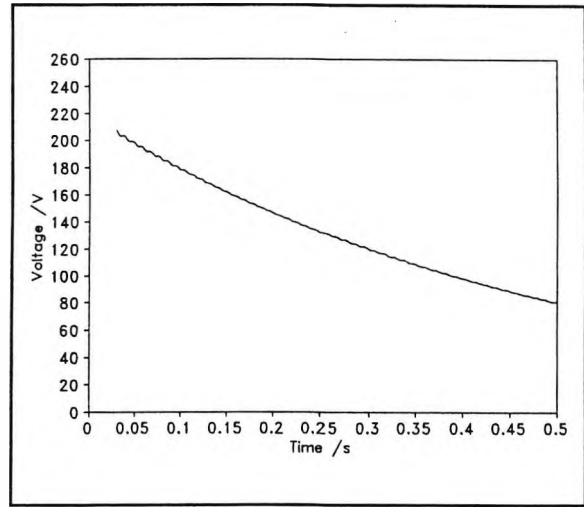


Figure 5.2(b) Extracted fundamental amplitude

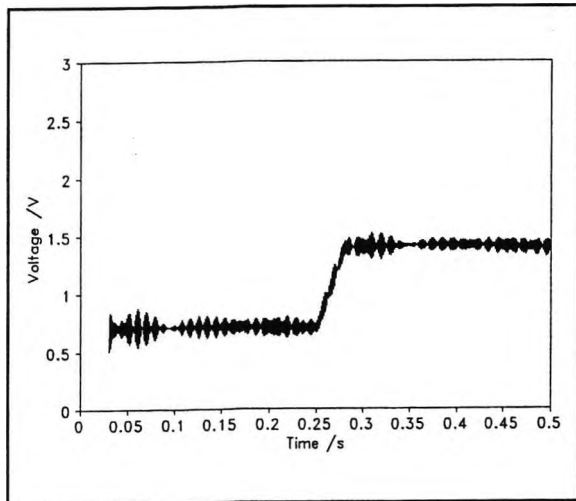


Figure 5.2(c) Extracted 15th harmonic amplitude

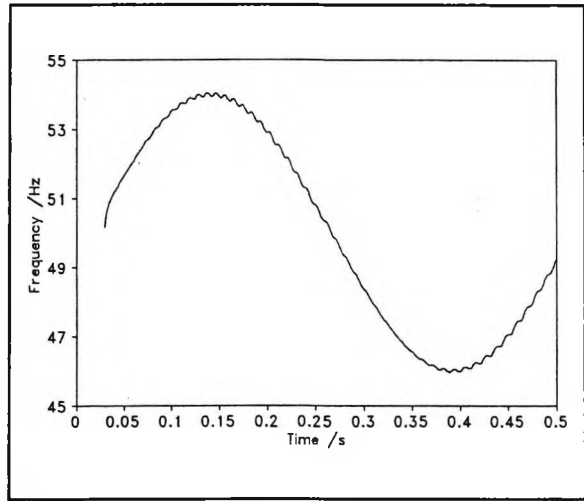


Figure 5.2(d) Extracted frequency variation

#### 5.1.4 Real Application of the System

In order to show that the system can keep track of the real world data to perform frequency and harmonic evaluations, the system is installed on site at a reputable commercial centre, City Plaza, in Hong Kong and a real-time waveform of 0.5 s is shown in Figure 5.3(a). The major load is a VVVF drive for an air-handling unit together with other power electronic loads such as personal computers and electronic gears for fluorescent lamps etc. Again, a 30 ms measurement window is adopted for the entire process. The length of the

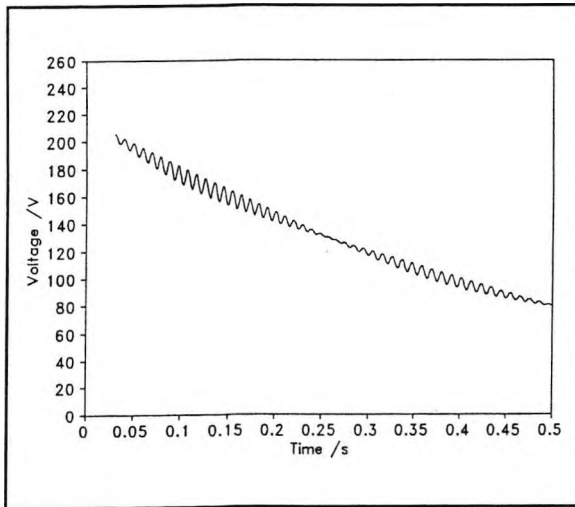


Figure 5.2(e) Extracted fundamental based on DFT

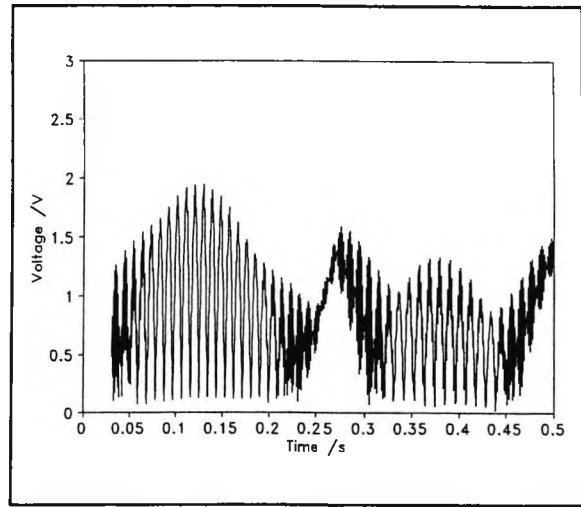


Figure 5.2(f) Extracted 15 th harmonic amplitude based on DFT

measurement window is arbitrary under the proposed algorithms and this is one of the merits of the whole system. From Figure 5.3(b), it can be seen that there is a slight variation of r.m.s. phase voltage over the period of monitoring but, in general, the voltage can be kept constant at around 223 V.

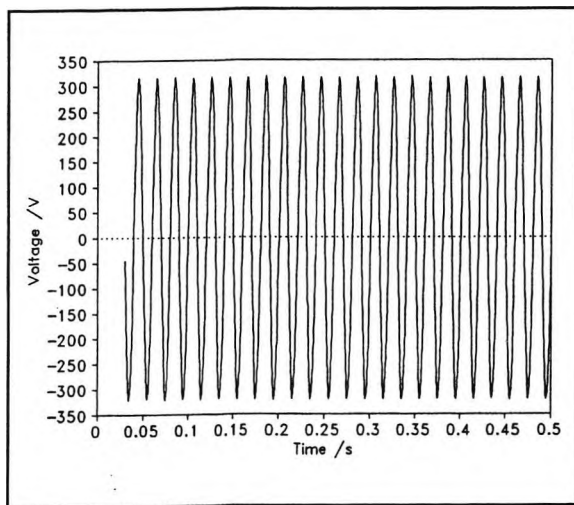


Figure 5.3(a) Instantaneous supply voltage waveform

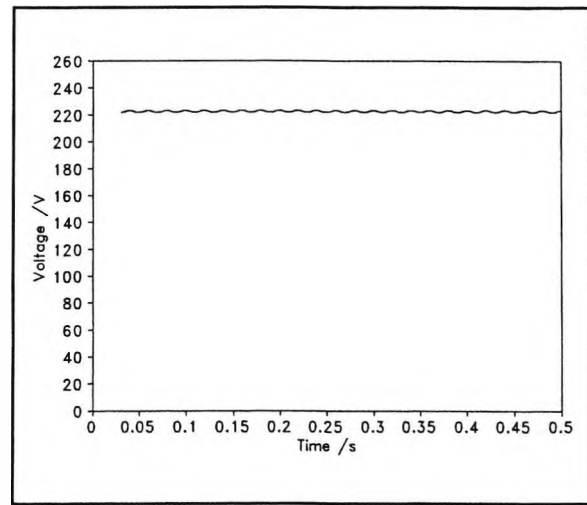


Figure 5.3(b) Extracted fundamental voltage by neural network

Figure 5.3(c) shows the amplitudes of the 3rd and 5th harmonics by the neural network system while Figure 5.3(d) shows the variation in mains frequency. It should be noted that there is continuous variation in the mains frequency and the absolute value is not at 50 Hz (49.92 Hz on average as given by the output of the neural-network), which cannot be handled

by the conventional DFT approach. Figure 5.3(e) and Figure 5.3(f) show the harmonics spectrum in terms of both amplitude and phase at time equal to 0.5 s.

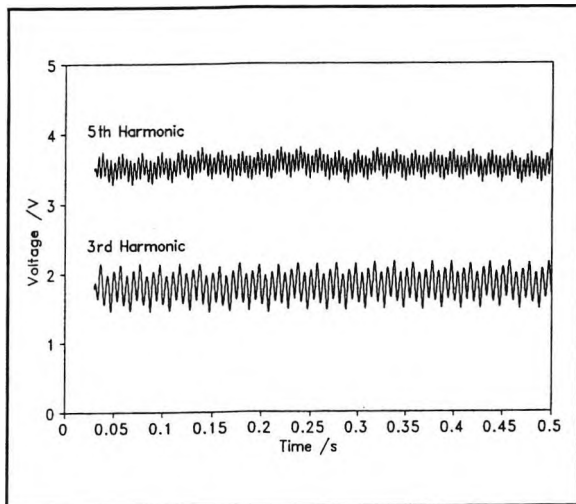


Figure 5.3(c) Extracted 3rd and 5th harmonic by neural network

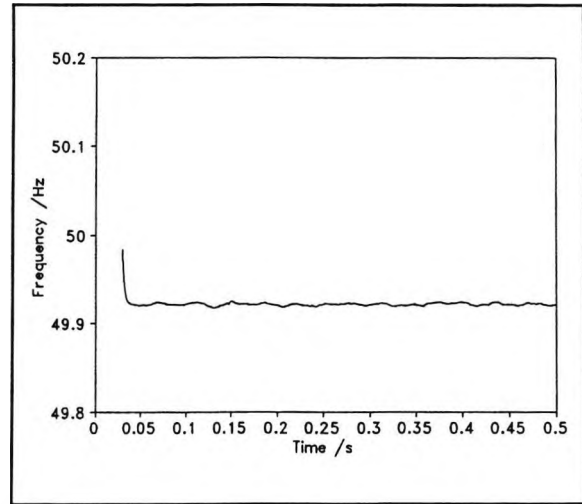


Figure 5.3(d) Extracted main frequency by neural network

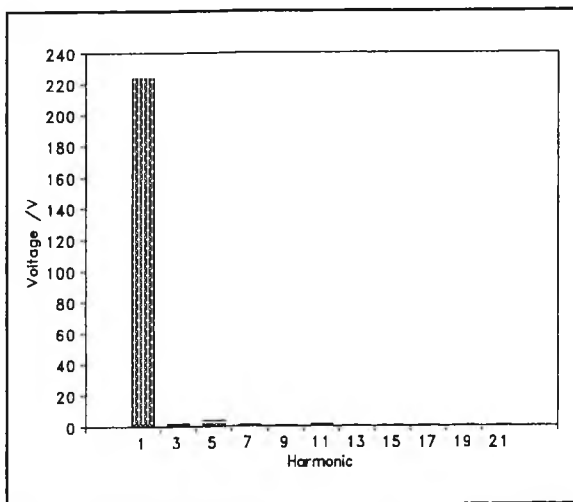


Figure 5.3(e) Extracted voltage harmonics spectrum at  $t = 0.5$  s

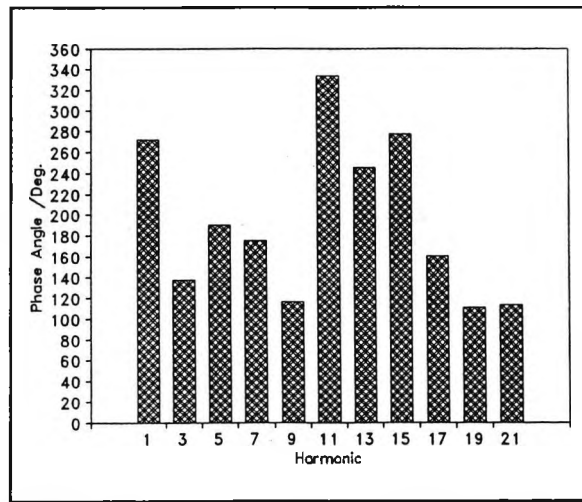


Figure 5.3(f) Extracted phase spectrum at  $t = 0.5$  s

The proposed method is designed to deal simultaneously with the measurement of the varying frequency, main-component amplitude and any harmonic component(s) present in the continuously changing power system. There is no theoretical restriction in the number of harmonic components to be evaluated except that the complexity of the neural network will be increased as the number of harmonic components is increased, the quantity of neurons

being proportional to the number of harmonic components to be evaluated. The computational loading simply increases rapidly as the expected number of harmonics becomes large. This imposes constraints on real-time tracking and it can be solved by parallel processing or the solution becomes obvious as the computational speed is greatly improved in the near future as technology is advancing. The estimation of all a's, b's and f in the network is parallel and thus a very high computational speed can be attained. The separation of f from a's and b's into two neural networks is a very particular choice because that will highly simplify the equation set, reducing the high non-linearity of the whole system. This action not only simplifies the design of the network but also greatly improves the rate and probability of convergence. The two examples, one by simulation and one by on-site real measurement, presented in this section illustrate the reliability of the method in extracting the multi-aspect information in one single operation. The major varying features of the signals are truly deduced by the proposed method. The results are no longer critically dependent on the choice of the measurement window. In many power applications, only the mains frequency and the fundamental voltage amplitude are of concern in the monitoring. Provided that harmonics pollution is the only form of contamination in the system, and the highest significant order of harmonic present can be established with confidence beforehand, the frequency and voltage information can be extracted by the proposed system with high fidelity under a real-time basis.

### 5.2 COMPLEX ARTIFICIAL NEURAL NETWORKS

ANNs have been proven to be capable of learning from raw data. They can be used to identify internal relations within raw data not explicitly given or even known by human experts and there is no need to assume any linear relationship between data. ANNs represent the promising new generation of information processing networks [75]. Advances have been made in applying such systems for problems found intractable or difficult for traditional computation. ANNs can supplement the enormous processing power of the von Neumann digital computer with the ability to make sensible decisions and to learn by ordinary experience. ANNs have widely been used in electric power engineering [10]. For energy management, load-flow [76] and optimal-power-flow problems were solved by ANNs [77].

However, most existing ANNs for electric power applications have been designed using real numbers. In power engineering, applications such as load flow analysis, phasor evaluation, signal processing and image processing etc. would mainly involve complex numbers. Although conventional ANNs are able to deal with complex numbers by treating the real parts and the imaginary parts independently, it will be shown in this paper that their behaviour is not so satisfactory. A new approach is introduced in this chapter where a computational ANN, particularly designed for manipulation of complex numbers in electric power systems, is described. It will be shown that this new "complex" ANN has a superior performance on operations and computations of complex numbers as compared with the conventional "real" counterparts. The "complex" ANN is implemented to estimate busbar voltages in a load flow problem.

### 5.2.1 Conventional ANN for Real Numbers

Figure 5.4 shows a typical ANN for real numbers where there are  $n$  number of input nodes,  $m$  number of hidden nodes and  $l$  number of output nodes, totally 3 layers. Of course, this network is freely extensible to any number of layers. All  $x$ 's and  $w$ 's in the network are real numbers and all outputs  $o$ 's are real numbers within an interval  $[0, 1]$ . The pre-superscript of each  $w$  identifies the layer to which that  $w$  belongs. A set of desirable outputs,  $d_k$ 's for  $k=1, \dots, l$ , corresponding to a set of inputs,  $x_j$ ,  $j=1, \dots, n$ , is used as a training set. The standard sigmoid function is employed and the following equations hold:

$$O_k = \frac{1}{1 + e^{-\sum_{i=1}^m {}^2 w_{ki} h_i}} \quad k = 1, \dots, l$$

$$h_i = \frac{1}{1 + e^{-\sum_{j=1}^n {}^1 w_{ij} x_j}} \quad i = 1, \dots, m$$
(5.6)

The following energy function,  $E$ , is being minimised,

$$E = \frac{1}{2} \sum_{k=1}^l [O_k - d_k]^2 \tag{5.7}$$

to obtain an optimal set of  $w$ 's using the "hill climbing" algorithm at the  $p$ th iteration step, and the following holds:

$$[w]^{p+1} = [w]^p - \lambda \nabla E$$

where  $\lambda = \text{step size} = 1.5$

$$\nabla E = \left[ \frac{\partial E}{\partial^2 w_{ki}} \Big|_{i=1, \dots, m} \quad \frac{\partial E}{\partial^1 w_{ij}} \Big|_{j=1, \dots, n} \right]^T \tag{5.8}$$

$$\frac{\partial E}{\partial^2 w_{ki}} = (O_k - d_k) O_k (1 - O_k) h_i$$

$$\frac{\partial E}{\partial^1 w_{ij}} = \sum_k (O_k - d_k) O_k (1 - O_k)^2 \cdot w_{ki} h_i (1 - h_i) x_j$$

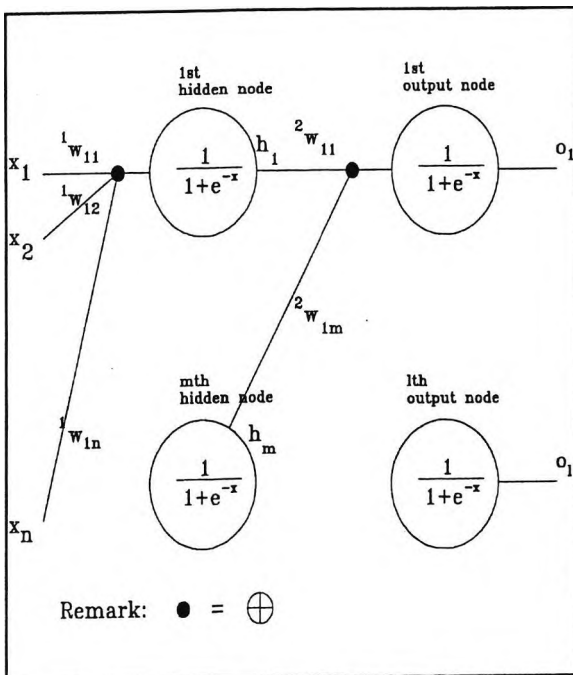


Figure 5.4 A Typical ANN for Real Numbers

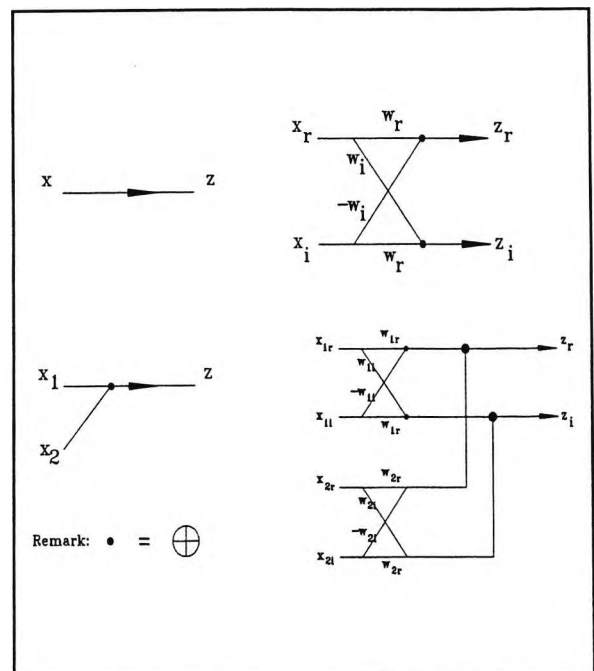


Figure 5.5 Basic Elements of Newly Designed "Complex" ANN

### 5.2.2 New ANN for Complex Numbers

Figure 5.5 shows the basic elements of the newly designed ANN for complex numbers. For the operation of a basic function, say  $z = w x$ , where  $x$  is the input complex number;  $w$  is the weighting and  $z$  is the output complex number, the upper part of Figure 5.5 is referred to and the operation is shown by equation (5.9). For the addition of two complex numbers,  $x_1$  and  $x_2$ , the operation is clearly shown in the lower part of Figure 5.5.

$$\begin{aligned} z_r + j z_i &= (w_r + j w_i) (x_r + j x_i) \\ &= (w_r x_r - w_i x_i) + j (w_i x_r + w_r x_i) \end{aligned} \quad (5.9)$$

$$\text{where } j = \sqrt{-1}$$

These basic elements form the foundation of the newly designed ANN for complex numbers. This new ANN was first proposed in 1996 [26]. The full configuration is shown in Figure 5.6 where it basically follows the format of Figure 5.4 but utilising new basic elements. Similarly, there are  $n$  number of input nodes,  $m$  number of hidden nodes and  $l$  number of output nodes. It should be noted that all nodes and weights are complex, a subscript of  $r$  indicating the real part while a subscript of  $i$  indicating the imaginary part.

The sigmoid function is similar to that used in the real ANN but it is a complex operation, as shown by equation (5.10).

$$\begin{aligned} \frac{1}{1 + e^{-(z_r + j z_i)}} &= \frac{1}{1 + e^{-z_r} \cos z_i - j e^{-z_r} \sin z_i} \\ &= \frac{\left[ 1 + e^{-z_r} \cos z_i \right] + j e^{-z_r} \sin z_i}{\left( 1 + e^{-z_r} \cos z_i \right)^2 + \left( e^{-z_r} \sin z_i \right)^2} \end{aligned} \quad (5.10)$$

Since this sigmoid function is highly non-linear and complicated,  $\nabla E$  needs to be done numerically. The method is to perturb each  $w$  by a very small amount while all other  $w$ 's

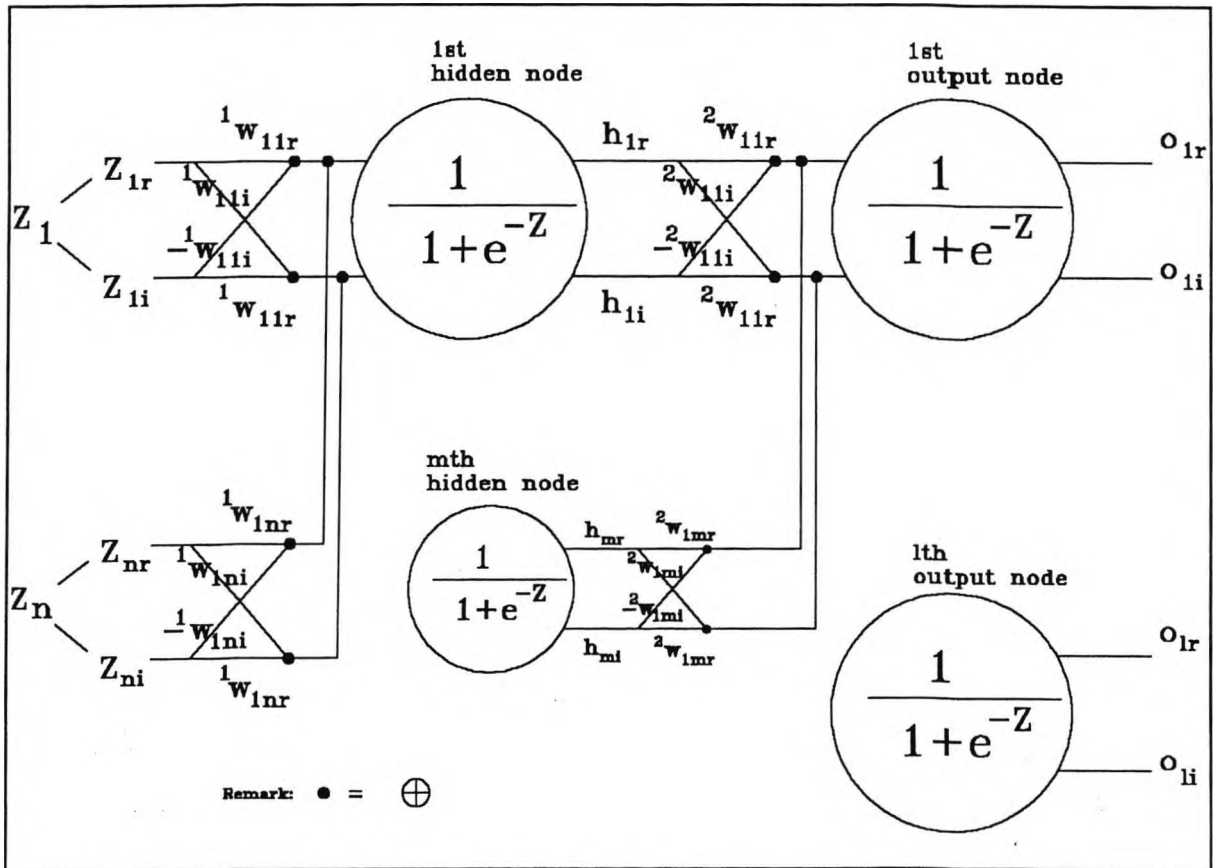


Figure 5.6 The New ANN for Complex Numbers

are kept constant. A new value of  $E$  is then evaluated. The ratio of the difference of the new  $E$  from the old  $E$  due to the perturbation gives the corresponding element in  $\nabla E$ .  $E$  itself now becomes a complex number and the gradient function refers to its magnitude, i.e.  $\|E\|^2$ , as defined by the following equation (5.11).

$$E = \frac{1}{2} \sum_{k=1}^l (O_{kr} - d_{kr}) + j (O_{ki} - d_{ki}) \tag{5.11}$$

$$\|E\|^2 = \frac{1}{2} \sum_{k=1}^l [ (O_{kr} - d_{kr})^2 + (O_{ki} - d_{ki})^2 ]$$

### 5.2.3 Comparison of the Two ANNs by Computer Simulation

In order to test the performance of the newly developed "complex" ANN versus the conventional "real" ANN in handling complex numbers, a simple function shown in equation

(5.12) is used.

$$O = x + \frac{1}{x} \tag{5.12}$$

$$\text{or } O_r + j O_i = x_r + j x_i + \frac{1}{x_r + j x_i}$$

A data set with nine training examples are available and shown in Table 5.1. During the training process, the total squared error of the output from the 9 training sets was continuously recorded. For the implementation on the conventional "real" ANN, there are 2 input nodes, 6 hidden nodes and 2 output nodes. For the implementation on the new "complex" ANN, there are 1 input complex node, 3 hidden complex nodes and 1 output complex node. All w's for both the conventional and new ANNs are set to "1" initially before training, i.e. a fair initial guess, and the step size,  $\lambda$ , is arbitrarily set to 1.5. The history of the squared error of the 9 training examples of the two ANNs during training is

O	x
5.1 - j4.9	0.1 + j0.1
2.1 - j3.8	0.1 + j0.2
1.1 - j2.7	0.1 + j0.3
4.2 - j1.9	0.2 + j0.1
2.7 - j2.3	0.2 + j0.2
1.74 - j2	0.2 + j0.3
3.3 - j0.9	0.3 + j0.1
2.61 - j1.34	0.3 + j0.2
1.97 - j1.37	0.3 + j0.3

Table 5.1

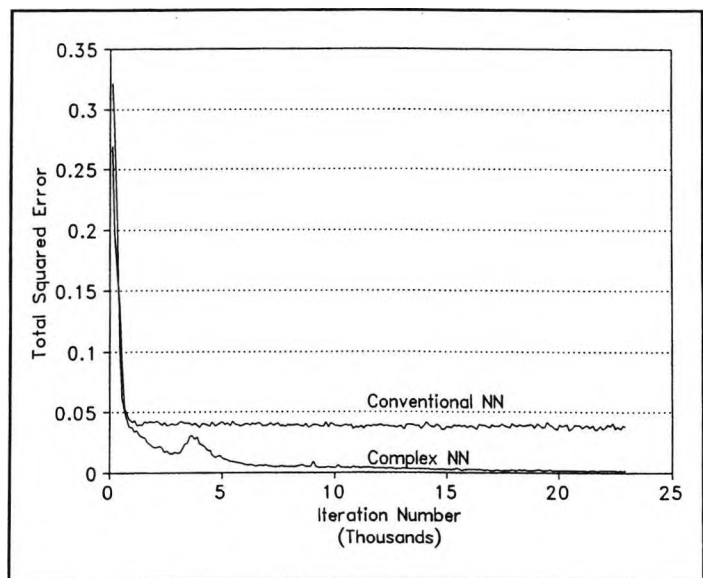


Figure 5.7 Error History of 2 ANNs under Training

shown in Figure 5.7. It can be seen that it takes 23,000 iterations for the "complex" ANN to arrive at a total squared error of  $10^{-3}$  or below while the "real" ANN can only achieve a total squared error of  $3.8 \times 10^{-2}$  after 23,000 iterations. After the two ANNs have been

trained up, a value of  $x = 0.25 + j0.25$  is fed into the two networks while the correct answer expected should be  $2.25 - j1.75$ . The "real" ANN gives an output of  $1.85 - j1.4$ , i.e. 19% error, while the "complex" ANN gives an output of  $2.3 - j1.75$ , i.e. 1.8% error. From this illustrative example, it can be concluded that it is better to use a "complex" ANN to handle systems involving complex numbers instead of using a "real" ANN to handle the real parts and imaginary parts separately. As mentioned in the introduction of this paper, complex numbers are widely used in electric power systems and thus, the "complex" design should be adopted whenever ANNs are applied to electric power systems. One typical example of applying the "complex" ANN to load flow analysis is shown in the following section.

### 5.2.4 Application of "complex" ANN to Load Flow Analysis

It was shown by Sprecher, Hornik, Funahashi and Cybenko that a multilayer feedforward

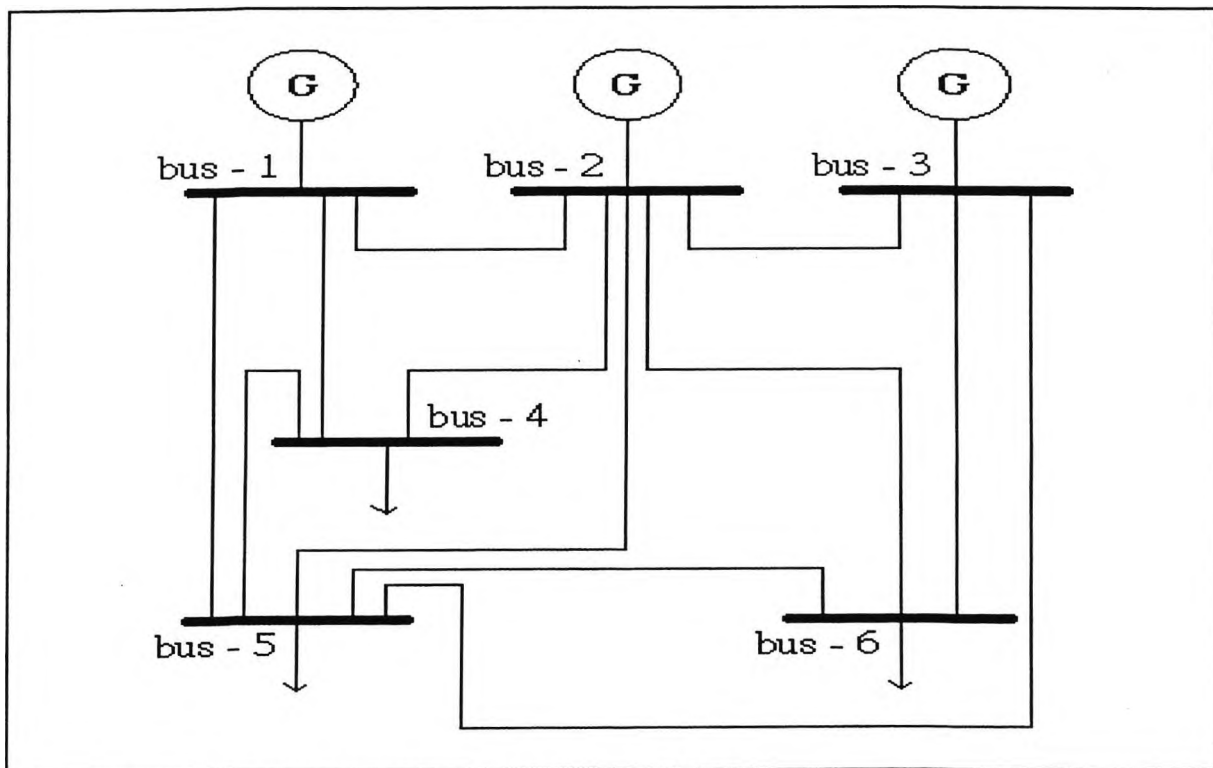


Figure 5.8 The 6-Bus Network for Load Flow Computation

neural network with one or more hidden layers is sufficient in order to approximate any continuous non-linear function arbitrarily well on a compact interval, provided sufficient

hidden neurons are available [78]. Power load flow problem is by itself a non-linear problem and hence, it can be analyzed with the help of an ANN. A 6-bus network, as shown in Figure 5.8, has been used to test the performance of the newly developed "complex" ANN. Bus-1, bus-2 and bus-3 are generator buses while Bus-1 is the swing bus. Bus-4, bus-5 and bus-6 are ordinary load buses where the P (active power) and Q (reactive power) are to be specified.

The details of the network parameters are shown in the two tables below:

From	To	R(p.u.)	X(p.u.)	B(p.u.)
bus-1	bus-2	0.1	0.2	0.02
bus-1	bus-4	0.05	0.2	0.02
bus-1	bus-5	0.08	0.3	0.03
bus-2	bus-3	0.05	0.25	0.03
bus-2	bus-4	0.05	0.1	0.01
bus-2	bus-5	0.1	0.3	0.02
bus-2	bus-6	0.07	0.2	0.025
bus-3	bus-5	0.12	0.26	0.025
bus-3	bus-6	0.02	0.1	0.01
bus-4	bus-5	0.2	0.4	0.04
bus-5	bus-6	0.1	0.3	0.03

Table 5.2

Bus	P <sub>load</sub>	Q <sub>load</sub>	P <sub>gen</sub>	V <sub>spec</sub>
bus-1	0	0	---	1.05
bus-2	0	0	0.5	1.05
bus-3	0	0	0.6	1.07
bus-4	P <sub>4</sub>	Q <sub>4</sub>	---	---
bus-5	P <sub>5</sub>	Q <sub>5</sub>	---	---
bus-6	P <sub>6</sub>	Q <sub>6</sub>	---	---

Table 5.3

The training example is generated by an ordinary load flow software using Newton-Raphson algorithms. This is just an illustrative example and therefore, in a real application, the "complex" ANN will continuously monitor the real-time state of the network in terms of voltage, P and Q.

14 training examples, as shown in Table 5.4, have been generated by the software package for learning by the two ANNs. In this case, the voltage at Bus-5 is to be estimated while the three generators are charged with the requirement of maintaining constant voltages at the corresponding busbars. Therefore, inputs to each ANN consist of P<sub>i</sub> and Q<sub>i</sub>, i = 4,5 and 6,

## Chapter V

i.e. 6 inputs to the "real" ANN and 3 inputs to the "complex" ANN. The output of each ANN is  $V_5$ , i.e. 2 output nodes for the "real" ANN and 1 output node for the "complex" ANN. Here, the subscript refers to the number of the load bus. All the other parameters associated with the network would remain unchanged during the trial test. The power load flow network is learned by the "real" and "complex" ANN under 14 combinations of  $P_4$ ,  $P_5$ ,  $P_6$ ,  $Q_4$ ,  $Q_5$ ,  $Q_6$  and  $V_5$ . The "real" ANN is a 6-2-2 network while the "complex" ANN is a 3-2-1 network so that the total number of weights inside the ANN is conserved. The initial values of all weights are random. Since the output of an ordinary sigmoid function for "real" ANN has a range  $[0, 1]$  and it is not suitable for this application, the sigmoid function was slightly modified to the following form:

$$\frac{2}{1 + e^{-x}} - 1 = \frac{1 - e^{-x}}{1 + e^{-x}} = \tanh\left(\frac{x}{2}\right) \quad (5.13)$$

The limit of iterations for both ANNs is set to 230,000 as in the case of section 5.2.3. Figure 5.9 shows the variation of the total squared error of the two ANNs with respect to the number of iteration.

$P_4 + jQ_4$ (p.u.)	$P_5 + jQ_5$ (p.u.)	$P_6 + jQ_6$ (p.u.)	$V_5$ (p.u.)
0.7+j0.7	0.7+j0.7	0.7+j0.7	0.975-j0.089
0.9+j0.9	0.9+j0.9	0.9+j0.9	0.864-j0.137
0.9+j0.7	0.7+j0.7	0.7+j0.7	0.969-j0.101
0.7+j0.9	0.7+j0.7	0.7+j0.7	0.960-j0.088
0.7+j0.7	0.9+j0.7	0.7+j0.7	0.962-j0.115
0.7+j0.7	0.7+j0.9	0.7+j0.7	0.944-j0.084
0.7+j0.7	0.7+j0.7	0.9+j0.7	0.964-j0.108
0.7+j0.7	0.7+j0.7	0.7+j0.9	0.951-j0.086
0.9+j0.7	0.9+j0.9	0.9+j0.9	0.883-j0.137
0.7+j0.9	0.9+j0.9	0.9+j0.9	0.872-j0.125
0.9+j0.9	0.9+j0.7	0.9+j0.9	0.903-j0.142
0.9+j0.9	0.7+j0.9	0.9+j0.9	0.882-j0.108
0.9+j0.9	0.9+j0.9	0.9+j0.7	0.894-j0.140
0.9+j0.9	0.9+j0.9	0.7+j0.9	0.880-j0.116

Table 5.4

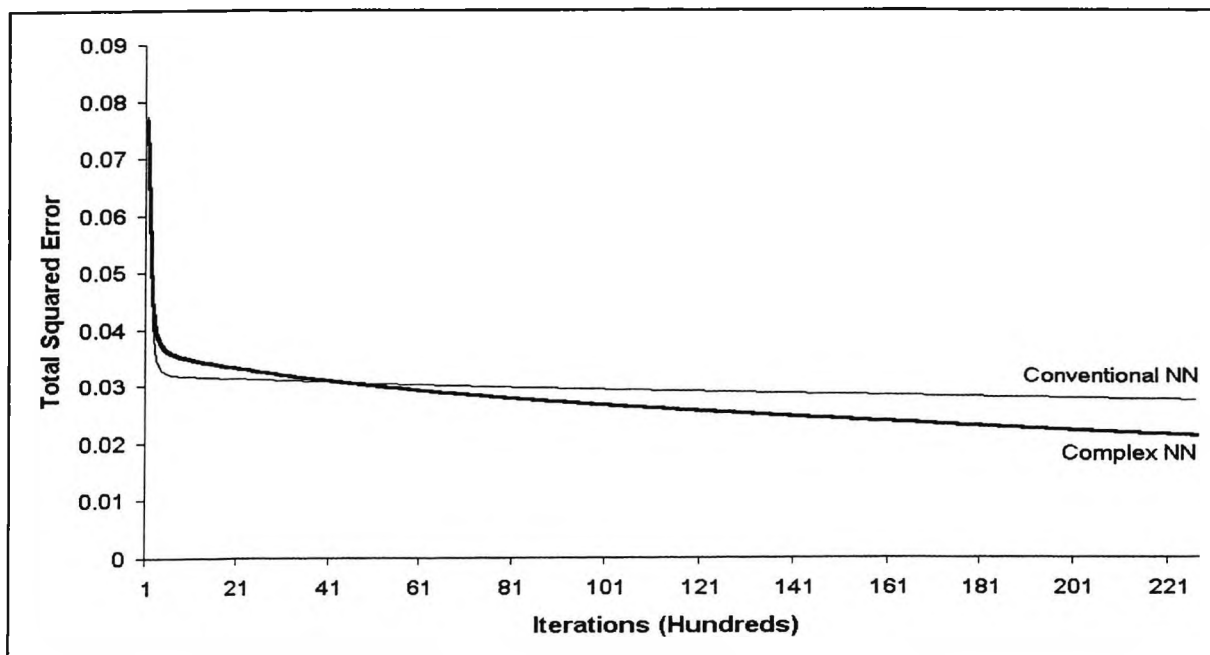


Figure 5.9 Training Errors of 2 ANNs for Power Load Flow

Although there are only 14 training examples, it can be seen that initially, the total squared error of the "real" ANN is smaller than that of the newly developed "complex" ANN. Actually, after 500 iterations, the total squared error of the "real" ANN has already attained a steady-state value, around 0.032. After 4,300 iterations, the "complex" ANN catches up with the "real" ANN and the total squared error is improving. After 23,000 iterations, the error is only 0.019. Actually, by comparing Figure 5.9 with Figure 5.7, one very interesting result can be noted. It seems that the "real" ANN can easily get itself into a minimum after a small number of iterations whereas, the "complex" ANN can continuously improve itself during the learning process. This is one merit of the newly developed "complex" ANN. After the two ANNs have been trained up, they are used to estimate  $V_5$  under different testing samples of  $P_i$ 's and  $Q_i$ 's,  $i = 4, 5$  and  $6$  as listed in Table 5.5.

Case	$P_4 + jQ_4$	$P_5 + jQ_5$	$P_6 + jQ_6$
1	0.77+j0.82	0.75+j0.79	0.84+j0.73
2	0.72+j0.76	0.88+j0.81	0.77+j0.80
3	0.83+j0.87	0.72+j0.79	0.82+j0.89
4	0.75+j0.77	0.82+j0.89	0.80+j0.76
5	0.84+j0.81	0.71+j0.77	0.79+j0.82
6	0.88+j0.81	0.83+j0.87	0.75+j0.82
7	0.80+j0.80	0.80+j0.80	0.80+j0.80
8	0.61+j0.69	0.92+j0.95	0.78+j0.67
9	0.58+j0.69	0.76+j0.94	0.97+j0.88
10	0.79+j0.87	0.61+j0.57	0.94+j0.68
11	0.60+j0.60	0.60+j0.60	0.60+j0.60
12	1.00+j1.00	1.00+j1.00	1.00+j1.00

Table 5.5

There are two categories of testing samples, first set being those  $P$ 's and  $Q$ 's randomly selected in between the limits of  $P$ 's and  $Q$ 's given in Table 5.4. Another set is randomly

selected outside the limits to test the ability of generalisation of the two ANNs. The results are shown in Table 5.6.

Case	$V_5$ /Correct	$V_5$ /Real NN	$V_5$ /Complex NN
1	0.941 $\angle$ -6.65	0.927 $\angle$ -6.88	0.938 $\angle$ -6.61
2	0.931 $\angle$ -7.09	0.927 $\angle$ -6.69	0.929 $\angle$ -7.17
3	0.918 $\angle$ -6.44	0.930 $\angle$ -7.10	0.925 $\angle$ -6.33
4	0.924 $\angle$ -6.84	0.928 $\angle$ -6.74	0.926 $\angle$ -7.07
5	0.937 $\angle$ -6.19	0.930 $\angle$ -7.04	0.936 $\angle$ -6.19
6	0.914 $\angle$ -7.10	0.931 $\angle$ -7.29	0.917 $\angle$ -7.08
7	0.931 $\angle$ -6.91	0.929 $\angle$ -6.99	0.928 $\angle$ -6.93
8	0.930 $\angle$ -6.98	0.925 $\angle$ -6.27	0.929 $\angle$ -7.05
9	0.903 $\angle$ -6.68	0.926 $\angle$ -6.51	0.928 $\angle$ -7.43
10	0.980 $\angle$ -6.33	0.930 $\angle$ -6.92	0.976 $\angle$ -6.24
11	0.995 $\angle$ -3.69	0.917 $\angle$ -4.82	0.962 $\angle$ -3.69
12	0.803 $\angle$ -12.2	0.939 $\angle$ -8.64	0.903 $\angle$ -10.2

Table 5.6

Table 5.5 and 5.6 are referred to for the following discussion. The first seven testing samples have been randomly selected in between the limits of [0.7, 0.9] of both P's and Q's. The "complex" ANN behaves better without exception in all cases. However, when five alternative testing samples, selected outside the limits, are tried, the "complex" ANN behaves better except in case 9. It appears that, in general, the "complex" ANN is more preferable for the present application and its readiness of generalisation is particularly useful.

It is generally accepted that the learning power of ANNs is useful in electric power system analysis. At present, most ANNs are built upon the environment of real numbers. However, it is well known that in computations related to electric power systems, complex numbers are extensively involved due to the existence of phase differences between different parameters. Naturally, the design of ANNs for electric power system analysis must shift towards the "complex" environment. A new "complex" ANN was developed for the relevant

applications. Operational elements, such as addition, subtraction and multiplication are shown graphically. A corresponding sigmoid function utilising a complex function is devised, resulting in a new gradient function for back propagation. In order to demonstrate that the newly designed "complex" ANN is superior to the conventional "real" ANN towards the manipulation of complex numbers, a simple function with 9 training samples is used. For illustration purposes, without loss of generality, a simple application of this novel technique is carried out in the load flow analysis of an electric power network consisting of six buses. A commercially available software package is used to generate 14 training samples and the voltage at a particular bus is estimated using the two trained ANNs. It is concluded that the "complex" ANN is superior to the conventional "real" ANN in three aspects. First, the "complex" ANN will not easily be trapped in a local minimum. Secondly, it has an improved ability of generalisation to evaluate cases not falling within the training zone. Finally, the sigmoid function employed in the ANN automatically handles the whole complex space with an absolute magnitude smaller than or equal to one. However, the user needs to suitably adjust the sigmoid function of a conventional "real" ANN when different output requirements are encountered. It is anticipated that this approach will be useful to other problems involving complex numbers such as signal processing and circuit analysis etc.

*Chapter VI***EVOLUTIONARY PROGRAMMING  
APPLICATION IN SUBSTATIONS**

Induction motors are the workhorses of many different industrial applications due to their ruggedness and versatility. They are used in power substations as fans and pumps. Although rotating machines are usually well constructed and robust, the possibility of incipient faults is inherent due to the stresses involved in the conversion of electrical energy to mechanical energy. Furthermore, the motors could well be exposed to different hostile environments and manufacturing defects. Internal motor faults as well as external motor faults are inevitable. In this chapter, an evolutionary programming approach is used for machine parameters estimation. Those parameters may be useful in the detection of motor fault at an early stage when the parameters estimated start to deviate from the nominal values. To become an intelligent substation, it is necessary to monitor the machinery inside the substation and detect any possible failure as soon as possible. The method described in this chapter is very useful and can be easily applied in intelligent substations.

**6.1 EVOLUTIONARY COMPUTATION**

Evolutionary computation comprises machine learning optimisation and classification paradigms roughly based on mechanisms of evolution such as biological genetics and natural selection. The evolutionary computation field includes genetic algorithms (GA), evolutionary programming (EP), genetic programming (GP) and evolution strategies (ES). The concept of chromosomes is central to genetic algorithms. Chromosomes are structures in cells or bodies that transmit genetic information. Individual patterns, or strings, in evolutionary computation systems are basically analogous to chromosomes in a biological system. Genetic algorithms are simple and powerful general purpose stochastic optimisation methods, which have been inspired by the Darwinian evolution theory of a population subject to reproduction, crossover and mutation in a selective environment where the fittest can survive. In

## Chapter VI

mathematical terms the goal of the GA is to maximise an objective function  $F(S_k)$ , where  $S_k$  is the search candidate which is the  $k_{th}$  individual in the population  $S$  (where the population is the set of possible solutions). The individuals of the population are expressed in a binary string form (chromosome) and the GA then manipulates these strings by using genetic operators (reproduction, crossover, mutation) to obtain improved solution (where the fittest individuals survive), until the optimal solution is obtained. Since GA uses stochastic operators instead of deterministic rules to search for a solution and also that many points in the space instead of a single point are searched simultaneously, it has a reduced chance of converging to a local minima. In addition to the production of a more global search, GA searches for many optimum points in parallel. Due to their robustness, speed, efficiency and flexibility, GAs have been used in various power engineering problems [10]. GAs can be used for combinatorial search problems that cannot be formulated as well-structured linear or non-linear optimisation problems. During each iteration step, which is called a generation, structures in the current population are evaluated and new generations are formed. The structures of the population are chosen by a randomised selection process, which ensures that the expected number of times that a structure is chosen, is approximately equal to that structure's fitness relative to the rest of the population. The less fit individuals in the population would die, and in order to search other points in the space, some variations are introduced into new population by using genetic recombination operators (crossover and mutation). Thus the fitter individuals are bred, i.e. two individuals are mated (crossover) and the offspring of the mated pair receives some characteristics of the parents. Fit individuals carry on mating, some of them mutate, thus the population undergoes various generation changes. After many generations, a population emerges, where the individuals will solve the problem well. Evolutionary programming algorithms are similar to genetic algorithms, but do not incorporate crossover. They rely on the survival of the fittest and mutation. EP works on real quantities and hence no chromosome encoding is required. Furthermore, crossover operator is not required to make the evolution process simpler and quicker. Although the rate of convergence of EP may be a little bit slower than that of GA, the overall speed could be faster than that of GA.

## 6.2 MOTOR INCIPIENT FAULT DETECTION

The monitoring, diagnosis and incipient fault detection of motors are important and difficult topics. With proper machine monitoring and incipient fault detection schemes, early warning can be achieved for preventive maintenance, improved safety and reliability of different operations. The importance of incipient fault detection is found in cost savings since one could detect potential machine failures before they occur. Breakdown maintenance is expensive because of the unplanned down time and possible consequential damages caused by equipment failures. In contrast, preventive maintenance is based on the belief that since degradation generally occurs before failures, monitoring the trend of machine degradation allows the degraded behaviour or faults to be corrected before they result in abrupt failure and machine breakdown. Early fault detection allows preventative maintenance to be scheduled for machines during a planned down time and it would prevent an extended period of down time resulting from extensive motor failure, hence improving the overall availability of the system. With proper system monitoring and fault detection schemes, the costs of maintaining the motors can be greatly reduced, while the availability of these machines can be significantly increased. On-line monitoring of induction machines in critical applications has been increasingly necessary to improve the machines' reliability and to minimise catastrophic failures. Microprocessor-based monitoring systems are of particular interest because they can be used for regular analyses of machine variables and for predicting possible fault conditions. Preventive maintenance can then be organised in a cost-effective manner. Different invasive and non-invasive methods for motor incipient fault detection have been reported [79,80]. Non-invasive schemes are those which are based on easily accessible and inexpensive measurements to predict the motor condition without dismantling the motor. These schemes are most suitable for on-line monitoring and fault detection purposes. The parameter estimation technique is widely used, even though it requires an accurate mathematical model and an elaborate understanding of the system dynamics based on a set of system parameters. These system parameters are usually chosen to reflect the motor conditions. There are many methods for machine parameter estimation including Extended Kalman Filter [81], Extended Luenberger Observer [82], ARMA estimation [83] and Genetic Algorithms [84] etc. However, all these methods have suffered the same problem in that the

serious power harmonics generated by the inverter of vector-controlled drives have not been carefully considered in detail. During the process of estimating the machine parameters, sinusoidal current and voltage waveforms are normally assumed and then appropriate control actions are carried out. However, that is not true for all PWM drives where substantial power harmonics exist. Therefore, errors are obtained by existing methods of parameter estimation. It can be clearly revealed from the conventional model matrix employed by researchers, such as the one shown below [65]:

$$\frac{d}{dt} \begin{bmatrix} i_{1d} \\ i_{1q} \\ \lambda_{2d} \\ \lambda_{2q} \end{bmatrix} = \begin{bmatrix} A & \omega_o & B & C \\ -\omega_o & A & -C & B \\ D & 0 & -\frac{R_2}{L_2} & E \\ 0 & D & -E & -\frac{R_2}{L_2} \end{bmatrix} \begin{bmatrix} i_{1d} \\ i_{1q} \\ \lambda_{2d} \\ \lambda_{2q} \end{bmatrix} + \frac{1}{L_s} \begin{bmatrix} V_{1d} \\ V_{1q} \\ 0 \\ 0 \end{bmatrix} \quad (6.1)$$

$$\begin{aligned} A &= -\frac{R_1}{L_s} - \frac{R_2 M^2}{L_2^2 L_s}; \quad B = \frac{R_2 M}{L_2^2 L_s} \\ \text{where} \quad C &= \frac{p \omega_r M}{L_2 L_s}; \quad D = \frac{R_2 M}{L_2} \\ E &= \omega_o - p \omega_r \end{aligned}$$

Here,  $\omega_o$  denotes the electrical stator angular speed whose definition is only physically realistic when the current waveforms are sinusoidal, i.e. without substantial harmonics. When current harmonics are serious, as in most cases of power electronics inverters, it is quite difficult to assume a well-defined magnetic flux rotating at an angular speed of  $\omega_o$ . The most updated research work in induction motor parameter determination [86] still made use of the assumption of sinusoidal waveforms due to the application of an equivalent circuit model. Another problem is that the three phase power supply to the A.C. machine from the inverter is never balanced. But most research studies [86] in the past few years assumed a balanced situation which was, in practice, quite difficult to achieve. Hence, the existence of power harmonics, the imbalance of inverter supply and the variation of rotor frequency must be taken into account when the machine parameters are to be identified. These are the major contributions of this chapter.

## 6.3 THE MACHINE MODEL

The conventional state equations of a general squirrel-cage induction machine are used [87] where the three phase voltages and currents are transformed to the 2-phase co-ordinate system, a, b in the stator and d, q in the rotor, are all referred to the stator. The basic matrix involving stator voltages, stator currents and rotor currents are shown below:

$$\begin{bmatrix} V_a \\ V_b \\ 0 \\ 0 \end{bmatrix} = \begin{bmatrix} R_1 + L_1 p & 0 & 0 & M p \\ 0 & R_1 + L_1 p & M p & 0 \\ M p & M \omega_r & L_2 \omega_r & R_2 + L_2 p \\ -M \omega_r & M p & R_2 + L_2 p & -L_2 \omega_r \end{bmatrix} \begin{bmatrix} i_a \\ i_b \\ i_d \\ i_q \end{bmatrix} \quad (6.2)$$

where  $p$  is the differential operator  $d/dt$ .  $i_d$  and  $i_q$  belong to the rotor;  $R_1$  and  $L_1$  belong to the stator;  $R_2$  and  $L_2$  belong to the rotor.  $M$  is the mutual inductance.  $\omega_r$  is the real-time rotating speed of the rotor. To re-arrange the equation for the ease of implementation in the computational program, the following abbreviations are employed.

$$\begin{aligned} X(t) &= \begin{bmatrix} i_a \\ i_b \\ i_d \\ i_q \end{bmatrix}; \quad B = \frac{1}{L_2 L_2 - M^2} \begin{bmatrix} L_2 & 0 \\ 0 & L_2 \\ -M & 0 \\ 0 & -M \end{bmatrix}; \quad u(t) = \begin{bmatrix} V_a \\ V_b \end{bmatrix} \\ A &= \frac{1}{L_2 L_2 - M^2} \begin{bmatrix} -L_2 R_1 & M^2 \omega_r & M R_2 & M L_2 \omega_r \\ -M^2 \omega_r & -L_2 R_1 & -M L_2 \omega_r & M R_2 \\ M R_1 & -M L_1 \omega_r & -L_1 R_2 & -L_1 L_2 \omega_r \\ M L_1 \omega_r & M R_1 & L_1 L_2 \omega_r & -L_1 R_2 \end{bmatrix} \end{aligned}$$

The general state space equation can be obtained:

$$\dot{X} = AX + Bu \quad (6.3)$$

The solution is:

$$\mathbf{X}(t) = e^{At}\mathbf{X}(0) + \int_0^t e^{A(t-\tau)}\mathbf{B}u(\tau)d\tau \quad (6.4)$$

and the approximate discrete solution is

$$\mathbf{X}(n+1) = e^{AT}\mathbf{X}(n) + \left[\int_0^T e^{A(T-t)}\mathbf{B}dt\right]\mathbf{u}(n) \quad (6.5)$$

where  $T$  is the sampling period which is equal to  $10^{-5}$  s in this case and  $\mathbf{X}(n)$  is the state at time  $nT$ .

#### 6.4 THE PARAMETER ESTIMATION

From equation (6.2), five useful unknown parameters need to be estimated, namely  $L_1$ ,  $R_1$ ,  $L_2$ ,  $R_2$  and  $M$ . However, two more parameters, namely  $i_d$  and  $i_q$ , though not so useful, need to be estimated as well, particularly because their initial values,  $i_{d0}$  and  $i_{q0}$ , at the beginning of a measuring window since they are not readily measurable as compared with  $i_a$  and  $i_b$ . Actually, the method is also good enough to estimate the real time rotor speed,  $\omega_r$ . However, in the experimental set-up, the speed sensor is available. For the sake of simplicity, within every measuring window of 100 samples, seven unknown variables are to be identified, i.e.  $L_1$ ,  $R_1$ ,  $L_2$ ,  $R_2$ ,  $M$ ,  $i_{d0}$  and  $i_{q0}$ . It is difficult to arrive at a global minimum for such highly non-linear situations by conventional methods of optimisation, such as hill climbing etc. In this case, techniques in evolutionary programming (EP) are employed instead. To use EP, a fitness function,  $F$ , is required, and it is similar to the cost function in conventional approaches. A measuring window consists of 100 samples, i.e. a period of 1/100 second, as the sampling rate is 10 kHz. Within this short period,  $\omega_r$  can be assumed constant and measured by the speed sensor. Initial values of the seven unknown parameters are randomly created and put into equation (6.3). It should be noted that  $V_a$ ,  $V_b$ ,  $i_a$  (and hence  $i_{a0}$ ) and  $i_b$  (and hence  $i_{b0}$ ) are all measurable. For each time step,  $t_i$ , within the measuring window, one can obtain  $i_{aci}$  and  $i_{bci}$  from equation (6.5) where 'c' denotes 'calculated'. For the  $i$ th time step, one has the measured  $i_{ami}$  and  $i_{bmi}$  where 'm' denotes 'measured'. The cost function,  $C$ ,

is then formulated as below:

$$C = \sum_{i=0}^{N_w - 1} \left[ (i_{ami} - i_{aci})^2 + (i_{bmi} - i_{bci})^2 \right] \quad (6.6)$$

where  $N_w$  ( $= 100$  in this case) is the number of samples within one measuring window. Then, by EP techniques, the seven parameters are iterated until the final solution is obtained. It should be noted that the fitness function,  $F$ , is generally chosen to be the reciprocal of the cost function, i.e.  $F = 1/C$ . Figure 6.1 are examples of the motor currents involved. The difference between the curves is the cost function.

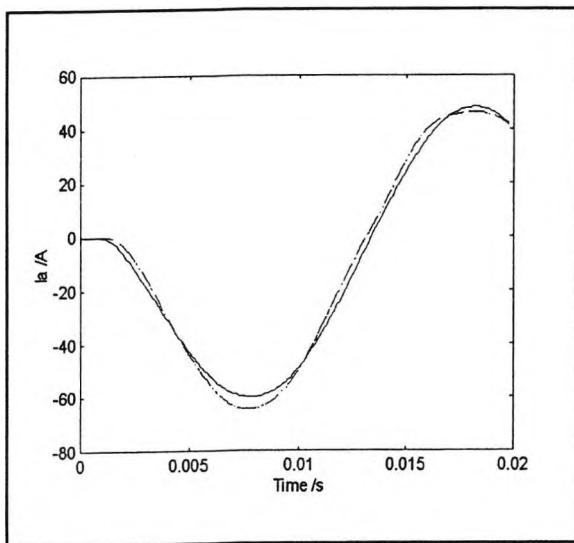


Figure 6.1(a) Waveform of  $i_{ac}$  and  $i_{am}$ (dash)

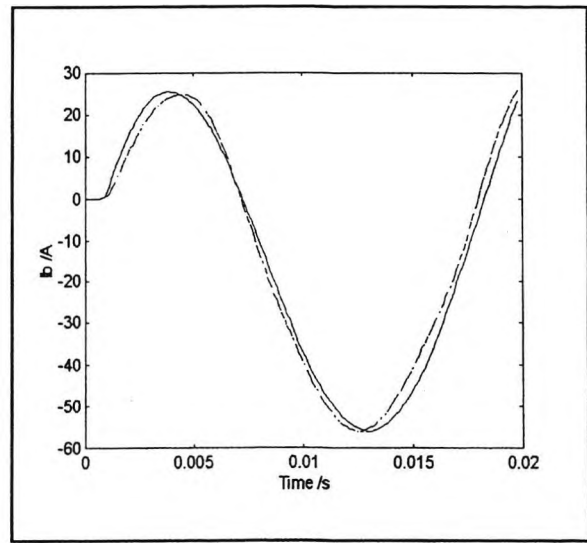


Figure 6.1(b) Waveform of  $i_{bc}$  and  $i_{bm}$ (dash)

### 6.5 EVOLUTIONARY PROGRAMMING

EP is a computationally intelligent method in which an optimisation algorithm has three steps, namely, natural selection, mutation and competition. The applications of EP on electric power engineering are not new [88]. According to the nature of the problem, each step could be modified and configured in order to achieve the optimal result. Each possible solution to the problem is called an individual. The mathematical form of the  $i$ th individual is:

$$p_i = [A_k^i] \quad k = 1, 2, \dots, m \quad (6.7)$$

where  $m$  is the number of parameters in any possible solution and  $A_{\min} < A_k^i < A_{\max}$ . In order to use EP, the mathematical model should be capable of dealing with the data type and structure of individuals. The EP algorithm has four main stages:

*Initialisation:* The initial population consists of individuals and is created randomly. The fitness score  $f_i$  of each  $p_i$  is obtained by a fitness function.

*Statistics:* The maximum fitness, minimum fitness, sum of fitness and average fitness of this generation are calculated.

*Mutation:* Each  $p_i$  is mutated in order to generate a new population.

*Competition:* Each individual  $p_i$  in the combined population has to compete with some other individuals to get its chance to be transcribed to the next generation.

The number of generations is determined by test or by monitoring the convergence of the system, e.g. the difference between maximum and minimum fitness. For clarity, the algorithm of EP adopted in this research is listed below in the form of pseudo code ('//' denotes a remark).

```
// start with an initial generation
g := 0;
// initialize a random (or reasonably known) population // of individuals
initpopulation P (g);
// evaluate fitness of all initial individuals of population
evaluate P (g);
// test for termination criteria (maximum number of // generations, fitness, etc.)
while not done do
// perturb the whole population stochastically
P' (g) := mutate P (g);
// evaluate its new fitness
```

```

    evaluate  $P'$  ( $g$ );
// select the survivors from actual fitness
     $P(g+1) := \text{survive } P(g), P'(g)$ ;
// increase the generation counter
 $g := g + 1$ ;
end while

```

The mutation method used is:

$$A_{i+m}^j = A_i^j + N(0, \beta)$$

where  $A_j^i$  is the  $j$ th element of the  $i$ th individual.  $N(0, \beta)$  is a Gaussian random variable with zero mean and variance  $\beta$ .  $\beta$  is controlling the mutation scale and it could be decreased during generations. The population size is arbitrarily chosen to be 30. After mutation, each generation will have 60 individuals. Afterwards, 30 most suitable individuals will be selected until the fitness function is maximised or the maximum number of generations, i.e. 10,000 in this case, has been attained.

## 6.6 THE EXPERIMENTAL SETUP

The experimental investigations were carried out under controlled loading conditions using a test bed capable of simulating a wide range of operating conditions, the test rig being equipped with a comprehensive instrumentation and PC-based data logging system enabling accurate control and measurement of the necessary thermal, mechanical and electrical parameters. The testing bed, as shown in Figure 6.2, consists of a 5.5 kW ABB induction motor (930 r.p.m., 12.7 A, 380-420 V delta connected, Class F, star connected in this experiment) coupled to a 10 kVA ABB DC generator (1000 r.p.m., Class F, 394 V<sub>max</sub>, 32.9 A<sub>max</sub>) via a HBM Alpha 3000 Torque Transducer that continuously monitors the dynamic torque on a real time basis. A variable speed drive, as shown in Figure 6.3, is used to control the speed of the induction machine. The output of the generator is controlled using a four quadrant converter. Electrical parameters, including voltage of each phase and current of each phase, real-time torque and motor speed are continuously sampled by a Yokogawa

DL708E digital scope, as shown in Figure 6.4, at a rate of 10 kilo-samples per second per channel for a total of eight channels.

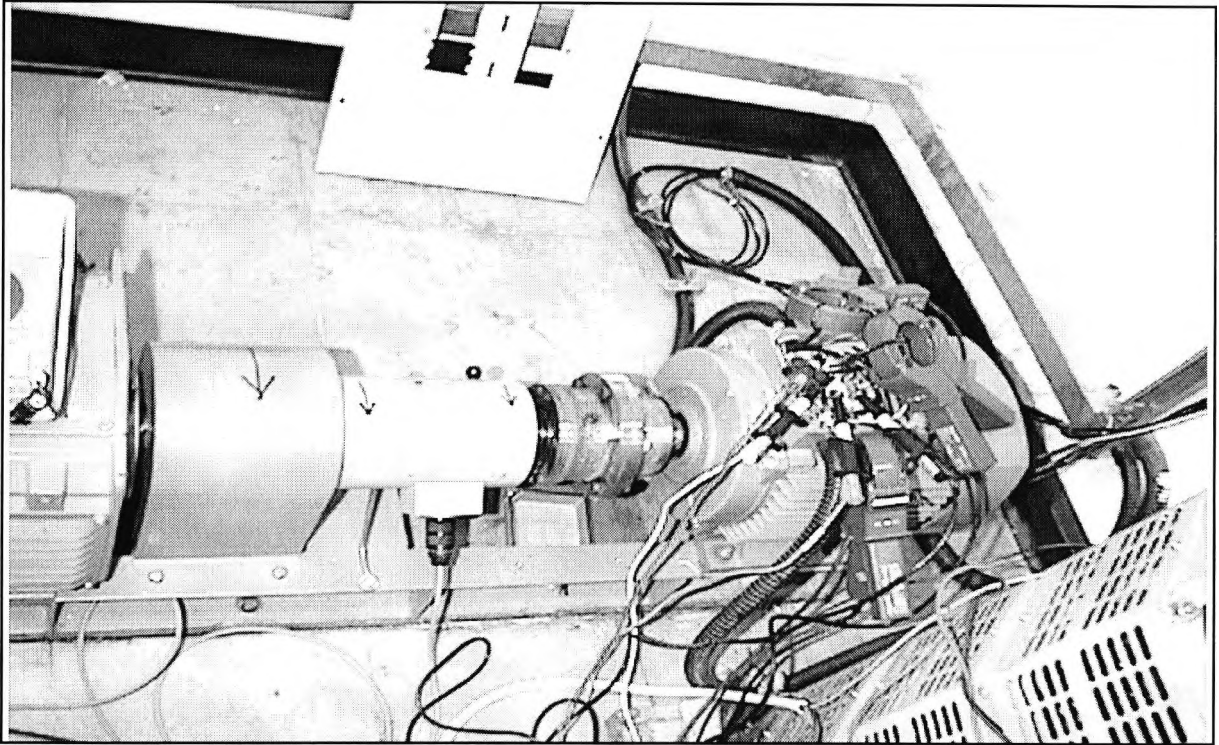


Figure 6.2 The A.C. motor - D.C. generator test bed



Figure 6.4 Yokogawa High Speed Digital Recorder

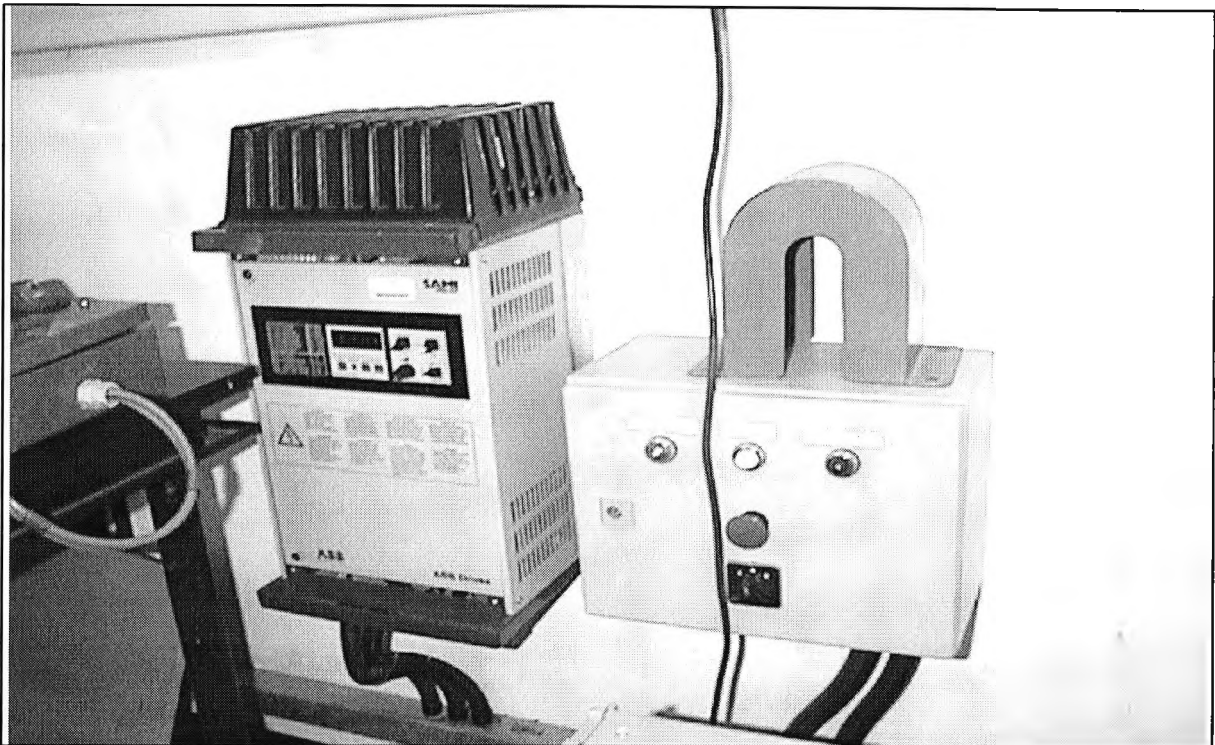


Figure 6.3 The ABB Variable Speed Drive

## 6.7 EXPERIMENTAL RESULTS

The A.C. induction motor was first started up without any load by direct-on-line method. Figure 6.5 shows the waveform of start-up current of the phase for the start-up period of one second. Figure 6.6 shows the torque variation during that start-up period of one second. Figure 6.7 shows the voltage waveform of red phase during start-up while Figure 6.8 shows the variation of rotor speed during start-up. Using the EP techniques, the machine parameters during the one second start-up period were estimated as follows:

$$R_1 = 2.335 \, \Omega; R_2 = 2.364 \, \Omega; L_1 = 0.416 \, \text{H}; L_2 = 0.402 \, \text{H}; M = 0.393 \, \text{H}.$$

As a comparative illustration, conventional method, conventional optimisation using steepest descent was employed. Three initial guesses by random generation were prepared and the final squared error in accordance with equation (6.6) are presented in Table 6.1 after the optimisation procedure is completed.

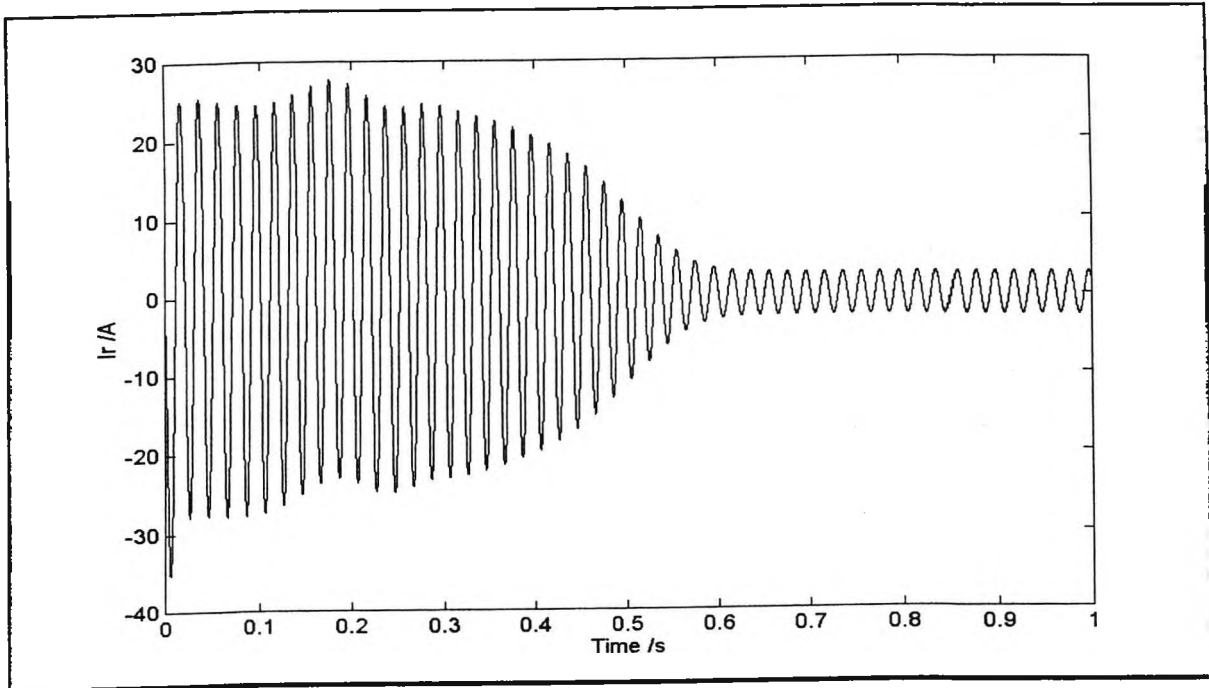


Figure 6.5 Start-up Current of Red Phase by DOL

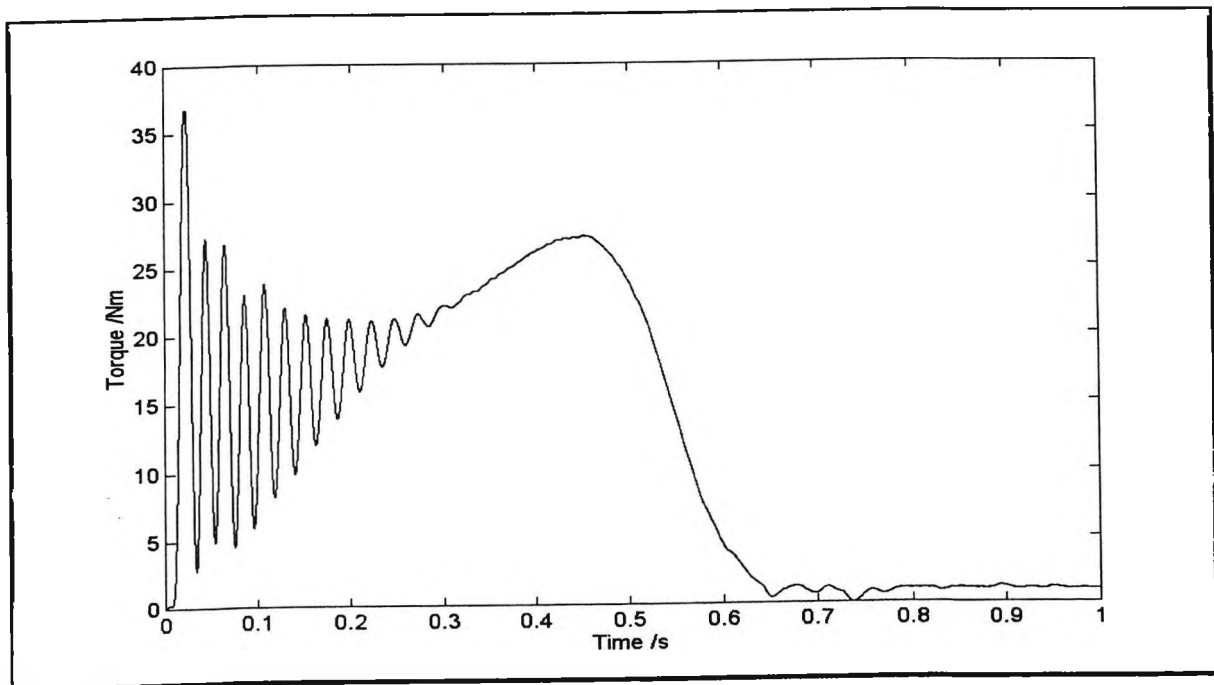


Figure 6.6 Torque Variation during Start-up by DOL

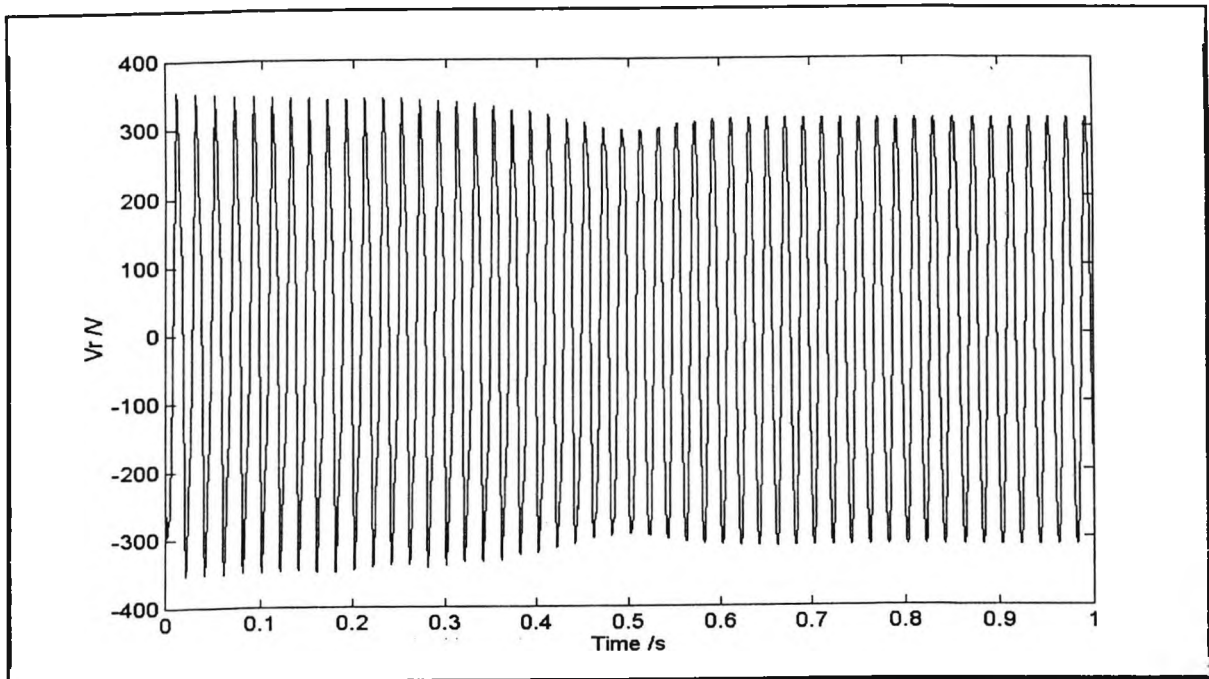


Figure 6.7 Start-up Voltage of Red Phase by DOL

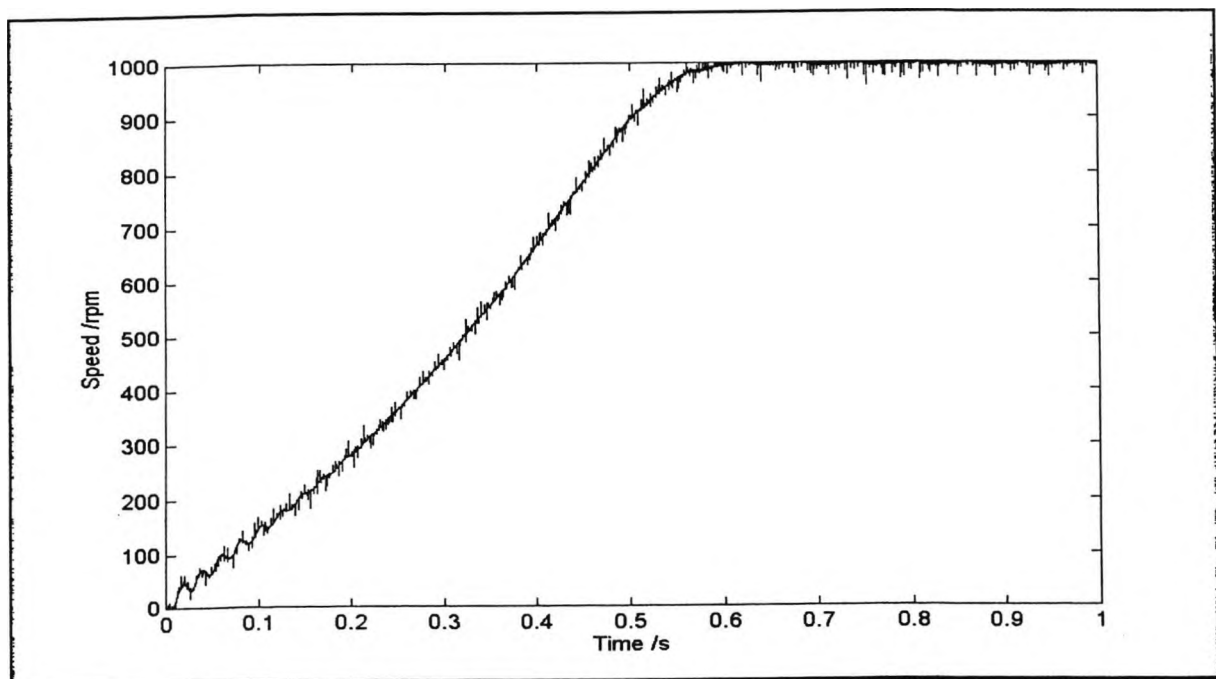


Figure 6.8 Rotor Speed Variation during Start-up (DOL)

In Table 6.1, the first three results were obtained by the conventional technique of hill-climbing while the last one was obtained by EP. It can be clearly revealed from Table 6.1

that the optimisation procedure is very dependent on the initial guesses and it can be easily trapped at a local minimum. For EP-based optimisation, a randomly selected initial guess is used and the squared error is the minimum as compared with the other three. Based on a literature review of EP research, it is believed that it is much easier to arrive at the global minimum by using EP. This is the strong justification why one need to adopt EP techniques to handle this problem.

	$R_1$	$R_2$	$L_1$	$L_2$	M	Error
initial guess	0.100	0.100	0.120	0.100	0.100	
final	0.149	0.159	0.311	0.009	0.051	1472
initial guess	0.500	0.500	0.300	0.400	0.300	
final	0.620	0.652	0.562	0.083	0.209	1405
initial guess	5.000	2.000	0.500	0.400	0.390	
final	4.955	1.966	0.317	0.541	0.393	3606
final	2.335	2.364	0.416	0.402	0.393	1399

Table 6.1

Next, the A.C. machine was started up using the ABB variable speed drive using a built-in soft start-up algorithm. The whole start-up event took about 1.5 second. For clarity, only the first 0.5 second event is shown for the voltage and current waveforms. Figure 6.9 shows the current waveform of the red phase during the soft start-up. Figure 6.10 shows the voltage waveform of the red phase during the soft start-up. From Figure 6.10, it can be seen that the harmonics contents within the voltage waveforms were extremely serious, making all conventional methods of machine estimation fail or produce unacceptable errors. Furthermore, as seen from Figure 6.9, the supply frequency varied significantly within the 0.5 second interval of soft start-up. Hence, if the supply frequency was unknown at any point during the start-up process and FFT was employed to identify the supply frequency as

in conventional approaches, substantial spectral leakage could be the major problem in making the machine parameter estimation fail as well.

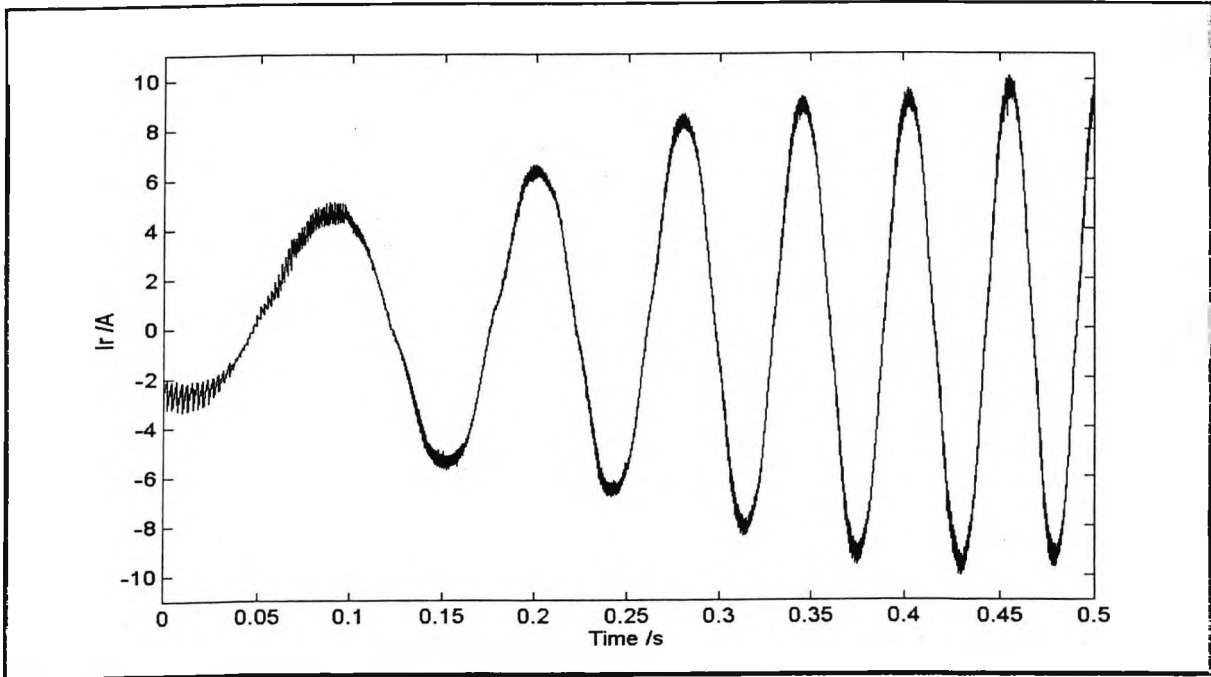


Figure 6.9 Current Waveform during Soft Start-up

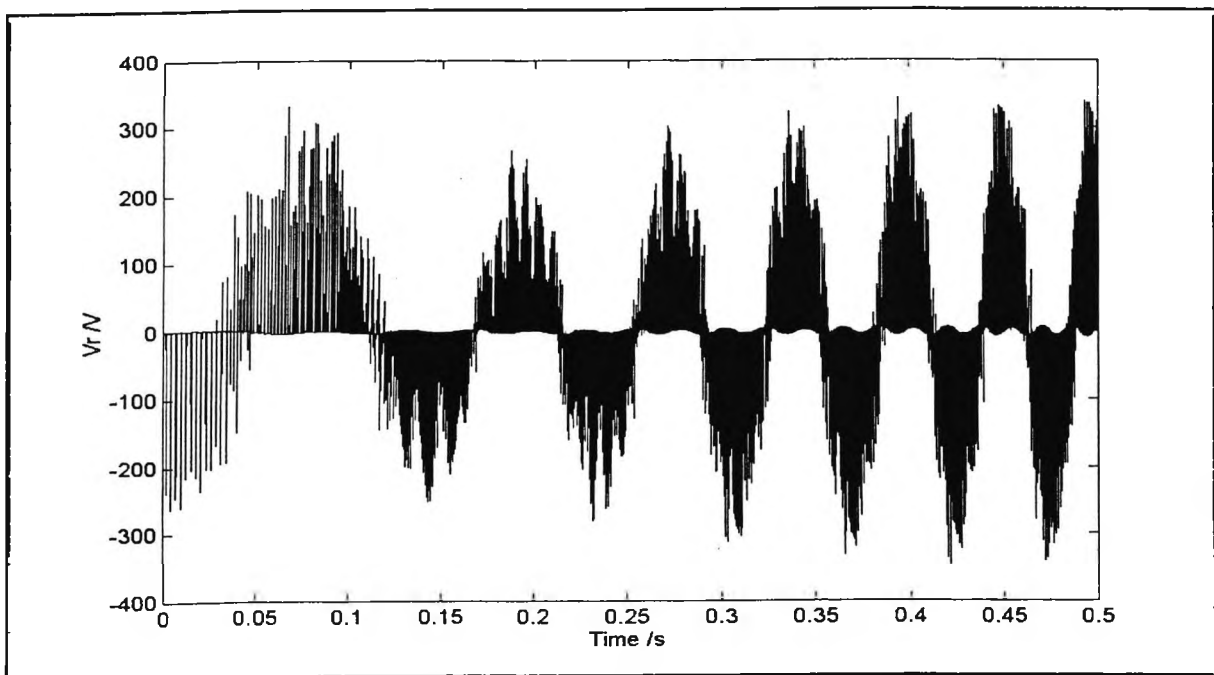


Figure 6.10 Voltage Waveform during Soft Start-up

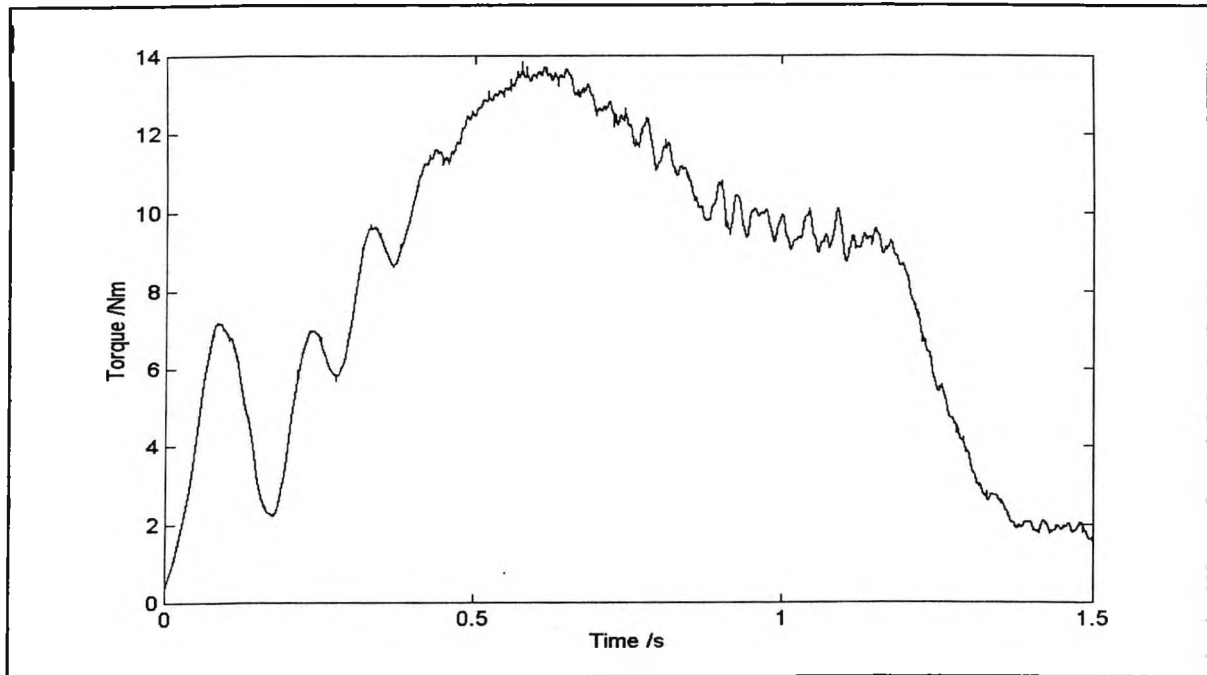


Figure 6.11 Torque Variation during Soft Start-up

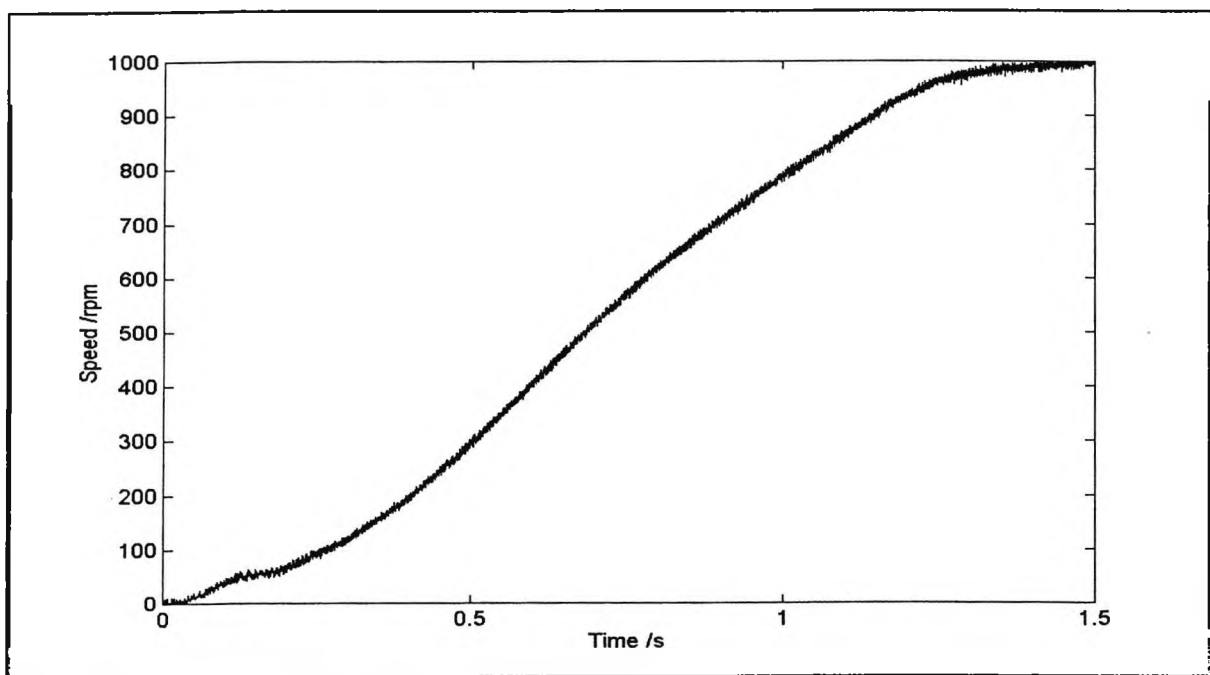


Figure 6.12 Rotor Speed Variation during Soft Start-up

For the sake of completeness, Figure 6.11 shows the variation of torque during the soft start-up event of 1.5 second. Figure 6.12 shows the variation of rotor speed during the start-up

event. Using the EP techniques again, the machine parameters during the 1.5 second soft start-up period were estimated as follows:

$$R_1 = 2.339 \Omega; R_2 = 2.368 \Omega; L_1 = 0.414 \text{ H}; L_2 = 0.400 \text{ H}; M = 0.396 \text{ H}.$$

It can be seen that the machine parameters could be accurately estimated during the two totally different start-up processes. The direct-on-line start-up process did not involve substantial harmonics contents with both the voltage and current waveforms. Whereas, the soft start-up process using a vector-controlled drive did generate tremendous distortion in the voltage and current waveforms during the start-up transient period. The slight increase in the R's may probably be due to skin effect of the current harmonics.

### 6.8 APPLICATIONS IN INTELLIGENT SUB-STATIONS

Regarding on-line parameter estimation, it should be noted that if one starts the EP process with a randomly selected initial population, past experience has revealed that it normally takes thousands of generations for full convergence. And under this convergence rate, the system is not suitable for real-time parameter estimation under applications such as real-time field oriented control. However, it is possible for us to have a trial run with the machine and carry out off-line estimation up to a reasonable degree of accuracy. Then, one can always make use of these results as the initial population of the EP process during subsequent applications to achieve an on-line application. It is first addressed in the beginning of the chapter that on-line machine parameter estimation is also very useful for motor fault detection which is increasingly popular.

The philosophy here lies with the fact that if a transient model can truly reflect the real-time performance of the machine and this transient model is closely related to the voltage and current waveforms, the change in the transient model will reflect something to us. It may be the natural change in certain parameters that are speed or temperature dependent. At the same time, it may be due to some defects inside the machine. Therefore, the idea of using EP-based parameter estimation based on true waveforms for fault finding works provided that

two conditions are met. First, the transient model can really reveal the defect. Second, the human operators have got enough experience to identify the existence of defects based on the changes in the parameters. For the first condition, if one day a new transient model comes out that can represent the machine more accurately, the new model can immediately be switched in to integrate with this EP-based method. For the second condition, more experiments are needed to build up a comprehensive document of experience so that different faults can be identified without much difficulty. This condition also applies to the conventional fault detection of rotating machines using vibrational analysis.

Most conventional approaches in parameter estimation have not taken into account the four major problems, i.e. harmonics, frequency variation, imbalance of the three phases and the changes in resistance due to skin effect. A new approach has been developed where it is not necessary to assume a smooth rotating magnetic flux being produced by sinusoidal three phase currents. The equivalent circuit model adopted by most researchers also relies on sinusoidal voltages and currents which do not normally exist in the real world. In this model, different voltage waveforms can be injected into the three stator windings and results of the seven important machine parameters can be obtained with high accuracy, even under non-sinusoidal supply.

In order to arrive at the global minimum, evolutionary programming techniques have been employed and the result has been satisfactory. From references [84] and [88], it is known that the intelligent techniques, such as EP and GA, could achieve better results than that obtained by the conventional techniques, e.g. the Newton Raphson method. Actually, the author has clearly demonstrated this argument using the parameter estimation exercise, as shown in Table 6.1. For simplicity during development, the rotor speed is measured. But it is possible to treat rotor speed as another unknown variable as well during the estimation process, though more sampling points within a measuring window may be required. This point further justifies the usefulness of this new method. Furthermore, if a random population is always used as the beginning of the EP process, this approach cannot guarantee a real-time parameter estimation. But if values have been obtained during off-site estimation that are close enough to the true solution, on-line parameter updating is still possible. It is

## Chapter VI

anticipated that this approach has great potential in machine parameter estimation as one deals with sample-by-sample iteration. If a new machine transient model is invented in future, this method can easily be applicable to the new model as well.

**Chapter VII****CONCLUSION AND FURTHER WORKS**

In this thesis, the importance of power substations towards the whole electric power transmission system has been highlighted and comments have also been made on the shortcomings of existing power substations which are designed and constructed based on a conventional approach. The concept of an *intelligent substation* has been explained in the first chapter. In order to design and build a substation for the next century and to catch up with the level of information technology of the coming age, one needs the provision of intelligent substations in order to improve the reliability and efficiency of the electric power transmission system. As a summary, there are quite a number of achievements arising from the results of the various systems developed as reported in this thesis.

**7.1 MAJOR ACHIEVEMENTS**

Primarily, a fundamental design platform for distributed monitoring and control was developed. The hardware and software of this platform was well tested and trial running was satisfactory in three power substations of the CLP Power. A proprietary high speed communication network was used to link all the microcontrollers. Important data inside the power substation, including real-time status, were recorded, analyzed and further transmitted to a master personal computer inside the substation. Via standard modems, the data could be transmitted back to the control centre for further processing and logging. Moreover, computer vision and Internet based technologies were also introduced into the upgraded version. Here the computer vision helps to give the shift duty staff inside the control centre a solid picture of what is happening inside the substation on a real-time basis. Normally, the substation is a forbidden area, excluding any unauthorised person to break in to disturb the machines there and thus ensuring a high reliability of the transmission process. The computer vision system could take a snap shot of any unauthorised intruder and appropriate action could be taken by the control centre. Another common problem for duty engineers is the bad

## Chapter VII

weather, e.g. heavy rain results in flooding inside the substation. A real-time image could certainly help the staff in the control centre to discover the existence of any natural disaster. Conventionally, alarms are transmitted based on the feedback from a sensor but very often, the sensors give false alarms. As most power substations are quite remote from the control centre, it would be wasteful in manpower if one requires the engineers to attend the site and then discover that it is a false alarm. Computer vision can also give the duty staff some direct evidences as whether an alarm is genuine or false, thus saving lots of manpower.

The ingredients necessary for incorporation into an intelligent substation were described in detail in this thesis. Guidelines of upgrading existing substations into intelligent substations could be formulated based on the features stated in this thesis. All the experimental results have shown that the proposed intelligent substation was totally feasible. Actually, this concept had been extensively developed in the field of building automation, the major difference being that reliability and security should be given the proper emphasis as compared with that in building systems. The ability of promoting the concept of condition based maintenance in power substations as one major function could also be made easier. It is concluded that condition based maintenance is the most efficient way of ensuring the highest reliability of operation of each device with the lowest cost of maintenance.

Techniques in artificial intelligence were employed to upgrade the standard features of the basic platform of monitoring and control. An artificial neural network on the complex domain was developed so that the accuracy and speed of convergence on the applications in the load flow analysis could be improved. A fuzzy expert system was used to aid the diagnosis of power equipment for conditioned based maintenance. Later, fuzzy numbers were used of to represent the spectrum of power harmonics in terms of magnitude and phase angle. An optimisation function involving operations of fuzzy numbers was suggested and tested. The most recent development involves the adoption of evolutionary programming to estimate the parameters of a rotating machine inside a power substation. Real-time current and voltage waveforms were recorded for the purpose of fine-tuning the machine parameters. Furthermore, parameter estimation can be a useful tool for condition based maintenance of the machine as well.

## Chapter VII

Reactive power control has been a very important control aspect of the substation using capacitor bank switching and transformer tap changing. Conventionally, power factor has been the major control parameter. In this thesis, the idea of using both the power factor and the reactive power consumption as the control parameters was discussed and implemented with a fuzzy control system. Furthermore, facilities for power quality monitoring were developed. With the advent of power electronics, the power system is getting more and more polluted. In order to maintain a healthy transmission system, the power quality of all feeders should be closely monitored. The artificial neural network developed could evaluate the real-time frequency of the supply so as to arrive at a more accurate estimation of the power spectrum.

This project provides a foundation for engineers to extend the concept of intelligent substations to the low voltage consumer substations as well, i.e. those substations with transformers stepping down the electric power from 11 kV to 380 V. In this way, full integration via a wide area network of all substations from the generating plants down to the consumer transformer rooms could be accomplished. The idea of re-structuring as different power supply companies are going to share the same substation can be made successful more readily. Without this integrated communication link, it will be very difficult to implement such an idea. As the trend of energy concern is still growing, demand side management will become a major issue in the power industry. The system described in this thesis may form the hardware basis of such management strategy.

### 7.2 FUTURE WORKS

The concept of intelligent substations can be further developed to include newer technologies to enhance the functions and features of substations. Information technology will still be the major theme of development built on a multi-media environment. The improvement will depend mainly on the success of man/machine interface. Internet/Intranet based substation control could become popular in future.

It is well aware that most faults in the power system appear as localised hot spots in their

early stage of development. They then gradually grow into faults that are not remediable, such as a total insulation breakdown or even an explosion etc. Through the detection of hot spots and abnormal rise in working temperature of conductors or insulators, infrared thermography [89] is one of the most useful tools in identifying potential failures so that preventive measures can be taken to avoid occurrence of any hazard. Thermography has also been employed in medical diagnosis [90] and the diagnosis of advanced electronics consumer products [91]. Another major reason for the numerous applications of infrared thermography in electricity power supply industry is that many points of interest for temperature measurement are difficult to access and are hazardous. The plant can be large, remote, electrically live, rotating or very hot and a remote sensing technique capable of inspecting large areas quickly has obvious attractions. The infrared imager has a temperature range from  $-40^{\circ}\text{C}$  to  $950^{\circ}\text{C}$  with a maximum resolution down to  $0.01^{\circ}\text{C}$ , making it extremely sensitive to slight unbalance in heat dissipation. The power system apparatus as identified in this thesis include bare conductor of 400 kV transmission lines, 25 kV overhead lines feeding electric trains, high resistance spots in high voltage and low voltage switchgears and busbars, abnormal temperature rise of PVC insulation due to overloading of power cables and high impedance faults in power transformers etc.

Although a thermogram can reveal the hot spots, the appearance of an object on a thermogram is often very different from that on an optical picture. Human beings are familiar with analysing optical images rather than thermograms. Owing to the difficulty in analysing thermal images by most non-skilful technical personnel, 3D thermograms are needed so that all engineering staff can easily understand the images under an environment of virtual reality for power plant designing and planning as well as condition based maintenance. The hardware in the initial trial undertaken consisted of a distance measuring device, a thermal imager and a PC. The surface of the object under measurement was divided into grid points whose absolute coordinates were measured with the aid of a laser based distance measuring kit, the Leica Disto which has a RS-232 communication cord for sending the measured data back to a personal computer (PC). The resolution of Disto is 5 mm over a distance of 10 m. Panning and tilting functions are offered to the Disto by an assembly of two stepper motors. The horizontal and vertical angles of the assembly are

## Chapter VII

updated inside the PC with a resolution of  $0.36^\circ$ . This assembly was mounted on top of the infrared camera which was stationary. Therefore, the Disto with panning/tilting functions could give the absolute coordinates of each grid point on the power equipment while the thermal system could give the real time surface temperature of that grid point. When this information was fed into a tailor-made virtual reality based software package, a 3D thermal image could be displayed and manipulated. The major problem here was with the correspondence between the Disto and the thermal system, i.e. matching every point sensed by Disto onto a corresponding point on the thermal image, where further research work was necessary.

Recently, virtual reality (VR) techniques have been widely used in industry. Virtual environments (VEs) are being produced to simulate the real environments, just like our application. The author indeed tried to put the whole piece of electric power equipment into the computer, not just with the geometrical details but with the distribution of surface temperature as well. A 3-dimensional power transformer with surface temperature profile could be displayed on the screen and one can freely manipulate the viewing angle of it. VEs can be distinguished by their relation to a real environment in three aspects. The VE is actually a projection of some real environment. That real environment might be of very different scale [98] or at some distance from the viewer [99]. The latter is usually described by the term tele-presence. It must be pointed out that VE does not exist but is fairly realistic. Very often, the VE can be quite unreal. In the case being studied, the VE was the power plant where the user could manipulate existing and real objects, the power equipment. In order to enhance the feeling of immersion which is the feeling of a VR user that his/her VE is real, surface rendering and controllable angle viewing have been built in the developed system. The user could select two different modes of display, the geometrical mode where the grid of the object's surface was shown or the thermal mode where the surface of the object was coated with a pseudo colour scale to reveal the surface temperature of each point. Three transformations were built into the program, namely translation, scaling and rotation.

Furthermore, the user could freely adjust the viewing angle to concentrate himself on any particular part of the surface, thus fulfilling the full objective of producing a VR environment

for electric power equipment design and maintenance. This 3D thermography could serve two purposes. The first one was for designing power plants under the geometrical mode. The 3D information of all components was recorded inside the PC for proper 3D display. The designer could thus fly around the power plant to check any obstruction and improper placement of equipment. Such checking was more powerful than using the 2D drawings supplied by the manufacturers conventionally. After the power plant was commissioned, regular thermal imaging procedures could be carried out so that any hot spots on the equipment could immediately be identified manually where the physical locations of these hot spots could be cross checked against the geometrical 3D surface. A point to be noted is that a skilful technician in thermography is not required any more because any technical staff in power engineering can fully understand the 3D thermograms.

### 7.3 A FINAL REMARK

The studies contained in this thesis have been very fruitful and some of them have been included in a book published by the Kluwer Academic Publishers [100] in early 1999. Recently, the United States following the examples of the UK pool system has embarked on the most massive, complicated industrial reorganisation since the end of World War II, the deregulation of the electric utility industry. Letting the market, instead of a *pas de deux* between utilities and regulations, set prices is the necessary crux of the matter, and before this can be granted, conditions must be established to ensure that no party has sufficient market power, either globally or locally, to foreclose potential competition. When the policy of deregulation spreads around the whole world, the demand for sub-station automation and power quality monitoring will increase significantly. The achievements reported in this thesis will definitely help to ensure a successful implementation of deregulation for all developed countries around the world.

*References*

- [1] C.R. Bayliss, *Transmission and Distribution Electrical Engineering*, Butterworth-Heinemann, 1996.
- [2] E. Lakervi and E.J. Holmes, *Electricity Distribution Network Design*, Peter Peregrinus Ltd., IEE, 1995.
- [3] Kenneth Caird, "Integrating substation automation", *IEEE Spectrum*, August 1997, pp. 64-69.
- [4] S. Humphreys, "Substation automation systems in review", *IEEE Computer Applications in Power*, April 1998, pp. 24-30.
- [5] C. Booth, J.R. McDonald, R.W. Stewart, W.J. Laycock and A. Bennett, "Enhanced power system control and management via intelligent substations", *Proceedings of IEE 2nd International Conference on Advances in Power System Control, Operation and Management*, Hong Kong, December 1993. pp. 542-547.
- [6] B. Lundqvist, H. Kronander and A.J. Mackrell, "The integration of protection, monitoring, control and communication functions in modern electrical hv installations", *Proceedings of Developments in Power System Protection*, March 1997, pp. 176-179.
- [7] N.J. Nilsson, *Artificial Intelligence: A New Synthesis*, Morgan Kaufmann Publishers, 1998.
- [8] Y.H. Song, Allan Johns and Raj Aggarwal, *Computational Intelligence Applications to Power Systems*, Kluwer Academic Publishers, 1996.
- [9] Kevin Warwick, Arthur Ekwue and Raj Aggarwal (Ed.), *Artificial Intelligence Techniques in Power Systems*, IEE, 1997.
- [10] L.L. Lai, *Intelligent Systems Applications in Power Engineering - Evolutionary*

## References

- Programming and Neural Networks*, John Wiley & Sons Ltd., 1998.
- [11] M.E. El-Hawary (Ed.), *Electric Power Applications of Fuzzy Systems*, IEEE Press, 1998.
- [12] G.R. Allen and R. Cheung, "Integration of protection, control and monitoring functions for transmission and distribution substations", *IEEE Transaction on Power Delivery*, Vol. 13, No. 1, 1998, pp. 96-101.
- [13] J.A. Momoh, L.G. Dias and D.N. Laird, "An implementation of hybrid intelligent tool for distribution system fault diagnosis", *IEEE Transactions on Power Delivery*, Vol. 12, No. 2, 1997, pp. 1035-1040.
- [14] A.P. Alves da Silva, A.H.F. Insfran, P.M. da Silveira and G. Lambert-Torres, "Neural networks for fault location in substations", *IEEE Transactions on Power Delivery*, Vol. 11, No. 1, 1996, pp. 234-239.
- [15] M. Kezunovic and I. Rikalo, "Detect and classify faults using neural nets", *IEEE Computer Applications in Power*, October 1996, pp. 42-47.
- [16] H. Monsef, A.M. Ranjbar and S. Jadid, "Fuzzy rule-based expert system for power system fault diagnosis", *IEE Proc.-Gener. Transm. Distrib.*, Vol. 144, No. 2, 1997, pp. 186-192.
- [17] B. Kasztenny and M. Kezunovic, "Digital relays improve protection of large transformers", *IEEE Computer Applications in Power*, October 1998, pp. 39-45.
- [18] J.A. Palmer and J.K. Nelson, "Intelligent control of large power transformer cooling pumps", *IEE Proc.-Gener. Transm. Distrib.*, Vol. 143, No. 5, 1996, pp. 474-478.
- [19] I. Oki, T. Haida, S. Wakabayashi, R. Tsuge, T. Sakakibara and H. Murase, "Development of partial discharge monitoring technique using a neural network in a gas insulated substation", *IEEE Transactions on Power Systems*, Vol. 12, No. 2, 1997, pp. 1014-1021.
- [20] Wladyslaw Mielczarski (Ed.), *Fuzzy Logic Techniques in Power Systems*,

## References

- Physica-Verlag Heidelberg, 1998, pp. 241-276.
- [21] W.L. Chan, T.M. Chan, S.L. Pang and A.T.P. So, "A distributed on-line hv transmission condition monitoring information system", *IEEE Transactions on Power Delivery*, Vol. 12, No. 2, 1997, pp. 707-713.
- [22] W.L. Chan, A.T.P. So and L.L. Lai, "Internet based transmission substation monitoring", *IEEE Transactions on Power Systems*, Vol. 14, No. 1, 1999, pp. 293-298.
- [23] A.T.P. So, W.L. Chan and C.T. Tse, "Fuzzy logic based automatic capacitor switching controller for reactive power compensation", *Proceedings of Second International Forum on Applications of Neural Networks to Power Systems*, Yokohama, April 1993, pp. 41-46.
- [24] W.L. Chan and A.T.P. So, "Power harmonics pattern recognition by solving fuzzy equations", *Fuzzy Sets and Systems*, Vol. 67, No. 3, 1994, pp 257-266
- [25] L.L. Lai, W.L. Chan, C.T. Tse and A.T.P. So, "Real-time frequency and harmonic evaluation using artificial neural networks", *IEEE Transactions on Power Delivery*, Vol. 14, No. 1, 1999, pp. 52-59.
- [26] W.L. Chan and A.T.P. So, "Development of a new artificial neural network in complex space", *Proceedings of 2nd Biennial Australian Engineering Mathematics Conference*, Sydney, July 1996, pp. 225-230.
- [27] W.L. Chan, A.T.P. So and L.L. Lai, "Complex artificial neural networks and its initial applications to load flow analysis", submitted to *IEEE Transactions on Power Systems*.
- [28] W.L. Chan, A.T.P. So and L.L. Lai, "Evolutionary programming based machine parameters estimation for field oriented control", *Proceedings of IEEE International Electric Machines and Drives Conference*, Seattle, May 1999, pp. 534-536.
- [29] A.T.P. So, W.L. Chan, C.T. Tse and K.K. Lee, "Fuzzy logic based automatic diagnosis of power apparatus by infrared imaging", *Proceedings of Second*

## References

- International Forum on Applications of Neural Networks to Power Systems*, Yokohama, April 1993, pp. 187-192.
- [30] W.L. Chan, A.T.P. So and L.L. Lai, "3-dimensional thermal imaging for power equipment maintenance", submitted to *IEEE Transactions on Power Delivery*.
- [31] M. Kezunovic and B. D. Russell, "Microprocessor applications to substation control and protection", *IEEE Computer Applications in Power*, October 1988, pp. 16-20.
- [32] N. Fujimoto, B. Gupta, R. Morra, G. Ford, J. Meehan, J. Salovaara and T. Molony, "Diagnostics and monitoring for substations", *Ontario Hydro Public Reference Centre PRC1993-69*, November, 1993.
- [33] J. Reason, "Circuit breakers with on-line condition monitoring", *Electrical World*, February, 1995, pp. 21-26.
- [34] A.T.P. So and W.L. Chan, "A Computer-Vision based Power Plant Monitoring System", *Proceedings of International Conference on Advances in Power System Control, Operation & Management*, IEE, Hong Kong, November 1991, pp. 335-340
- [35] M.A. Pike et al ed. *Using the Internet*, 2nd Edition, Que Corp., Indianapolis, 1995.
- [36] A. Gaffin eds. *Everybody's Guide to the Internet*, MIT Press, Cambridge, 1994.
- [37] H. Hahn eds. *The Internet Complete Reference*, McGraw-Hill, Berkeley, 1994.
- [38] B.J. Thomas eds. *The Internet for Scientists and Engineers: On-line Tools and Resources*, CPIE Optical Engineering Press, Bellingham, 1995.
- [39] A.T.P. So and W.L. Chan, "Remote building system monitoring by internet", *Proceedings of 1996 Int. Conf. on Information Infrastructure*, Beijing, April, 1996, pp. 723-726.
- [40] A.T.P. So, W.L. Chan and W.L. Tse "Building automation systems on the

## References

- internet", *Facilities*, Vol. 15, No. 5/6, 1997, pp. 125-133.
- [41] A.T.P. So, W.L. Tse and W.L. Chan, "Development of a full degree course on internet", *Proceedings of 1996 IEEE International Conference on Multi-Media Engineering Education*, Melbourne, July, 1996, pp. 373-382.
- [42] L.A. Zadeh, "Outline of a new approach to the analysis of complex systems and decision processes", *IEEE Transactions System, Man and Cybernetics*, Vol. SMC-3, 1973, pp. 28-44.
- [43] C.T. Tse et al, "Automatic capacitor switching controller using reactive power as control parameter", *Proceedings of the 9th Conference on Electric Power Supply Industry*, Hong Kong, November 1992, Vol. 4, pp. 274-284.
- [44] T.J.E. Miller, *Reactive Power Control in Electric Systems*, New York, Wiley, 1982, pp. 181-222.
- [45] S.E. Haque and N.H. Malik, "Analysis and performance of a fixed filter-thyristor controlled reactor (ff-tcr) compensator", *IEEE Transactions on Power Systems*, Vol. PWRS-2, No. 2, 1987, pp. 303-309.
- [46] M. Kovács, "Stable embedding of ill-posed linear equality and inequality systems into fuzzified systems", *Fuzzy Sets and Systems*, Vol. 45, 1992, pp. 305-312.
- [47] H. Ishibuchi and H. Tanaka, "Fuzzy regression analysis using neural networks", *Fuzzy Sets and Systems*, Vol. 50, 1992, pp. 257-265.
- [48] C.H. Cheng and D.L. Mon, "Fuzzy system reliability analysis by interval of confidence", *Fuzzy Sets and Systems*, Vol. 56, 1993, pp. 29-35.
- [49] A.A. Mahmoud and R.D. Shultz, "A method for analysing harmonic distribution in ac power systems", *IEEE Transactions on Power Apparatus and Systems*, Vol. PAS-101, No. 6, 1982, pp. 1815-1824.
- [50] R.C. Dugan, W.T. Jewell and D.J. Roesler, "Harmonics and reactive power from line-commutated inverters in proposed photovoltaic subdivision", *IEEE Transactions on Power Apparatus and Systems*, Vol. PAS-102, No. 9, 1983,

## References

pp. 3205-3214.

- [51] S.K. Tso and W.L. Chan, "Dual-data acquisition system for high frequency and long duration signal", *Proceedings of HKIE CAI Symposium of Instrumentation & Control*, Hong Kong, January, 1991, pp. 121-128.
- [52] S.K. Tso and W.L. Chan, "Distributed monitoring system for harmonics penetration study", *Proceedings of IEE 1st International Conference on Advances in Power System Control, Operation and Management*, Hong Kong, November, 1991, pp. 744-750.
- [53] T.H. Ottmeyer, N. Kakimoto, T. Hkyama and A.A. Hammam, "Harmonic performance of individual and grouped loads", *Proceedings of 3rd International Conference on Harmonics in Power Systems*, Indiana, 1988, pp. 277-283.
- [54] A. Kaufmann and M.M. Gupta. (Ed.), *Introduction to Fuzzy Arithmetic Theory and Applications*, Van Nostrand Reinhold, N.Y., 1985.
- [55] B.D. Bunday and G.R. Garside (Ed.), *Optimisation Methods in Pascal*, (Edward Arnold, 1987) 54-56.
- [56] T. H. Ortmeyer, K. R. Chakravarthi and A. A. Mahoud, "The effects of power system harmonics on power system equipment and loads", *IEEE Transactions on Power Apparatus and Systems*, Vol. PAS-104, No. 9, September 1985, pp. 2555-2563.
- [57] T. A. George and D. Bones, "Harmonic power flow determination using the fast fourier transform", *IEEE Transactions on Power Delivery*, Vol. 6, No. 2, April 1991, pp. 530-535.
- [58] J. Arrillaga, D. A. Bradley and P. S. Bodger, *Power System Harmonics*, John Wiley & Sons, 1985.
- [59] J. T. Broch, *Principles of experimental frequency analysis*, Elsevier Science Publishers Ltd., 1990, ch 4.
- [60] A. A. Girgis and F. M. Ham, "A qualitative study of pitfalls in FFT", *IEEE Transactions on Aerospace and Electronic Systems*, Vol. AES 16, No 4, July

## References

- 1980, pp. 434-439.
- [61] S.A. McIlwaine, C.E. Tindall and W. McClay, "Frequency tracking for power system control", *IEE Proceedings*, Part C, Vol. 133, No. 2, 1986, pp. 95-98.
- [62] M.M. Begovic, P.M. Djuric, S. Dunlap and A.G. Phadke, "Frequency tracking in power networks in the presence of harmonics", *IEEE Transactions Power Delivery*, Vol. 8, No. 2, 1993, pp. 480-486.
- [63] L.L. Lai, A.D. Wang, Y.Z. Ge, A.O. Ekwue and K.L. Lo, "A simple method for measuring power system frequency", *Proceedings of the Third International Symposium on Electricity Distribution and Energy Management*, Vol 2, IEEE Singapore Section, pp. 784-789.
- [64] A.G. Phadke, J.S. Thorp and M.G. Adamiak, "A new measurement technique for tracking voltage phasors, local system frequency and rate of change of frequency", *IEEE Transactions Power Apparatus and Systems*, Vol. PAS-102, No. 5, 1983, pp. 1025-1038.
- [65] A.G. Phadke et al (Working Group H-7), "Synchronized sampling and phasor measurements for relaying and control", *IEEE Transactions Power Delivery*, Vol. 9, No. 1, 1994, pp. 442-452.
- [66] M.S. Sachdev and M.M. Giray, "A least error squares technique for determining power system frequency", *IEEE Transactions Power Apparatus and Systems*, Vol. PAS-104, No. 2, 1985, pp. 437-443.
- [67] H.M. Beides and G.T. Heydt, "Dynamic state estimation of power system harmonics using Kalman filter methodology", *IEEE Transactions on Power Delivery*, Vol. 6, No. 4, October, 1991, pp. 1663-1670.
- [68] S.K. Tso and W.L. Chan, "Frequency and harmonic evaluation using non-linear least-squares technique", *Journal of Electrical and Electronics Engineering*, Vol. 14, No. 2, 1994, pp 124-132.
- [69] V. Terzija, M. Djuric and B. Kovacevic, "A new self-tuning algorithm for the frequency estimation of distorted signals", *IEEE Transactions Power Delivery*,

## References

- Vol. 10, No. 3, 1995, pp. 1779-1785.
- [70] R.K. Hartana and G.H. Richards, "Harmonic source monitoring and identification using neural networks", *IEEE Transactions on Power Systems*, Vol. 5, No. 4, November, 1990, pp. 1098-1104.
- [71] S. Osowski, "Neural network for estimation of harmonic components in a power system", *IEE Proceedings*, Part C, Vol. 139, No. 2, March, 1992, pp. 129-135.
- [72] P.E. Gill, Walter Murray and M.H. Wright, *Practical Optimization*, Academic Press, 1981, pp. 133-139.
- [73] S.V.B. Aiyer, M. Niranjan and F. Fallside, "A theoretical investigation into the performance of the Hopfield model", *IEEE Transaction on Neural Networks*, Vol. 1, 1990, pp. 204-215.
- [74] Y. Takefuji, *Neural Network Parallel Computing*, Kluwer Academic Pub., Boston, 1992, pp. 157-176.
- [75] J.M. Zurada, Eds. *Introduction to Artificial Neural Systems*, info Access, Singapore, 1992, pp. 1-3.
- [76] T.T. Nguyen, "Load-flow parallel processing system, conjugate-gradient neural network architecture", *Electric Power Systems Research*, vol. 39, 1996, pp. 73-79.
- [77] T.T. Nguyen, "Neural network optimal-power-flow", *Proceedings of IEE 4nd International Conference on Advances in Power System Control, Operation and Management*, Hong Kong, November, 1997, pp. 266-271.
- [78] J.A.K. Suykens, J.P.L. Vandewalle and B.L.R. De Moor, *Artificial Neural Networks for Modelling and Control of Non-linear Systems*, Kluwer Academic Publishers, Boston, 1996.
- [79] S.L. Ho, H.W. Leung and W.L. Chan, "Application of statistical signal processing for condition monitoring of rotor faults in induction motor", *Proceedings of Sixth International Conference on Electrical Machines and*

## References

- Drives*, September 1993, pp. 97-102
- [80] M.Y. Chow, *Methodologies of using Neural Network and Fuzzy Logic Technologies for Motor Incipient Fault Detection*, Word Scientific Publishing Co. Pte. Ltd., 1997.
- [81] D.J. Atkinson, P.P. Acarnley and J.W. Finch, "Observers for induction motor state and parameter estimation", *IEEE Transactions on Industry Applications*, Vol. 27, 1991, pp. 1119-1127.
- [82] T. Du, P. Vas and F. Stronach, "Design and application of extended observers for joint state and parameter estimation in high-performance AC drives", *IEE Proceedings - Electr. Power Applic.*, Vol. 142, No. 2, pp. 71-78, 1995.
- [83] L. Ljung, *System Identification: Theory for the User*, Englewood Cliffs, J.J., Prentice Hall, 1987.
- [84] P. Pillay, R. Nolan and T. Haque, "Application of genetic algorithms to motor parameter determination for transient torque calculations", *IEEE Transactions on Industry Applications*, Vol. 33, No. 5, 1997, pp. 1273-1281.
- [85] I. Miki, O. Nakao and S. Nishiyama, "A new simplified current control method for field-oriented induction motor drives", *IEEE Transactions on Industry Applications*, Vol. 27, No. 6, 1991, pp. 1081-1086.
- [86] Nangsue P., P. Pillay and S. Conry, "Evolutionary algorithms for induction motor parameter determination", *IEEE Transactions on Energy Conversion*, PE-256-EC-0-2-1988, in press.
- [87] A.M. Trzynadlowski, *The Field Orientation Principle in Control of Induction Motors*, Kluwer Academic Publishers, Norwell, 1994.
- [88] L.L. Lai, A.G. Sichanie and B.J. Gwyn, "Comparison between evolutionary programming and a genetic algorithm for fault-section estimation", *IEE Proceedings-Gener. Transm. Distrib.*, Vol. 145, No. 5, 1998, pp. 616-620.
- [89] S.G. Burnay, T.L. Williams and C.H. Jones *Application of Thermal Imaging*, Adam Hilger, 1988.

## References

- [90] F.H.Y. Chan and A.T.P. So, "A 3-camera system for medical thermography", *Proceedings of BME'92, Biomedical Engineering Symposium*, Hong Kong, April, 1992, pp. 5-8.
- [91] F.H.Y. Chan and A.T.P. so, "Application of thermography in advanced consumer electronics", *Proceedings of the International Symposium on Consumer Electronics*, Beijing, October, 1992, pp. 337-340.
- [92] W.J. Gordon and R.F. Riesenfeld, *B-spline Curves and Surfaces, Computer Aided Geometric Design*, New York, Academic Press, 1974, pp. 95-126.
- [93] B.D. Bunday and G.R. Garside, *Optimisation Methods in Pascal*, Edward Arnold, 1987, pp. 54-56.
- [94] I. Sobel, "On calibrating computer controlled cameras for perceiving 3D scenes", *Artificial Intelligence*, Vol. 5, 1974, pp. 185-198.
- [95] D.B. Gennery, "Stereo-camera calibration", *Proceedings of Image Understanding Workshop*, 1979, pp. 101-108.
- [96] R.K. Lenz, and R.Y. Tsai, "Techniques for calibration of the scale factor and image center for high accuracy 3D machine metrology", *IEEE Transactions on Pattern Analysis and Machine Intelligence*, Vol. 10, No. 5, 1988, pp. 713-720.
- [97] O.D. Faugers and G. Toscani, "The calibration problem for stereo", *Proceedings of CVPR'86*, Miami, 1986, pp. 15-20.
- [98] R.M. Taylor, W. Robinett, V.L. Chi, F.P. Brooks, W.V. Wright, R.S. Williams and E.J. Snyder, "The nanomanipulator: a virtual reality interface for a scanning tunnelling microscope", *Computer Graphics*, Vol. 27, 1993, pp. 127-134.
- [99] G.M.H. Clifford and A. Shaffer, "A real-time robot arm collision avoidance system", *IEEE Transactions Robotics and Automation*, Vol. 8, No. 2, 1992.
- [100] A.T.P. So and W.L. Chan, ed. *Intelligent Building Systems*, Kluwer Academic Publishers, Norwell, 1999.